Alma Mater Studiorum · University of Bologna

School of Science
Department of Physics and Astronomy
Master Degree in Physics

A next-to-leading order calculation of the impact of primordial magnetic fields into cosmological observables

Supervisor:
Prof. Roberto Casadio

Co-supervisors:
Dr. Fabio Finelli
Dr. Daniela Paoletti

Submitted by:
Alex Ciabattoni

Academic Year 2021/2022

Abstract

In this thesis, we perform a next-to-leading order calculation of the impact of primordial magnetic fields (PMF) into the evolution of scalar cosmological perturbations and the cosmic microwave background (CMB) anisotropy. Magnetic fields are everywhere in the Universe at all scales probed so far, but their origin is still under debate. The current standard picture is that they originate from the amplification of initial seed fields, which could have been generated as PMFs in the early Universe. The most robust way to test their presence and constrain their features is to study how they impact on key cosmological observables, in particular the CMB anisotropies. The standard way to model a PMF is to consider its contribution (quadratic in the magnetic field) at the same footing of first order perturbations, under the assumptions of ideal magneto-hydrodynamics and compensated initial conditions. In the perspectives of ever increasing precision of CMB anisotropies measurements and of possible uncounted non-linear effects, in this thesis we study effects which go beyond the standard assumptions. We study the impact of PMFs on cosmological perturbations and CMB anisotropies with adiabatic initial conditions, the effect of Alfvén waves on the speed of sound of perturbations and possible non-linear behavior of baryon overdensity for PMFs with a blue spectral index, by modifying and improving the publicly available Einstein-Boltzmann code SONG, which has been written in order to take into account all second-order contributions in cosmological perturbation theory. One of the objectives of this thesis is to set the basis to verify by an independent fully numerical analysis the possibility to affect recombination and the Hubble constant.

Contents

Introduction

Magnetic fields are everywhere in the Universe on all scales probed so far, from planets and stars to galaxies and galaxy clusters. Despite an extraordinary amount of data, their origin still represents one of the biggest open questions of modern cosmology. A compelling possibility is that they are the result of an amplification (through dynamos or gravitational compression) of relics from the early Universe, which were generated prior to recombination and are known as *primordial magnetic fields* (PMFs).

PMFs have a strong impact on the main cosmological observables, in particular on the anisotropies of the cosmic microwave background (CMB), hence allowing them to have powerful tools to test their existence and properties. However, the presence of PMFs involves a treatment of plasma physics which goes beyond the standard treatment of CMB physics and the assumptions of linearity and ideal magneto-hydrodynamics (MHD) to be exhaustively described. So far, these effects were mostly studied in the framework of small-scales MHD simulations, but an extensive and rigorous treatment of this kind of physics in the standard Einstein-Boltzmann approach and a quantitative discussion of its impact on CMB anisotropies is still lacking. The ever increasing precision of CMB anisotropies measurements makes the development of robust predictions from these non-trivial effects a necessity and, at the same time, a fascinating challenge for present and future studies.

This thesis consists in a step towards this direction, that is to study the impact of PMFs on cosmological perturbations and CMB anisotropies with adiabatic initial conditions by making use of the Einstein-Boltzmann code SONG, that is able to compute the key cosmological observables up to second order in cosmological perturbation theory and that we properly modified to include the desired magnetic contributions. In particular, we took into account the PMF energy-momentum tensor, which is treated as a first order perturbation and hence gravitates at linear level, the Lorentz force, which affects the baryon velocity and indirectly also photons, and the increasing of the speed of sound due to Alfvén velocity, which has the effect to enhance the effective pressure of the fluid. Particularly important for us is the impact of PMFs on baryon overdensities and their possible non-linear behavior for PMFs with a blue spectral index. In fact, an intriguing possibility is that baryon inhomogeneities of appreciable amplitude induced by the presence of PMFs may affect the recombination history and consequently change

the measurement of the Hubble constant from CMB data, leading to a possible relieving of the tension with the measurements from supernovae.

This thesis is structured as follows:

1. In Chapter 1 we give a brief overview of the basic notions about the standard cosmological model and the mechanism of inflation.

2. In Chapter 2 we present the relativistic cosmological perturbation theory, going through the perturbed Einstein and Boltzmann equations and showing how the initial conditions for the perturbations are fixed in the adiabatic case.

3. In Chapter 3 we give a review of CMB anisotropies, which is the key cosmological observable for this thesis, describing in details the temperature angular power spectrum and its dependence on the cosmological parameters.

4. In Chapter 4 we present the cosmological perturbation theory at second order, in particular by emphasizing the additional complexities with respect to the linear case; we also introduce the code SONG, how it works and the improvements we needed to implement for our purposes; we also show a few second-order spectra for ΛCDM obtained with it.

5. In Chapter 5 we give a review of primordial magnetic fields, showing the main mechanisms of their generation and how the electrodynamics is formulated in an expanding Universe.

6. In Chapter 6 we present a detailed review of the impact of PMFs on CMB anisotropy, showing the main results in the literature for compensated initial conditions; we then give our first original results for adiabatic initial conditions, showing in particular how the CMB angular power spectrum is affected by the contributions of the Lorentz force and the PMF energy-momentum tensor in the Einstein equations.

7. In Chapter 7 we discuss *i*) the impact of PMFs on baryon inhomogeneities and their behavior around recombination, in particular for blue spectral indices, *ii*) the effect of Alfvén waves on the speed of sound, whose contribution is usually neglected in the standard literature because of its non-linear nature.

Throughout this thesis, we assume natural units in which $c = \hbar = k_B = 1$ (unless otherwise specified) and work with the metric signature (-,+,+,+). For tensors, we use Greek letters for spacetime indices ($\mu = 0, ..., 3$) and Latin letters for spatial ones ($i = 1, ..., 3$).

Chapter 1

The Standard Big-Bang Cosmological Model

In the last century an extraordinary amount of activities and discoveries in both theoretical and observational cosmology led our understanding of the Universe to unimaginable levels. The standard theory of cosmology, also known as hot Big-Bang model, represents nowadays the most successful theory for describing the evolution of the Universe as a whole. Since the formulation of the theory of General Relativity (GR) by Albert Einstein in 1916, scientists were able to provide a rigorous mathematical framework for the construction of cosmological models. Friedmann in 1922 [28] and than Lemaitre in 1927 [51] derived the solutions of GR assuming homogeneity and isotropy of the Universe, leading to the Friedmann-Lemaitre-Robertson-Walker (FLRW) metric. In fact, cosmological observations suggest that the Universe is nearly isotropic, at least considering scales larger than ~ 100 Mpc; we can then directly infer its homogeneity if we assume that there are no special observers in the Universe (*Copernican principle*). Homogeneity and isotropy of the Universe constitute what is known as *Cosmological principle*, which represents the starting point of our discussion and whose validity is mostly verified *a posteriori*.

Another crucial fact for modern cosmology was the discovery, in 1929, of the expansion of the Universe by Edwin Hubble [36], who found that galaxies were receding from us with radial velocities proportional to their distances. Moreover, in 1998, observations of distant type Ia supernovae [75] showed that such expansion is accelerating, leading scientists to hypothesize the existence of an additional, unknown component in the Universe, the Dark Energy (DE).

Few decades later the discovery by Hubble, one more key step was made thanks to the detection of the Cosmic Microwave Background radiation (CMB) by Penzias and Wilson in 1965 [68], which gave the first clear hint of an early hot *Big-Bang* stage in the history of the Universe.

The other kind of component which completes the *dark* side of our Universe together with the DE is the Dark Matter (DM), whose existence was necessary to explain the

rotational curves of spiral galaxies and is now supported by many other astrophysical and cosmological data. The model which includes DE in the form of a cosmological constant (Λ) and non-relativistic, or cold, DM (CDM) is called ΛCDM. Despite some theoretical issues, it is currently the most economic model (we need only 6 parameters to define it), which at the same time is in agreement with the largest number of observations. The abundance of the light elements from primordial nucleosynthesis, the expansion of the Universe and the CMB data are some of the most relevant successes of the concordance model and at the same time provide for it remarkable constraints to the cosmological parameters. In addition to the ordinary evolution of the Universe, the existence of an early stage of accelerated expansion, called inflation, is necessary to solve some problems which arise in the standard picture, as we will see in this chapter.

1.1 General Relativity

The dynamics of the Universe on large scales is driven mostly by gravity. A consistent gravitational theory is therefore necessary for the construction of a cosmological model. The best candidate so far is the theory of General Relativity, whose validity has been reinforced several times in the last century by many experimental tests. It is based on the Principle of General Relativity, which states that the laws of physics are the same in all reference frames, and on the Equivalence Principle, according to which we can always construct in a sufficiently small neighborhood of any spacetime point in a arbitrary gravitational field a local inertial frame in which gravity is absent.

The metric

In this framework, we assign to a generic event one temporal coordinate and three spatial ones, allowing us to interpret it as a point in the 4-dimensional spacetime manifold with coordinates $x^\mu = (x^0, x^1, x^2, x^3) = (t, x, y, z)$.

The key object of GR is the 2-rank symmetric tensor $g_{\mu\nu}$, which is called *metric* tensor and encodes all the information about the geometry of the manifold and determines how distances are computed. Given two infinitesimally nearby spacetime points (x^0, x^1, x^2, x^3) and $(x^0 + \mathrm{d}x^0, x^1 + \mathrm{d}x^1, x^2 + \mathrm{d}x^2, x^3 + \mathrm{d}x^3)$, their distance $\mathrm{d}s$ is defined as

$$\mathrm{d}s^2 = g_{\mu\nu}(x)\, \mathrm{d}x^\mu \mathrm{d}x^\nu \ . \tag{1.1}$$

In Special Relativity, the metric is constant everywhere, $g_{\mu\nu} = \mathrm{diag}(-1, 1, 1, 1)$, while in GR it generally depends on the spacetime point, $g_{\mu\nu} = g_{\mu\nu}(t, \mathbf{x}) \equiv g_{\mu\nu}(x)$. This spacetime dependence is what encodes the effect of gravity and is determined by the distribution of matter and energy in the Universe.

The geodesic equation

The evolution of a test particle in a curved spacetime without any non-gravitational forces is governed by the geodesic equation. A *geodesic* is a curve which extremizes the particle's action between two fixed spacetime points through the variational principle. In the flat space it is just a straight line, so we can intuitively picture it as the shortest path for a particle to move between two points, generalized to curved manifolds. Varying the particle's action in a curved spacetime and setting it to zero, we obtain the geodesic equation

$$\frac{\mathrm{d}^2 x^\mu}{\mathrm{d}\lambda^2} + \Gamma^\mu_{\rho\sigma} \frac{\mathrm{d}x^\rho}{\mathrm{d}\lambda} \frac{\mathrm{d}x^\sigma}{\mathrm{d}\lambda} = 0 \ , \tag{1.2}$$

where the $\Gamma^\mu_{\rho\sigma}$ are the Christoffel symbols defined as[1]

$$\Gamma^\mu_{\rho\sigma} = \frac{1}{2} g^{\mu\alpha} \big(g_{\alpha\rho,\sigma} + g_{\alpha\sigma,\rho} - g_{\rho\sigma,\alpha} \big) \tag{1.3}$$

and λ is what parametrizes the geodesic and grows monotonically with time.

We can rewrite the geodesic equation in a slightly different form by introducing the *4-velocity*

$$U^\mu \equiv \frac{\mathrm{d}x^\mu}{\mathrm{d}\lambda} \ , \tag{1.4}$$

which allows us to write equation (1.2) as

$$\frac{\mathrm{d}U^\mu}{\mathrm{d}\lambda} + \Gamma^\mu_{\rho\sigma} U^\rho U^\sigma = 0 \ . \tag{1.5}$$

We can further manipulate the last equation to obtain the following expression:

$$U^\alpha \big(U^\mu{}_{,\alpha} + \Gamma^\mu_{\alpha\beta} U^\beta \big) \equiv U^\alpha \nabla_\alpha U^\mu = 0 \ , \tag{1.6}$$

where in the second term we have define the *covariant derivative* of U^μ.

Using the definition of *4-momentum* $P^\mu \equiv m U^\mu$, where m is the mass of the particle, we can rewrite equation (1.6) as[2]

$$P^\alpha P^\mu{}_{,\alpha} + \Gamma^\mu_{\alpha\beta} P^\alpha P^\beta = 0 \ . \tag{1.7}$$

[1] Here we define the inverse metric $g^{\mu\alpha}$ such that $g_{\mu\nu} g^{\mu\alpha} = \delta^\alpha_\nu$, while the commas are partial derivatives: $g_{\mu\nu,\alpha} \equiv \frac{\partial g_{\mu\nu}}{\partial x^\alpha}$.

[2] We stress that this equation holds for both massive and massless particles, where in the latter case P^μ has to be interpreted as the 4-momentum of a massless particle.

The Einstein field equations

All the information about the dynamics are contained in the *Einstein field equations*:

$$G_{\mu\nu} \equiv R_{\mu\nu} - \frac{1}{2} g_{\mu\nu} R = 8\pi G\, T_{\mu\nu} \ , \tag{1.8}$$

where $G_{\mu\nu}$ is the Einstein tensor, $R_{\mu\nu}$ the Ricci tensor, $R \equiv g^{\mu\nu} R_{\mu\nu}$ the Ricci scalar and $T_{\mu\nu}$ the energy-momentum tensor (EMT). These are ten (with only six independent) highly non-linear partial differential equations, which relate the geometry of the manifold (in $G_{\mu\nu}$) to the matter content (in $T_{\mu\nu}$). This leads to an innovative picture of GR, according to which gravity is not meant just as an external force, like in the Newton's law, rather it has a geometrical interpretation: the matter content of the Universe determines its geometry and, vice versa, the geometry affects the dynamic of the matter.

The Ricci tensor is a contraction of the Riemann tensor, $R_{\mu\nu} = R^{\lambda}{}_{\mu\lambda\nu}$, which is defined as follows:

$$R^{\lambda}{}_{\mu\nu\rho} = \Gamma^{\lambda}_{\mu\nu,\rho} - \Gamma^{\lambda}_{\mu\rho,\nu} + \Gamma^{\lambda}_{\alpha\rho}\Gamma^{\alpha}_{\mu\nu} - \Gamma^{\lambda}_{\alpha\nu}\Gamma^{\alpha}_{\mu\rho} \ . \tag{1.9}$$

Thus, the Ricci tensor can be expressed in terms of the Christoffel symbols:

$$R_{\mu\nu} = \Gamma^{\lambda}_{\mu\nu,\lambda} - \Gamma^{\lambda}_{\mu\lambda,\nu} + \Gamma^{\lambda}_{\alpha\lambda}\Gamma^{\alpha}_{\mu\nu} - \Gamma^{\lambda}_{\alpha\nu}\Gamma^{\alpha}_{\mu\lambda} \ . \tag{1.10}$$

By construction the Riemann tensor satisfies the Bianchi identities:

$$R_{\mu\nu\lambda\rho;\sigma} + R_{\mu\nu\sigma\lambda;\rho} + R_{\mu\nu\rho\sigma;\lambda} = 0 \ , \tag{1.11}$$

where $R_{\mu\nu\lambda\rho;\sigma} \equiv \nabla_\sigma R_{\mu\nu\lambda\rho}$ and $R_{\mu\nu\lambda\rho} = g_{\mu\alpha} R^{\alpha}{}_{\nu\lambda\rho}$.

As a consequence, the Einstein tensor is covariantly conserved:

$$\nabla_\mu G^{\mu}{}_{\nu} = 0 \ , \tag{1.12}$$

which in turn implies, through equation (1.8), the conservation law for the EMT:

$$\nabla_\mu T^{\mu}{}_{\nu} = 0 \ . \tag{1.13}$$

These constraints make the number of independent equations in (1.8) decrease from ten to six.

The field equations (1.8) can be obtained directly from the action principle. The full action of the theory is given by the Einstein-Hilbert term, describing the geometrical part, together with the matter term:

$$S = \int \mathrm{d}^4x \sqrt{-g} \left[\frac{R}{16\pi G} + \mathcal{L}_{\mathrm{matter}} \right] \ , \tag{1.14}$$

where $g \equiv \det[g_{\mu\nu}]$ and $\mathrm{d}^4x\sqrt{-g}$ represents the invariant volume element.

With this procedure, we also find a formal definition of the EMT, which relates it to the matter lagrangian density $\mathcal{L}_{\mathrm{matter}}$ as follows:

$$T_{\mu\nu} \equiv \frac{-2}{\sqrt{-g}} \frac{\delta(\sqrt{-g}\mathcal{L}_{\mathrm{matter}})}{\delta g^{\mu\nu}} = -2\frac{\delta \mathcal{L}_{\mathrm{matter}}}{\delta g^{\mu\nu}} + g_{\mu\nu}\mathcal{L}_{\mathrm{matter}} \ . \tag{1.15}$$

1.2 FLRW metric and the Friedmann equations

Solving the field equations (1.8) is in general very difficult, if not impossible, without making any simplifying assumption. In this sense, assuming the existence of symmetries can help to constrain the form of the metric and makes the mathematical apparatus manageable. Formally, it is useful to introduce the concepts of *isometries* and *Killing vectors*.

An isometry is a transformation $x \to x'$ which leaves the functional form of the metric invariant, namely

$$g'_{\mu\nu}(x) = g_{\mu\nu}(x) \quad \forall x \ . \tag{1.16}$$

If we consider an infinitesimal transformation like

$$x'^{\mu} = x^{\mu} + \epsilon\, \xi^{\mu} \quad \text{with } \epsilon \ll 1 \ , \tag{1.17}$$

we obtain an isometry if the 4-vector ξ^{μ} satisfies the *Killing equations*:

$$\xi_{\mu;\nu} + \xi_{\nu;\mu} = 0 \ , \tag{1.18}$$

in which case ξ^{μ} is called Killing vector of the metric $g_{\mu\nu}(x)$. It can be proven that a N-dimensional manifold can be equipped with at most $N(N+1)/2$ Killing vectors and, in the special case in which it possesses exactly $N(N+1)/2$ of them, it is called *maximally symmetric space*. An important property of those spaces in the case of $N \geq 3$ is that they possess a constant Ricci scalar.

1.2.1 Geometry of the Universe

As already mentioned, our basic assumption is the cosmological principle, which considerably simplifies the mathematical formulation. This principle states that at each instant of *time* the Universe (both the spatial geometry and the matter content) is homogeneous and isotropic. What should be stressed here is the meaning of the time being referred to as well as for which observer such principle holds. This can be better clarified by assuming that the Universe can be foliated by a regular set of spacelike hypersurfaces Σ_t and there exists fundamental observers whose world lines x^i are a set of non-intersecting geodesics orthogonal to Σ_t. The time t is then the parameter which labels a particular spacelike hypersurface, while the aforementioned observers are those who perceive the Universe to be homogeneous and isotropic.

Within the formalism introduced above, this means that these 3-dimensional spacelike hypersurfaces are maximally symmetric spaces, which are characterized by 3 spacelike Killing vectors generating spatial translations (which mathematically determines homogeneity) and 3 spacelike Killing vectors generating rotations (which mathematically determines isotropy).

The metric of the Universe is then uniquely identified by the cosmological principle and takes the following form:

$$\mathrm{d}s^2 = -\mathrm{d}t^2 + a^2(t)\gamma_{ij}\mathrm{d}x^i\mathrm{d}x^j \ , \tag{1.19}$$

where $a(t)$ is the *scale factor*, $x^i \equiv \{x^1, x^2, x^3\}$ are the *comoving coordinates* and

$$\gamma_{ij} = \delta_{ij} + k\frac{x_i x_j}{1 - k(x_k x^k)} \ . \tag{1.20}$$

Note that homogeneity and isotropy have reduced the independent components of the metric to just the scale factor and a constant, the curvature parameter k. The latter can take the values $k = -1, 0, +1$, denoting an hyperbolic, flat or spherical geometry respectively. Measurements of CMB [72] strongly suggest a nearly flat Universe, that is $k \approx 0$. The metric (1.19) is known as the *Friedmann-Lemaitre-Robertson-Walker* (FLRW) *metric* and is more commonly expressed in spherical coordinates (t, r, θ, ϕ):

$$\mathrm{d}s^2 = -\mathrm{d}t^2 + a^2(t)\left[\frac{\mathrm{d}r^2}{1 - kr^2} + r^2(\mathrm{d}\theta^2 + \sin^2\theta\,\mathrm{d}\phi^2)\right] \ , \tag{1.21}$$

because it makes the symmetries of the space manifest. It also enjoys a rescaling symmetry $a \to \lambda a$, $r \to r/\lambda$, $k \to \lambda^2 k$, with which we can always set the scale factor to unity today[3].

Another useful expression of the FLRW metric can be obtained by introducing the *conformal time* $\mathrm{d}\tau = \mathrm{d}t/a(t)$, which allows us to write

$$\mathrm{d}s^2 = a^2(\tau)\left[-\mathrm{d}\tau^2 + \frac{\mathrm{d}r^2}{1 - kr^2} + r^2\mathrm{d}\Omega^2\right] \ , \tag{1.22}$$

where $\mathrm{d}\Omega = \mathrm{d}\theta^2 + \sin^2\theta\,\mathrm{d}\phi^2$ and $a(\tau)$ is the conformal scale factor. In what follows, an overdot will denote a derivative with respect to the cosmic time t, while a prime will denote a derivative with respect to the conformal time τ.

It should be remarked again that the form of the FLRW metric has been obtained exclusively through symmetries considerations, without ever referring to the expression of $T_{\mu\nu}$, nor the Einstein equations, which instead are necessary to know the functional form of the scale factor $a(t)$.

1.2.2 Kinematics of the Universe

In order to understand how particles evolve in the cosmological context, we should apply the geodesic equation (1.7) to the FLRW metric (1.19). We need then to compute the

[3] In this case, $a(t)$ becomes dimensionless, while r and $k^{-1/2}$ take the dimension of length.

Christoffel symbols for this metric and one can show that the only non-zero components are Γ^0_{ij}, Γ^i_{0j} and Γ^i_{jk}; furthermore, the homogeneity of the Universe implies $\partial_i P^\mu = 0$. These two considerations allow us to rewrite the geodesic equation (1.7) as

$$P^0 \frac{\mathrm{d}P^\mu}{\mathrm{d}t} = -(2\Gamma^\mu_{0j} P^0 + \Gamma^\mu_{ij} P^i) P^j \ . \tag{1.23}$$

We can now consider two cases:

- Massive particles at rest in the comoving frame ($P^j = 0$) stay at rest:

$$P^j = 0 \quad \Rightarrow \quad \frac{\mathrm{d}P^\mu}{\mathrm{d}t} = 0 \ . \tag{1.24}$$

- Not requiring the particles to be at rest and considering the $\mu = 0$ component, after a bit of mathematical manipulation equation (1.23) becomes

$$\frac{\dot{p}}{p} = -\frac{\dot{a}}{a} \quad \Rightarrow \quad p \propto \frac{1}{a} \ , \tag{1.25}$$

  where $p^2 \equiv g_{ij} P^i P^j$ is the physical 3-momentum and we used the explicit expressions of the Christoffel symbols in the FLRW spacetime. So, for both massive and massless particles, the physical 3-momentum decays with the expansion of the Universe; in the massless case, since $p = E$, it is the energy which gets diluted.

Cosmological redshift and Hubble law

All the information we have about the Universe come from the radiation we receive from distant sources. So, in order to correctly infer the properties of what we are observing, we should take into account that, in accordance with the equation (1.25), the energy of the photons (or the wavelengths of the electromagnetic waves in the classical picture) gets stretched by the expansion of the Universe.

Quantitatively, the relation between the observed wavelength λ_o at time t_0 and the emitted one λ_e at time t is

$$\frac{\lambda_o}{\lambda_e} = \frac{a(t_0)}{a(t)} \equiv 1 + z \ , \tag{1.26}$$

where z is called *redshift*. Since $a(t_0) > a(t)$, the wavelength also increases, $\lambda_o > \lambda_e$, as expected.

If the source is sufficiently close, we can expand the scale factor in power series:

$$a(t) = a(t_0)[1 + (t - t_0)H_0 + ...] \ , \tag{1.27}$$

where we have defined the *Hubble constant* as

$$H_0 \equiv \frac{\dot{a}(t_0)}{a(t_0)} \ . \tag{1.28}$$

From the definition (1.26) of z we then get $z = H_0(t_0 - t) + \dots$. Since for nearby objects $t_0 - t$ just coincides with the physical distance d ($c = 1$), we then find a linear relation between the redshift and the distance:

$$z \simeq H_0\, d \ . \tag{1.29}$$

This is the famous *Hubble law*, which was proposed by Edwin Hubble who observed that the recessional velocities $v_{\rm gal}$ of galaxies were indeed proportional to their distances: $v_{\rm gal} = Hd$ (H here is the *Hubble parameter* which is a function of time; H_0 is just H evaluated today) [36].

The Hubble constant, by definition, is a measure of the current expansion rate of the Universe. Its numerical value has undergone numerous changes in the last decades and still nowadays its measurement is not without uncertainties. Since H_0 enters in almost every cosmological quantity, by convention it is usually defined as

$$H_0 \equiv 100\, h\, \text{km s}^{-1}\text{Mpc}^{-1} \ , \tag{1.30}$$

where the parameter h is conveniently used to keep track of all the uncertainties that H_0 may introduce in the other cosmological parameters. According to the latest Planck results, we now have $h \approx 0.674 \pm 0.005$ [72], but its precise value is still under debate. Measurements from the local universe, in fact, suggest values which are not compatible (considering the uncertainties) with the ones coming from the early time observations, leading to the so-called Hubble tension.

Distances

The concept of distance in cosmology is not trivial. One can have in fact different definitions of distance which in general do not coincide. The spatial part of the metric (1.19), $\mathrm{d}\chi^2 \equiv \gamma_{ij}\mathrm{d}x^i\mathrm{d}x^j$, has the meaning of *comoving distance*. It does not account for the expansion of the universe, since the scale factor is factorized out its definition, but its expression generally depends on the curvature of the Universe; in the flat case ($k = 0$) it just coincides with the usual Euclidean distance: $\mathrm{d}\chi^2 = \delta_{ij}\mathrm{d}x^i\mathrm{d}x^j$. The physical distance, instead, is given by $r = a(t)\chi$. We would like to relate these theoretical distances to what we really measure, that is the redshift. Let us then consider the propagation of light from the source to us; this is described by the radial null geodesic ($\mathrm{d}s^2 = 0$, $\mathrm{d}\theta = \mathrm{d}\phi = 0$), which allows us to write $\mathrm{d}\chi = \mathrm{d}t/a(t)$. Integrating from the time of emission $t_{\rm em}$ to the time of observation $t_{\rm obs}$, we find that the comoving distance travelled by the photon is

$$\chi(t_{\rm em}, t_{\rm obs}) = \int_{t_{\rm em}}^{t_{\rm obs}} \frac{\mathrm{d}t}{a(t)} \quad \Rightarrow \quad \chi(z) = \frac{1}{a_0}\int_0^z \frac{\mathrm{d}z}{H(z)} \ , \tag{1.31}$$

where in the second expression we have used the definition of the Hubble parameter and the relation between $a(t)$ and z as in (1.26); we refer to it as the *distance-redshift law*.

It is interesting to notice that, in conformal time, equation (1.31) becomes

$$\chi(\tau_{\rm em}, \tau_{\rm obs}) = \int_{\tau_{\rm em}}^{\tau_{\rm obs}} {\rm d}\tau = \tau_{\rm obs} - \tau_{\rm em} \ . \tag{1.32}$$

Let us now see other two commonly used definitions of distance, which are mostly applied in the observational sector.

- *Luminosity distance.* Standard candles, whose absolute luminosity L is known for theoretical reasons (like type Ia supernovae), are used to infer their (luminosity) distance d_L by measuring their fluxes F and using the following relation:

$$F = \frac{L}{4\pi d_L^2} \ . \tag{1.33}$$

  In a FLRW spacetime, we should consider two effects: *i*) temporal dilation which makes the rate of arrival of photons decreases by a factor $(1+z)^{-1}$ and *ii*) the redshifting of photons by a factor $(1+z)^{-1}$. Accounting for these contributions we then have that $L \to L(1+z)^{-2}$ and equation (1.33) becomes

$$F = \frac{L}{4\pi\chi^2(1+z)^2} \equiv \frac{L}{4\pi d_L^2} \quad \Rightarrow \quad d_L \equiv \chi(1+z) \ , \tag{1.34}$$

  where we have now assumed flat geometry ($k = 0$).

- *Angular diameter distance.* Equivalently to the idea of standard candles, standard rulers are objects whose physical size D is already known. Measuring the angular size $\delta\theta$ of a source, if $\delta\theta \ll 1$ (always true for cosmological objects), its (angular) distance d_A is given by the Euclidean geometry:

$$d_A = \frac{D}{\delta\theta} \ . \tag{1.35}$$

  In the cosmological context it is expressed in terms of the comoving distance through the following relation:

$$d_A = \frac{\chi}{1+z} \ , \tag{1.36}$$

  where again we assumed flat space. Comparing with the definition of luminosity distance we have

$$d_A = \frac{d_L}{(1+z)^2} \ . \tag{1.37}$$

Horizons

Since the Universe has a finite age, the information we receive from the travelling radiation can come only from a finite volume of the entire Universe. This leads to the concept of *particle horizon* (or cosmological horizon), which is the distance travelled by a photon since the Big-Bang up to a certain time t; it is obtained, in comoving coordinates, from equation (1.31) by setting $t_{\rm em} = 0$ and $t_{\rm obs} = t$:

$$\chi_{\rm ph}(t) = \int_0^t \frac{{\rm d}t'}{a(t')} \ . \tag{1.38}$$

Since the speed of light is the upper limit velocity, this represents the maximum comoving distance any particle could have travelled up to the time t. If evaluated today, it gives the maximum extension of our past light cone and therefore the size of the observable Universe (for the ΛCDM model $\chi(t_0) \simeq 14000$ Mpc).

Another useful quantity is the *Hubble radius*, which is the physical distance travelled by light in a Hubble time H^{-1}. Its comoving definition is therefore[4]

$$L_H(t) = \frac{1}{a(t)H(t)} \ . \tag{1.39}$$

Conceptually, it is an horizon outside which objects recede from us faster than light[5] due to the relation $v = Hr$. If we consider a constant expansion, this would imply that objects outside the Hubble radius will never enter in causal contact with us; if instead the expansion slows down, an increasing number of objects will eventually enter the Hubble horizon, while the opposite situation occurs if the Universe experiences an accelerated expansion.

Finally, it is worth mentioning the *event horizon*, which is complementary to the particle horizon and defined as

$$\chi_e(t) = \int_t^{t_f} \frac{{\rm d}t'}{a(t')} \ , \tag{1.40}$$

where t_f is the final time for the Universe and $t_f = \infty$ in the case of infinite expansion. No signals can ever reach us in the future from an event which occur at time t and whose comoving distance is $\chi > \chi_e$.

1.2.3 Dynamics of the Universe

The dynamical evolution of the Universe is determined by the Einstein field equations (1.8). We have already constrained the form of the metric to be the FLRW one, thanks to

[4]Recall that $c = 1$, so the Hubble radius coincides with the Hubble time.

[5]This fact does not violate special relativity, since there is no information which really travel faster than light.

the assumptions of homogeneity and isotropy of space. We need then to specify possible expressions for the energy-momentum tensor $T_{\mu\nu}$ and finally put all together and solve for the unknown function $a(t)$.

The energy-momentum tensor

The cosmological principle forces the EMT to be the one of a *perfect fluid*,

$$T^{\mu\nu} = (\rho + P)U^\mu U^\nu + P g^{\mu\nu} \ , \tag{1.41}$$

where U^μ is the 4-velocity of the fluid relative to the observer, while $\rho = \rho(t)$ and $P = P(t)$ are the proper density and the proper pressure of the fluid, respectively. In the frame comoving with the observer, $U^\mu = (1, 0, 0, 0)$ and hence the EMT assumes the simple form:

$$T^{\mu\nu} = \begin{pmatrix} \rho & 0 \\ 0 & P g^{ij} \end{pmatrix} \quad \Rightarrow \quad T^\mu_\nu = \mathrm{diag}(-\rho, P, P, P) \ . \tag{1.42}$$

Assuming a perfect fluid and the FLRW metric, the 0-component of the conservation law (1.13) leads to the energy conservation equation

$$\dot\rho + 3\frac{\dot a}{a}(\rho + P) = 0 \ . \tag{1.43}$$

Cosmic fluids

In order to complete the information about the fluid, additionally to its EMT we need to specify an equation of state, that is $P = P(\rho)$. In the cosmological context, we assume an equation of state of the form $P = \omega\rho$, where ω is a constant. The equation (1.43) then becomes

$$\frac{\dot\rho}{\rho} = -3(1+\omega)\frac{\dot a}{a} \quad \Rightarrow \quad \rho \propto a^{-3(1+\omega)} \ . \tag{1.44}$$

The Universe is filled with a mixture of cosmic fluids. It is useful to consider three different cases, specified by different values of the parameter ω.

- *Matter* $\rightarrow$ $P = 0$ $\rightarrow$ $\omega = 0$.
  It comprises all forms of matter for which the pressure is negligible with respect to the energy density, which is the case of non-relativistic particles. Examples in our Universe are *Dark Matter* and *baryons*[6]. Setting $\omega = 0$, equation (1.44) becomes

  $$\rho_m \propto a^{-3} \ , \tag{1.45}$$

  that is, the energy density of matter just dilutes with the expansion of the Universe.

[6] In cosmology, the term *baryon* is (incorrectly) used to denote ordinary matter, although technically it is not always the case (electrons, for example, are leptons).

- *Radiation* $\rightarrow$ $P = \frac{1}{3}\rho$ $\rightarrow$ $\omega = \frac{1}{3}$.
  This is the case of a gas of relativistic particles[7], when the energy density is dominated by the kinetic energy. Examples in our Universe are *photons* and *neutrinos*. Setting $\omega = \frac{1}{3}$ in equation (1.44) gives

$$\rho_r \propto a^{-4} \ . \tag{1.46}$$

  The faster dilution of radiation with respect to matter is due to the redshifting of the energy, $E \propto a^{-1}$, according to (1.25).

- *Dark Energy* $\rightarrow$ $P = -\rho$ $\rightarrow$ $\omega = -1$.
  In order to explain the current acceleration of the expansion of our Universe, we need to hypothesize the existence of a component with a negative pressure, leading to an exotic equation of state never experienced in laboratory. A reasonable candidate comes from the quantum field theory as *vacuum energy*, although its predicted value is hugely distant from the observed one. Inserting $\omega = -1$ in the continuity equation gives

$$\rho_{de} \propto a^0 \ , \tag{1.47}$$

  which means that the energy density does not dilute with expansion.

Friedmann equations

We can now finally use the Einstein equations to determine how the scale factor evolves in time. Assuming the FLRW metric (1.19) and the energy-momentum tensor of a perfect fluid as in equation (1.41), the 00- and the ii- components of the Einstein equations (1.8) lead to the *Friedmann equations*:

$$\left(\frac{\dot{a}}{a}\right)^2 = \frac{8\pi G}{3}\rho - \frac{k}{a^2} \ , \tag{1.48}$$

$$\frac{\ddot{a}}{a} = -\frac{4\pi G}{3}(\rho + 3P) \ , \tag{1.49}$$

where now ρ and P are meant to be the sum of all contributions to the energy density and pressure we can have, that is $\rho = \sum_i \rho_i$ and $P = \sum_i P_i$ (with the subscript i we denote γ for photons, ν for neutrinos, c for cold dark matter, b for baryons and Λ for dark energy). The equation (1.49) is actually the truly dynamical equation for $a(t)$ (second order differential equation), whereas equation (1.48) acts as a constraint and sets the

[7] The reason why $\omega = \frac{1}{3}$ in the relativistic case can be seen by looking at the EMT of, for example, a plane wave moving along the x axis, which is $T^\mu_\nu = \mathrm{diag}(-E, P, 0, 0)$. The mass-shell condition ($E = P$) then implies that the trace T of the EMT vanishes and since the trace is invariant under rotations, this holds in every reference frame, that is $T = -\rho + 3P = 0$ and hence $P = \frac{1}{3}\rho$.

initial condition for $a(t_0)$ and $\dot{a}(t_0)$. Moreover, it is better to specify that the system is really closed if we include also the continuity equation (1.43).

Even without specifying an equation of state, it is however possible to understand some interesting feature of our Universe just looking at the Friedmann equations. For ordinary matter and radiation, the quantity $\rho + 3P$ is always positive and therefore $\ddot{a} < 0$, which means decelerating expansion. This is clearly in contrast with the current observation of an accelerating expansion, which then suggests that our Universe today must be dominated by some unknown component (Dark Energy) which satisfies $\rho + 3P < 0$. Furthermore, we know that $a > 0$ (by definition) and $\dot{a}/a > 0$ (since we observe redshifts). Thus, the function $a(t)$ must be concave downward and therefore it must have reached $a(\tilde{t}) = 0$ at some finite time $\tilde{t}$ in the past [92]. This the Big-Bang *singularity* problem: at this initial moment energy and pressure are predicted to be infinite and General Relativity stops working.

The first Friedmann equation (1.48) is usually written in terms of the Hubble parameter H as

$$H^2 = \frac{8\pi G}{3}\rho - \frac{k}{a^2} \ . \tag{1.50}$$

It is useful to define the *density parameter* of the i-th component as

$$\Omega_i \equiv \frac{\rho_i}{\rho_{\rm crit}} = \frac{8\pi G}{3H^2}\rho_i \ , \tag{1.51}$$

where $\rho_{\rm crit}$ is the critical density for which the Universe is flat, as one can see setting $\rho = \rho_{\rm crit}$ in equation (1.48) (it should be remarked that its value varies with time, as it depends on the Hubble parameter). The value of the total density parameter, $\Omega_{\rm tot} = \sum_i \Omega_i$, discriminates between an open ($\Omega_{\rm tot} < 1$), flat ($\Omega_{\rm tot} = 1$) and closed ($\Omega_{\rm tot} > 1$) Universe. Equation (1.50) can then be conveniently rewritten as

$$H^2(z) = H_0^2[\Omega_{r,0}(1+z)^4 + \Omega_{m,0}(1+z)^3 + \Omega_{k,0}(1+z)^2 + \Omega_{\Lambda,0}] \ , \tag{1.52}$$

where with the subscripts m and r we mean matter and radiation, respectively, while $\Omega_{k,0} \equiv -k/(a_0 H_0)^2$ accounts for the curvature contribution. The subscript 0 means instead that the quantities are evaluated today and from now on we will always use this notation.

Another useful way to express the Friedmann equations is to write them in conformal time. After having defined the conformal Hubble parameter $\mathcal{H} \equiv a'/a = aH$, equations (1.48) and (1.49) can take the following equivalent form:

$$\mathcal{H}^2 = \frac{8\pi G}{3}a^2\rho - k \ , \tag{1.53}$$

$$\mathcal{H}' = -\frac{4\pi G}{3}(\rho + 3P)a^2 \ . \tag{1.54}$$

1.3 Inflation

1.3.1 Problems of the Standard Big-Bang Theory

Despite its several successes, the Big-Bang theory as described so far is incomplete. It does not explain, for example, why we do not observe magnetic monopoles, why our Universe is incredibly close to be spatially flat and why the CMB radiation is isotropic on large scales with extremely tiny fluctuations.
Let us briefly discuss all of them.

- *The flatness problem.*
  Current observations [72] bound the Universe to be almost perfectly spatially flat. The coincidence of having zero curvature can be seen as a fine tuning in the standard cosmology. The Universe in fact does not naturally evolve towards a zero curvature and this condition must be verified already in its initial conditions. The problem can be better visualized by rewriting equation (1.50) in terms of the total density parameter $\Omega(t)$,

  $$\Omega(t) - 1 = \frac{k}{(aH)^2} \ . \tag{1.55}$$

  The value of Ω at the initial time t_i (denoted as Ω_i) is then

  $$\Omega_i - 1 = (\Omega_0 - 1)\frac{(a_0 H_0)^2}{(a_i H_i)^2} = (\Omega_0 - 1)\left(\frac{\dot{a}_0}{\dot{a}_i}\right)^2 \leq 10^{-60} \ , \tag{1.56}$$

  which means that, in order to have a current flatness of $\Omega_0 - 1 \leq 10^{-2}$, we need the primordial Universe to be flat with extremely high precision, leading to the fine tuning problem. We need therefore some mechanism which could have dynamically led the Universe to such condition in the early epochs.

- *The horizon problem.*
  The CMB radiation is observed to have a very isotropic temperature. The problem here is that the photons we receive from sufficiently distant portions of the sky were never in causal contact at the moment of photon decoupling, which is when the CMB photons scattered for the last time before reaching us. In other words, they could never have reached thermal equilibrium up to that moment, since the particle horizon at the time of decoupling was too small to allow it. The angle subtended in the sky by the comoving horizon at recombination is $\theta_{\rm hor} \simeq 1.15°$, so if two regions are separated by an angle greater than $2\theta_{\rm hor}$, in principle they should not emit CMB photons sharing the same temperature. Indeed, the CMB map is made of about 10^4 disconnected patches of space.

- *The monopole problem.*
  Grand Unified Theories (GUT), which try to govern the particle physics at extremely high energy ($\sim 10^{16}$ GeV) like in the very first moments of the Universe, predict the production of topological defects, like cosmic strings and magnetic monopoles. Their expected density is large, but we do not observe such things.

1.3.2 The inflationary solution

Shrinking the Hubble radius

The flatness and horizon problems are associated with the fact in the standard picture the comoving Hubble radius is an increasing function of time. In order to see this, let us suppose that the Universe is dominated by a single fluid with equation of state $P = \omega\rho$. Thus, the comoving Hubble radius becomes

$$(aH)^{-1} = H_0^{-1} a^{\frac{1}{2}(1+3\omega)} \tag{1.57}$$

As long as we deal with familiar matter content, we have that $1 + 3\omega > 0$ (it is known as strong energy condition, SEC) and therefore the comoving Hubble radius always increases with the expansion. It is useful to express the particle horizon χ in terms of $(aH)^{-1}$, as follows:

$$\chi_{\rm ph}(t) = \int_0^t \frac{{\rm d}t'}{a} = \int_{a_i}^a \frac{{\rm d}a}{a\dot{a}} = \int_{\ln a_i}^{\ln a} (aH)^{-1} {\rm d}\ln a \ . \tag{1.58}$$

Thus, we see that we can relate the causal structure to the comoving Hubble radius. Inserting (1.57) in (1.58), we obtain

$$\chi_{\rm ph}(a) = \frac{2}{H_0(1+3\omega)} \left[a^{\frac{1}{2}(1+3\omega)} - a_i^{\frac{1}{2}(1+3\omega)} \right] \equiv \tau - \tau_i \ . \tag{1.59}$$

Since approaching to the Big-Bang $a_i \to 0$ and also $\omega > -\frac{1}{3}$ assuming the SEC, we then have $\tau_i \to 0$.

A possible solution of these problems can therefore be quite straightforward: we may assume in the early Universe a sufficiently long period of *decreasing Hubble radius*, that is

$$\frac{d}{dt}(aH)^{-1} < 0 \ . \tag{1.60}$$

This physically means that during this phase the SEC must be violated. The initial conformal time τ_i is now pushed to negative values, $\tau_i \to -\infty$, meaning that $\tau = 0$ no longer coincides with the singularity anymore, rather it represents the transition between the shrinking Hubble radius period and the standard Big-Bang theory evolution. Violating SEC also means that, from equation (1.49), we have a period of accelerated expansion, during which initially causal connected regions got separated beyond the

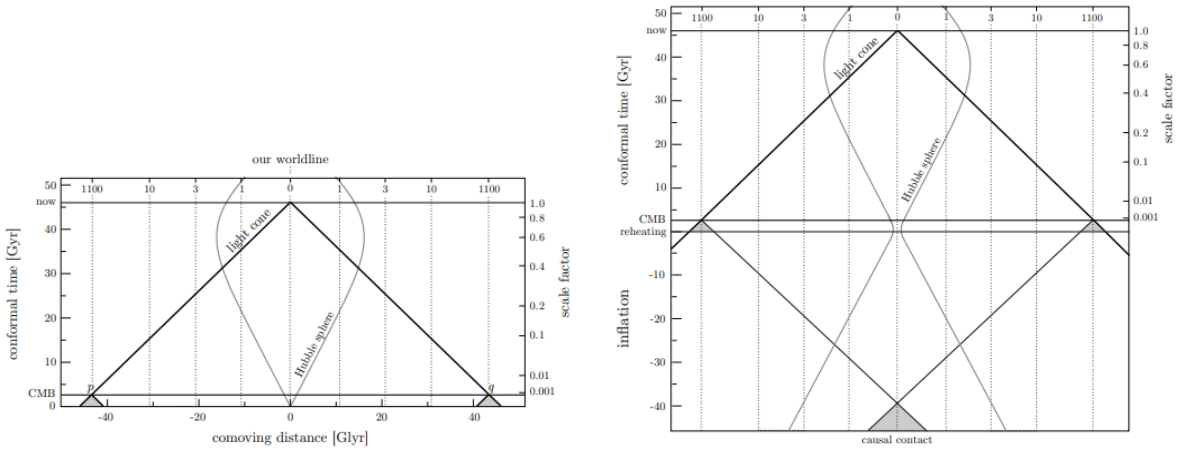

Figure 1.1: Schematic representations of the horizon problem in the standard Big-Bang model (*left*) and its solution with the inflationary mechanism (*right*), where now all CMB points have overlapping past light cones [6].

Hubble radius[8] and hence can now appear to be not in causal contact, although they were early on. This accelerated phase is called *inflation*.

Slow-roll inflation

As we have already seen, a period of accelerated expansion can be achieved by assuming a fluid with negative pressure. A simple toy model of inflation is given by a dynamical scalar field $\phi(x)$, called *inflaton*, associated with a potential energy density $V(\phi)$. This model, also known as *single-field inflation*, is just one of a broad collection of models that have been suggested so far, but it still represents a good candidate. We assume that during this phase the EMT of the inflaton dominates the Universe, so that it determines the evolution of the FLRW background.

The action of the scalar field minimally coupled to gravity is

$$S = \int \mathrm{d}^4x\sqrt{-g}\mathcal{L} = \int \mathrm{d}^4x\sqrt{-g}\left[-\frac{1}{2}\partial_\mu\phi\,\partial^\mu\phi - V(\phi)\right] . \tag{1.61}$$

The EMT of the field is

$$T_{\mu\nu} = -\partial_\mu\phi\,\partial_\nu\phi - g_{\mu\nu}\mathcal{L} . \tag{1.62}$$

Using the treatment of a perfect fluid, we can identify the energy density ρ_ϕ and pressure

[8] Using the Hubble radius to determine the causal region is just a more conservative way, since it is always smaller than the particle horizon.

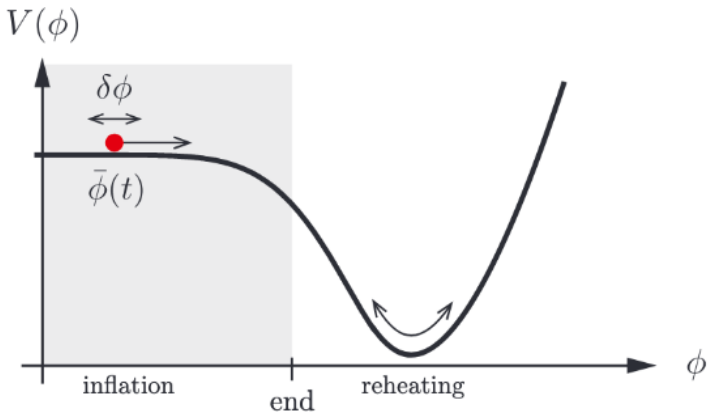

Figure 1.2: Example of a slow-roll potential. Inflation occurs in the shaded region [6].

P_ϕ of the field to be

$$\rho_\phi = \frac{1}{2}\dot{\phi}^2 + V(\phi) \ , \tag{1.63}$$

$$P_\phi = \frac{1}{2}\dot{\phi}^2 - V(\phi) \ , \tag{1.64}$$

where we are now assuming an homogeneous scalar field, $\phi = \phi(t)$, compatibly with the symmetries of the spacetime. The equation of state is then easily obtained:

$$\omega = \frac{P_\phi}{\rho_\phi} = \frac{\frac{1}{2}\dot{\phi}^2 - V(\phi)}{\frac{1}{2}\dot{\phi}^2 + V(\phi)} \ . \tag{1.65}$$

The Friedmann equation (1.50), trading the Newton constant G with the Planck mass $M_{\rm pl}$ ($G \equiv M_{\rm pl}^{-2}$) and setting $k = 0$, can be accordingly rewritten as

$$H^2 = \frac{8\pi}{3M_{\rm pl}^2}\left[\frac{1}{2}\dot{\phi} + V(\phi)\right] \ . \tag{1.66}$$

The dynamics of the inflaton is governed by the Klein-Gordon equation, that is

$$\ddot{\phi} + 3H\dot{\phi} + V_{,\phi} = 0 \ . \tag{1.67}$$

We note that the expansion of the Universe acts as a frictional force ($3H\dot{\phi}$) for the dynamics of the field.

Looking at the equation of state (1.65), we conclude that a scalar field can lead to an accelerated expansion ($\omega < -\frac{1}{3}$) if the potential energy dominates its kinetic energy, that is $\frac{1}{2}\dot{\phi}^2 \ll V$. This condition is called *first slow-roll condition* and leads to an equation of

state $P_\phi \simeq -\rho_\phi$, which causes the scale factor to grow exponentially, $a(t) \sim e^{Ht}$ (with H nearly constant). In order to solve the Big-Bang problems, we should also require that $|\ddot{\phi}| \ll |V_{,\phi}|$ (*second slow-roll condition*), which ensures that the slowly rolling of the scalar potential down its potential is maintained for a sufficient long period. The schematic behaviour is illustrated in Figure 1.2. Under these approximations, the Klein-Gordon (eq. (1.67)) and the Friedmann (eq. (1.66)) equations become

$$3H\dot{\phi} \simeq -V_{,\phi} \ , \tag{1.68}$$

$$H^2 \simeq \frac{8\pi}{3M_{\rm pl}^2} V(\phi) \ . \tag{1.69}$$

It is now useful to define the *potential slow-roll parameters* ϵ_V and η_V as follows:

$$\epsilon_V(\phi) \equiv \frac{M_{\rm pl}^2}{16\pi}\left(\frac{V_{,\phi}}{V}\right)^2 \ , \tag{1.70}$$

$$\eta_V(\phi) \equiv \frac{M_{\rm pl}^2}{8\pi}\frac{V_{,\phi\phi}}{V} \ . \tag{1.71}$$

The slow-roll conditions are then equivalent to requiring

$$\epsilon_V \ll 1 \ , \quad |\eta_V| \ll 1 \ . \tag{1.72}$$

Inflation ends when these conditions are violated, $\epsilon_V(\phi_{\rm end}) \approx 1$. It is customary to parametrize how much the scale factor grows during inflation in terms of the e-fold number N, which is

$$N \equiv \ln\frac{a(t_{\rm end})}{a(t_{\rm in})} = \int_{t_{\rm in}}^{t_{\rm end}} H\,{\rm d}t \simeq \frac{8\pi}{M_{\rm pl}^2}\int_{\phi_{\rm end}}^{\phi_{\rm in}} \frac{V}{V_{,\phi}}{\rm d}\phi \ , \tag{1.73}$$

where $t_{\rm in}$ and $t_{\rm end}$ denote the beginning and ending times of inflation, respectively. It can be shown that having $N \sim 60$ is enough to solve the aforementioned Big-Bang problems. In fact, the dramatic expansion during inflation led the density of magnetic monopoles to be diluted and hence hardly observable, while from equation (1.55) the exponential evolution of $a(t)$ makes the total density parameter Ω to be driven towards the unity, rather then away from it; finally, as we have already seen, the horizon problem is solved since regions which do not appear to be in causal connection today, actually were early on thanks to the shrinking Hubble radius during inflation.

Apart from solving these problems, inflation successfully provides a theory for the quantum generation of cosmological perturbations and hence for explaining the observed anisotropy in the CMB radiation. During inflation, quantum fluctuations of the field are generated on sub-Hubble scales, $\phi(t,\mathbf{x}) = \bar{\phi}(t) + \delta\phi(t,\mathbf{x})$, and their scales are then stretched out of the Hubble radius by the exponential expansion. Once they cross it, these

fluctuations become classical density perturbations, which eventually re-enter the Hubble radius during the standard evolution after the end of inflation and subsequently provide the seeds of cosmic structures. CMB gives us a snapshot of these primordial fluctuations at the time of photon decoupling and hence it represents a powerful instrument to validate or rule out possible models of inflation.

The statistical properties of these primordial fluctuations are encoded into the *primordial power spectrum*, which is the variance of the fluctuations in Fourier space. Instead of $\delta\phi$, it is more useful to use the *primordial curvature perturbation* $\mathcal{R}$, which has the property to be constant on super-Hubble scales for adiabatic perturbations (we will explain what adiabatic perturbations are in Chapter 2) and it is related to $\delta\phi$ by $\mathcal{R} = -H\delta\phi/\dot{\bar{\phi}}$. The power spectrum is parametrized as follows

$$\mathcal{P}_{\mathcal{R}}(k) = A_{\rm s}\left(\frac{k}{k_*}\right)^{n_{\rm s}-1}, \tag{1.74}$$

where $k = 2\pi/\lambda$ (with λ the comoving scale of the perturbation in real space) and k_* is a reference scale. Since different scales exit at different times with almost the same values of the potential $V(\phi)$, we expect a nearly scale invariant spectrum with an index that is slightly less than one to account for the end of inflation. This prediction has been verified to great accuracy by current CMB data [72]. The amplitude $A_{\rm s}$ instead is not predicted by the model and therefore we need to constrain it with observations.

When the inflation ends, a very complex process called *reheating* starts to produce Standard Model particles and the Universe as we know it today can begin its standard thermal evolution.

1.4 Thermal history of the Universe

The evolution of the Universe can be briefly summarized as a cooling history. At the earliest time, right after inflation and reheating, the Universe was in a hot and dense state and filled with a plasma of relativistic particles, including quarks, leptons, gauge bosons and Higgs bosons. In this period, its thermodynamical behavior was characterized by thermal equilibrium[9] However, departures from equilibrium are what really determine the key aspects of the evolution of the Universe and lead to what we observe today. Non-equilibrium dynamics, for example, is responsible for the acquisition of cosmological abundances from massive particles, for the origin of the CMB and for the formation of the light chemical elements.

[9]Rigorously, it is not possible for the Universe to be in thermal equilibrium, since the FLRW metric does not possess a timelike Killing vector. However, to a good approximation, we can state that the Universe evolved through a succession of nearly thermal states, with the temperature decreasing as a^{-1} [46].

A schematic way to understand the thermal evolution of the Universe is to compare the *rate of interactions* Γ with the *rate of expansion* H. In fact, while thermal equilibrium is kept by the interactions between particles, the expansion of the Universe makes the plasma more the diluted and hence interactions become progressively rarer. When $\Gamma \gg H$, interactions are efficient enough to keep the considered particles in thermal equilibrium; at $\Gamma \sim H$ [10], instead, the particles decouple from the thermal bath and evolve independently.

Let us now list the key events of the thermal history of the Universe [6].

- *Baryogenesis.*
  Since we currently observe an overabundance of matter over anti-matter, there must have been in the very early Universe some primordial matter-antimatter asymmetry, without which the annihilation processes would have led the overall baryon number to be zero. Models of baryogenesis try to explain such discrepancy in a dynamical way, *i.e.* without setting this primordial asymmetry as an arbitrary initial condition.

- *Electroweak phase transition.*
  At $\sim$ 100 GeV some of the gauge bosons and other particles acquire mass via the Higgs mechanism. This leads to a dramatic change in the strength of weak interactions.

- *QCD phase transition.*
  At $\sim$ 150 MeV, strong interactions between quarks and gluons become important and lead to the formation of color-singlet quark-triplet states (*baryons*) and color-singlet quark-antiquark states (*mesons*).

- *Dark Matter decoupling.*
  If DM is described by some form of particle, we expect that it decouples from the thermal bath very early on, since it interacts very weakly with the other Standard Model particles. For example, the WIMP (Weakly Interacting Massive Particle), which is a strong candidate for DM, decouples at around 1 MeV.

- *Neutrino decoupling.*
  Neutrinos are kept in equilibrium with the plasma only via weak interactions. Their decoupling occur at $\sim$ 0.8 MeV.

- *Electron-positron annihilation.*
  Shortly after neutrino decoupling, the annihilation between electrons and positrons takes place. The entropy in $e^{\pm}$ pairs is then transferred to the photons but not to

[10] This is just a rough criterion, the rigorous approach to evolve particle distributions out of equilibrium is to integrate the Boltzmann equation (its perturbed version will be extensively used in Chapter 2).

the neutrinos, which are already decoupled [11]. This is the reason why the photon temperature we measure today is greater than the neutrino one by a factor 1.4.

- *Big-Bang nucleosynthesis.*
  At ~ 100 KeV (about 3 minutes after the Big-Bang) the light elements were formed. The verification of its accurate predictions is considered one of the three main pillars of the original Big-Bang theory together with the Universe expansion and the CMB.

- *Matter-radiation equality.*
  At $z \sim 3400$ (after about 60 kyr since Big-Bang), the matter contribution becomes equal to that of the radiation, marking the end of the radiation-dominated era and the beginning of the matter-dominated one.

- *Recombination.*
  At $z \sim 1100$, electrons and protons start to combine and form hydrogen atoms, through the process $e^- + p^+ \rightarrow H + \gamma$; this happens because the temperature has become low enough and the efficiency of the reverse reaction is no longer high enough to keep the hydrogen ionized.

- *Photon decoupling.*
  With recombination, the fraction of free electrons drops and hence the Thomson scattering $e^- + \gamma \rightarrow e^- + \gamma$, which is the dominant process which was keeping electrons and photons in equilibrium so far, becomes inefficient. Thus, photons decouple and start to stream freely through the Universe; they constitute today the cosmic microwave background, with a temperature of $T = 2.725 \pm 0.001$ K.

1.5 ΛCDM model

Through observations we are able to constrain the free parameters of the theory. A remarkable feature of our Universe is that the density parameters sum up extremely closely to 1, that is $\Omega_{\rm tot} \simeq 1$ and then $\Omega_k \simeq 0$ (it represents less than 1% of the cosmic energy budget). This corresponds to having a current energy density almost equal to the critical one, which is $\rho_{\rm crit} \simeq 1.9 \times 10^{-26} h^2 \text{kg m}^{-3}$. In particular, the main contributions to the energy density today in the Universe come from matter and Dark Energy [72],

$$\Omega_m = 0.3153 \pm 0.0073 \ , \quad \Omega_\Lambda = 0.6847 \pm 0.0073 \ , \tag{1.75}$$

whereas the radiation contribution, $\Omega_r = \Omega_\gamma + \Omega_\nu \simeq 9.4 \times 10^{-5}$, is almost negligible. These relative abundances can be understood by simply looking at how densities of

[11] The duration of the neutrino decoupling causes the effective number of neutrinos to be predicted 3.046, instead of 3.

each species change with the expansion, as shown in equations (1.45), (1.46) and (1.47). In fact, we have that radiation dilutes faster than matter, which in turn dilutes faster than the DE, leading to a current Universe where the radiation contribution has become completely negligible compared to the other two components. At the same time, this also means that in the past, at redshift higher than some critical value ($z \sim 0.7$), matter was dominating over both radiation and DE, and going further back in time, before what is called matter-radiation equality ($z_{\rm eq} \sim 3400$), the Universe was in a radiation dominated era.

We have already seen that the matter contribution comes not only from ordinary matter, but also from Dark Matter, that is $\Omega_m = \Omega_b + \Omega_c$. In particular, $\Omega_b h^2 \sim 0.022$ and $\Omega_c h^2 \sim 0.12$, so DM is actually the dominant contribution for matter [72].

CMB observations at large scales help also to obtain information about the inflationary mechanism. The current values of the amplitude and the spectral index of the primordial power spectrum obtained by Planck are $A_{\rm s} = (2.100 \pm 0.030) \times 10^{-9}$ and $n_{\rm s} = 0.9649 \pm 0.0042$ [72].

The concordance cosmological model which accounts for a cosmological constant (Λ), cold Dark Matter (CDM) and a period of accelerated expansion (inflation) before the usual thermal evolution of the Universe is therefore called ΛCDM.

1.5.1 Dark Energy

An exotic component with negative pressure is necessary to motivate the current accelerated expansion of the Universe. It is mathematically modelled by introducing a cosmological constant Λ in the Einstein field equations. This approach was already proposed by Einstein himself but for a completely different purpose, that was to avoid the dynamical behaviour predicted by his equations and achieve a static Universe. The Einstein field equations with cosmological constant take the following form:

$$R_{\mu\nu} - \frac{1}{2} g_{\mu\nu} R - \Lambda g_{\mu\nu} = 8\pi G T_{\mu\nu} \ . \tag{1.76}$$

The idea of a static Universe lost its reliability after the discovery of the expansion of the Universe by Hubble and the use of the cosmological constant was soon abandoned. The subsequent observation of an accelerating expansion in 1998, however, made the introduction of the cosmological constant in the Einstein equations again necessary, since models without Λ do never predict an acceleration. The nature of this new component, commonly called *Dark Energy*, is one of the biggest open question in modern cosmology. A possibility (proposed for the first time by Lemaitre [50] and Eddington [22]), is that Dark Energy comes from the vacuum energy density, which is a prediction of quantum physics. However, its predicted value from the Standard Model of particle physics is much larger than the one actually observed in the Universe, and this is why possible extensions of the underlying theory or other candidates (like the quintessence, a scalar

field which could drive the accelerated expansion in a similar way of the inflaton during inflation) are often considered.

1.5.2 Dark Matter

The existence of a form of matter which interact only gravitationally with the other species and which therefore cannot be directly seen is one of the pillars of the ΛCDM model. The first robust evidence of "missing" non visible matter in our Universe (Dark Matter) comes from the observation of rotation curves of spiral galaxies, which can be theoretically explained only by assuming additional matter content in them. The presence of DM is further corroborated by several other astrophysical and cosmological data, like gravitational lensing of galaxy clusters, CMB radiation and structure formation. In particular, Dark Matter plays a crucial role in the formation of the large scale structures, whose observation strongly suggests a *cold* nature of DM (hence the name Cold Dark Matter, CDM), *i.e.* DM is dominated by non-relativistic matter.

One of the most reliable DM candidates is represented by WIMPs (Weakly-Interacting Massive Particles), hypothetical particles with masses of ~ 100 GeV which interact only through weak interactions and gravity with other species. Such particles naturally arise from supersymmetric extensions of the Standard Model of particle physics with properties (mass and cross section) which would lead to the observed relic abundance of DM (*WIMP miracle*). There are however several other candidates which span a wide range of masses, from light bosons (like axions or axion-like particles) to composite objects like the so-called massive compact halo objects (MaCHOs) or even primordial black holes.

Chapter 2

Cosmological Perturbation Theory

In the previous chapter, the basic assumption of all the discussion was the cosmological principle, that is homogeneity and isotropy of the Universe. However, what we observe around us is far from being homogeneous and isotropic, at least at enough small scales: it is sufficient to think of the distribution of galaxies, which shows a clustering behaviour at scales of tens of Mpc, or even of the CMB, whose direction-dependent fluctuations in temperature, even if tiny, are still a violation of perfect isotropy. We have already mentioned that the inflationary mechanism offers an elegant way to produce these perturbations from quantum fluctuations of the inflaton field, thus providing the seed for the observed CMB anisotropies and the formation of structures. How these perturbations evolve during the expansion of the Universe will be the topic of this chapter.

The standard approach is to split the description of the Universe in two sectors:

- an *homogeneous background*, which is described by the FLRW metric and evolves through the Friedmann equations, as discussed in Chapter 1;
- *small space-dependent perturbations*, whose evolution is governed by the perturbed Einstein and Boltzmann equations expanded around the homogeneous solution.

The assumption of *small* perturbations allows us to work within the framework of *perturbation theory*, which means that it will be possible to expand the equations of interest and eventually truncate the expansion at an arbitrary level of accuracy. The fact that the CMB map deviates from being perfectly isotropic by just a tiny amount ($\sim 10^{-5}$) permits, for most of the purposes, to stop the analysis at first order in perturbation theory, *i.e.* to work with the linearized versions of the Einstein and Boltzmann equations, thus simplifying (and not just a little) the mathematical treatment. It is however important to specify, especially for the purpose of this thesis, that the complete description and the associated predictions for cosmological observables of many cosmological effects requires to go beyond the linear order approximation. An example related to the topic of work is the generation of primordial magnetic fields by second order perturbations at

recombination, while other cases involve for example models of non-Gaussian signatures on the CMB. The direct way to perform a non-linear analysis is to go to second order perturbation theory, which is the approach we actually used in this work to study the impact of primordial magnetic fields into the CMB.

Generally, a perturbation has the tendency to grow and possibly collapse if the gravitational force exceeds the opposing pressure one. As dark matter perturbations start growing at early times after equivalence, baryons and photons remain tightly coupled until recombination, leading to a later start of the growth for baryons whereas photons free-streams after decoupling. After recombination both dark matter and baryon perturbations can grow and therefore we must consider the possibility for a perturbation to grow enough to start the gravitational collapse and subsequently form the structures we observe today. The critical scale over which a perturbation can collapse is called *Jeans scale*; below such scale, the perturbation does not grow but propagates through the Universe as an oscillating wave. When the gravitational collapse occurs, the perturbation can no longer be considered small and we enter in a full non-linear regime that requires full N-body simulations to be predicted. For the CMB case we are far from the gravitational collapse and we can assume a linear regime with a second order modelling of the interested effects.

In this chapter we will focus only on the linear theory and we will develop all the equations up to first order in the cosmological perturbations. The second order formalism and equations will be explored instead in Chapter 4. The main reference, especially for the used notation, is [70], which also gives the formalism and equations used in the numerical code SONG.

Notations

In this thesis, our notation for the Fourier transform is

$$\begin{aligned} Y(\mathbf{k},t) &= \int \mathrm{d}^3x\, e^{-i\mathbf{k}\cdot\mathbf{x}}\, Y(\mathbf{x},t)\ , \\ Y(\mathbf{x},t) &= \int \frac{\mathrm{d}^3k}{(2\pi)^3}\, e^{i\mathbf{k}\cdot\mathbf{x}}\, Y(\mathbf{k},t)\ , \end{aligned} \tag{2.1}$$

where Y is a generic function. We also consider the standard convention in which $a(t_0) = 1$, where t_0 is the present time.

2.1 Formalism of perturbation theory

Let us now briefly review the basic formalism of perturbation theory. If we have a cosmological field $X(t, \mathbf{x})$, its perturbative expansion reads

$$X(t, \mathbf{x}) = X^{(0)}(t) + \sum_{n=1}^{\infty} \epsilon^n X^{(n)}(t, \mathbf{x}) \ , \tag{2.2}$$

where we used ϵ as expansion parameter, while $X^{(n)}$ denotes the n-th order of perturbation of X. Note that the background value, $X^{(0)}$, depends only on time, since for our assumption the background cosmology relies on cosmological principle and hence a dependence on the position would violate homogeneity. Moreover, isotropy prevents $X^{(0)}$ to be a 3-vector, hence all velocity fields, for example, must have a vanishing background value. The inhomogeneous contribution is entirely given by the perturbation part, which by definition is what produces the deviation from the cosmological principle.

We have already mentioned that, since the temperature fluctuations of the CMB are really small ($\sim 10^{-5}$), stopping the perturbative expansion to the first order is an excellent approximation, at least for most of the purposes. Thus, we can simply write

$$X(t, \mathbf{x}) \simeq X^{(0)}(t) + \epsilon\, X^{(1)}(t, \mathbf{x}) \ . \tag{2.3}$$

From now on, in order to make the expressions more readable, we will absorb the expansion parameter in the definition of perturbative variable $X^{(n)}$, that is $\epsilon^n X^{(n)} \to X^{(n)}$. Moreover, we will often avoid to explicitly specify the perturbative order in our expressions, since in this chapter we will only keep linear terms.

A generic function of X can be Taylor expanded around $X^{(0)} \equiv \bar{X}$ as

$$f(X) = f(\bar{X}) + \sum_{n=1}^{\infty} \frac{1}{n!} \left(\frac{\partial^n f}{\partial X^n} \right)_{\bar{X}} (X - \bar{X})^n \ . \tag{2.4}$$

Up to linear order, further expanding $X \simeq X^{(0)} + X^{(1)}$, we can split $f(X)$ into its background and linear part as follows:

$$f(X)^{(0)} = f(\bar{X}) \ , \quad f(X)^{(1)} = \left(\frac{\partial f}{\partial X} \right)_{\bar{X}} X^{(1)} \ . \tag{2.5}$$

This perturbative approach allows us to conveniently split and solve the equations order by order. In particular, an equation for the n-th order is solved using the solutions for all the preceding orders. So, for example, if we want to stop at linear order and so we consider only the background and first order equations (or linearized equations), we do not need any information about higher-order equations. Hence, up to linear order, which is what we consider in this chapter, the linearized Einstein and Boltzmann equations, together with suitable initial conditions, are all we need in order to determine the evolution of the first-order cosmological perturbations.

2.2 Perturbations to the FLRW metric

The starting point is to perturb the FLRW metric $g^{(0)}_{\mu\nu}$ with small perturbations $\delta g_{\mu\nu}$ and so to write $g_{\mu\nu} = g^{(0)}_{\mu\nu} + \delta g_{\mu\nu}$. The general parametrization of the perturbed metric, in the flat case ($k = 0$) and in conformal time, is the following:

$$ds^2 = a^2(\tau)\big\{-(1+2\Psi)d\tau^2 + 2\omega_i dx^i d\tau + [(1-2\Phi)\delta_{ij} + 2\gamma_{ij}]dx^i dx^j\big\}\ , \tag{2.6}$$

where Ψ, Φ, ω^i and γ_{ij} are the metric perturbations with vanishing background. We note that, setting them to zero, we just recover the unperturbed FLRW metric, as expected. The perturbed variables contain 10 degrees of freedom, compatibly with a spacetime symmetric tensor: Ψ and Φ are scalars $(1+1)$, w^i is a 3-vector (3) and γ_{ij} is, by construction, a symmetric and traceless tensor (5), hence giving $1+1+3+5 = 10$ degrees of freedom (which can be reduced to 6 by performing a gauge fixing, as we will see later).

2.2.1 Scalar-Vector-Tensor decomposition

These 10 independent components of the perturbations to the metric are conveniently decomposed into scalar, vector and tensor (SVT) parts. The main advantage of this procedure is that, at linear order, scalar, vector and tensor perturbations evolve independently, which means that we will be able to decouple the Einstein and Boltzmann equations for these three kind of perturbations without any mixing. It is important to remark, however, that this property holds only at first order, while for second and higher orders different types of perturbations can source each other due to the presence of quadratic terms. We will better explore this issue in Chapter 4.

Given a generic spacetime tensor T, a first guess could be to think at T_{00}, T_{0i} and T_{ij} as its scalar, vector and tensor part, respectively. In fact, under a spatial coordinate transformation $x^i \to x'^i = x'^i(x^j)$, one has that T_{00} transforms as a scalar, T_{0i} as a 3-vector, while T_{ij} transforms as a 3-tensor. This decomposition is however not complete, since T_{0i} contains both scalar and vector degrees of freedom, while T_{ij} is a mixture of all the three types.

In order to extract the SVT degrees of freedom out of them, we introduce the projecting vectors $\xi^i_{[m]}$ and matrices $\chi^{ij}_{2,[m]}$, whose explicit expressions are found in Appendix B. The former, contracted with T_{0i}, gives its scalar ($m = 0$) and vector ($m = \pm 1$) component, while the latter, contracted with T_{ij}, yields its scalar ($m = 0$), vector ($m = \pm 1$) and tensor ($m = \pm 2$) component. The remaining scalar part of T_{ij} is given by its trace,

$\delta^i{}_j T_{ij}/3$. Summing up, we have

$$\begin{aligned}
&\text{Scalar } (m=0) \quad &\Longleftrightarrow \quad &\chi^{ij}_{2,[0]} T_{ij} \ , \quad \xi^i_{[0]} T_{i0} \ , \quad \delta^i{}_j T_{ij}/3 \ , \quad T_{00} \ . \\
&\text{Vector } (m=\pm 1) \quad &\Longleftrightarrow \quad &\chi^{ij}_{2,[\pm 1]} T_{ij} \ , \quad \xi^i_{[\pm 1]} T_{i0} \ . \\
&\text{Tensor } (m=\pm 2) \quad &\Longleftrightarrow \quad &\chi^{ij}_{2,[\pm 2]} T_{ij} \ .
\end{aligned}$$

It leads to 4 scalar, 4 vector and 2 tensor components of T; they are also known as *azimuthal modes*.

Within this formalism, the SVT decomposition of the metric is then the following:

- $\{\Psi, \Phi, \omega_{[0]}, \gamma_{[0]}\}$ are the 4 *scalar* components;
- $\{\omega_{[\pm 1]}, \gamma_{[\pm 1]}\}$ are the 4 *vector* components;
- $\{\gamma_{[\pm 2]}\}$ are the 2 *tensor* components;

where $\omega_{[m]} \equiv \xi^i_{[m]} g_{i0}$ and $\gamma_{[m]} \equiv \chi^{ij}_{2,[m]} g_{ij}$.

2.2.2 Gauge fixing

The use of General Relativity as the mathematical framework of the theory leads to the issue of gauge freedom. This means that the metric can undergo an infinitesimal coordinate transformation and still be a solution of the same Einstein equations.

In order to better visualize this issue, let us consider a general coordinate transformation from a coordinate system x^μ to another $\tilde{x}^\mu$ as follows [54]:

$$x^\mu \to \tilde{x}^\mu = x^\mu + d^\mu(x^\nu) \ , \tag{2.7}$$

where we write the time and spatial parts of d^μ as

$$\begin{aligned}
d^0 &= \alpha(x^\nu) \ , \\
d^i &= \partial^i \beta(x^\nu) + \epsilon^i(x^\nu) \ ,
\end{aligned} \tag{2.8}$$

with $\partial^i \beta$ being the longitudinal component ($\epsilon_{ijk} \partial^j \partial^k \beta = 0$) and ϵ^i the transverse one ($\partial_i \epsilon^i = 0$). Requiring the invariant line element ds^2 to remain untouched under this coordinate transformation leads to

$$\tilde{g}_{\mu\nu}(x) = g_{\mu\nu}(x) - g_{\mu\beta}(x) \partial_\nu d^\beta - g_{\alpha\nu}(x) \partial_\mu d^\alpha - d^\alpha \partial_\alpha g_{\mu\nu}(x) + \mathcal{O}(d^2) \ , \tag{2.9}$$

where both the right and the left hand side are evaluated at the same spacetime point x. If we consider d^μ to be of the same order as the metric perturbations Ψ, Φ, ω_i and γ_{ij},

from the transformation (2.9) we can find the relations between the metric perturbations in the two coordinate systems, as follows

$$\begin{aligned}
\tilde{\Psi}(x) &= \Psi - \alpha'(x) - \mathcal{H}\alpha(x) \ , \\
\tilde{\Phi}(x) &= \Phi(x) + \frac{1}{3}\partial_i\partial^i\beta(x) + \mathcal{H}\alpha(x) \ , \\
\tilde{\omega}_i(x) &= \omega_i(x) + \partial_i\alpha(x) - \partial_i\beta'(x) - \epsilon_i'(x) \ , \\
\tilde{\gamma}_{ij}(x) &= \gamma_{ij}(x) - \left[\left(\partial_i\partial_j - \frac{1}{3}\delta_{ij}\partial_k\partial^k\right)\beta(x) + \frac{1}{2}(\partial_i\epsilon_j + \partial_j\epsilon_i)\right] \ .
\end{aligned} \tag{2.10}$$

Hence, under a general infinitesimal coordinate transformation, we obtain a new set of metric perturbations, which is mathematically different from the old one but physically equivalent (*i.e.* the Einstein equations are still solved). It is clear then that the metric perturbations are gauge dependent and we need therefore to perform a gauge fixing. Although all the gauges are equivalent, one particular gauge might be better then another one from a practical point of view, possibly making the computations more manageable or some physical property more manifest.

A multitude of gauges has been proposed in the last decades for the study of cosmological perturbations. Surely, the most popular and used gauges in this context are the *Newtonian* gauge and the *Synchronous* gauge.

The Newtonian gauge (also known as Poisson or longitudinal gauge) is defined by the conditions that both g_{0i} and g_{ij} are transverse, that is, in terms of the metric variables,

$$\partial^i\omega_i = 0 \ , \quad \partial^j\gamma_{ij} = 0 \ . \tag{2.11}$$

In Fourier space, for $\mathbf{k}$ aligned with the polar axis, these conditions are equivalent to $\omega_{[0]} = 0$ and $\gamma_{[0]} = \gamma_{[\pm1]} = 0$. So, in the Newtonian gauge, we have in total 6 degrees of freedom, that is two scalar potentials (Ψ and Φ), one transverse vector potential (ω) and one transverse-traceless tensor potential (γ). A restricted version of this gauge is obtained by setting $\omega_i = \gamma_{ij} = 0$, which means that only the two scalar degrees of freedom are present. This restriction can be safely applied at linear order, but in a non-linear analysis one should be careful, since vector and tensor modes can be induced even if they initially vanish.

The synchronous gauge is instead obtained by confining all the perturbations to the spatial part of the metric, that is

$$\Psi = 0 \ , \quad \omega_i = 0 \ . \tag{2.12}$$

Although it is vastly used in literature, this choice may lead to two main problems. First of all, these conditions do not fix the gauge freedom completely and lead to the appearance of spurious gauge modes in the solutions to the equations for the density perturbations. Moreover, this gauge produces a more complicated angular dependence

in the Boltzmann equation at second order, leading to cubic and quartic terms in the photon direction [70]. For these reasons, in this thesis we will focus on the Newtonian gauge, which is also the gauge used in SONG.

2.3 The linearized Einstein equations

We can now write the linearized Einstein equations in Fourier space. They are expressed as

$$\delta G^{\mu}{}_{\nu} = 8\pi G\, \delta T^{\mu}{}_{\nu} \ . \tag{2.13}$$

Using the same formalism introduced in Sec. 2.2.1, we project the Einstein equations in its scalar, vector and tensor components, thus obtaining

$$\begin{aligned}
&\text{Time-time} && \iff && \delta G^{0}{}_{0} = 8\pi G\, \delta T^{0}{}_{0} \\
&\text{Trace} && \iff && \delta G^{i}{}_{i} = 8\pi G\, \delta T^{i}{}_{i} \\
&\text{Space-time} && \iff && i\xi^{i}_{[m]} \delta G_{i0} = 8\pi G\, i\xi^{i}_{[m]} \delta T_{i0} \\
&\text{Space-space} && \iff && \chi^{ij}_{2,[m]} \delta G_{ij} = 8\pi G\, \chi^{ij}_{2,[m]} \delta T_{ij}
\end{aligned}$$

We should underline the fact that the spatial indices refer to the up-down version of the Einstein equations, as in equation (2.13), hence, for example, T_{ij} is the spatial part of $T^{\mu}{}_{\nu}$ and not $T_{\mu\nu}$. We see that, while the time-time and trace equations each contain only 1 scalar degrees of freedom, the space-time one describes both scalar and vector degrees of freedom (1 and 2 respectively), while the space-space equation contains all the three types (1 scalar, 2 vectors and 2 tensors). In what follows, we neglect the first-order vector and tensor perturbations and let them contribute only from second order on. It is a safe approximation, since vector perturbations are rapidly redshifted with expansion, while tensor ones survive in small part only on large scales (moreover, the decoupling of modes at linear order guarantees that neither vectors nor tensors are sourced by scalar perturbations). Hence, at linear order we need to evolve just Ψ and Φ.

Let us now look at the energy-momentum tensor. It can be parametrized as the one of a fluid with energy density ρ, pressure P and 4-velocity U^{μ}, that is

$$T^{\mu}{}_{\nu} = (\rho + P) U^{\mu} U_{\nu} + \delta^{\mu}{}_{\nu} P + \Sigma^{\mu}{}_{\nu} \ . \tag{2.14}$$

$\Sigma^{\mu}{}_{\nu}$ is the anisotropic stress tensor, a symmetric and traceless tensor which quantifies the deviation of the fluid from being perfect. At background level it is zero, but at first order it can have a non-vanishing contribution mostly from neutrinos. Denoting the density and pressure perturbations as $\delta\rho$ and δP and their background values as $\bar{\rho}$ and $\bar{P}$, we

can expand the EMT up to first order as follows:

$$\begin{aligned} T^0{}_0 &= -(\bar{\rho} + \delta\rho) \ , \\ T^i{}_0 &= -(\bar{\rho} + \bar{P})V^i = -T^0{}_i \ , \\ T^i{}_j &= (\bar{P} + \delta P)\delta^i{}_j + \Sigma^i{}_j \ , \end{aligned} \tag{2.15}$$

where we have defined $V^i \equiv a\, U^i$.

The last step to obtain the Einstein equations is then to decompose the EMT via the usual SVT decomposition, which gives

$$\begin{aligned} T^0{}_0 &= -(\bar{\rho} + \delta\rho) \ , \\ T^i{}_i &= 3(\bar{P} + \delta P) \ , \\ \xi^i_{[m]} T_{i0} &= -(\bar{\rho} + \bar{P})V_{[m]} \\ \chi^{ij}_{2,[m]} T_{ij} &= \Sigma_{[m]} \ , \end{aligned} \tag{2.16}$$

where $V_{[m]} = \xi^i_{[m]} V_i$ and $\Sigma_{[m]} = \chi^{ij}_{2,[m]} \Sigma_{ij}$.

Finally, we can write the scalar Einstein equations at linear order and projected in Fourier space.

- Time-time equation:

$$6\mathcal{H}^2\Psi + 6\mathcal{H}\,\Phi' + 2k^2\Phi = 8\pi G a^2\, \delta T^0{}_0 \ . \tag{2.17}$$

- Trace equation:

$$6\ddot{\Phi} + \Psi(6\mathcal{H}^2 + 12\dot{\mathcal{H}}) + 6\mathcal{H}(\dot{\Psi} + 2\dot{\Phi}) + 2k^2(\Phi - \Psi) = 8\pi G a^2\, \delta T^i{}_i \ . \tag{2.18}$$

- Space-time equations:

$$-2k(\dot{\Phi} + \mathcal{H}\Psi) = 8\pi G a^2\, (i\xi^i_{[0]} \delta T_{i0}) \ . \tag{2.19}$$

- Space-space equations:

$$-\frac{2k^2}{3}(\Phi - \Psi) = 8\pi G a^2\, (\chi^{ij}_{2,[0]} T_{ij}) \ . \tag{2.20}$$

Let us make some final comments. The EMT in the right hand sides of each equation is meant to be the sum of the EMTs of each species, that is photons, neutrinos, baryons and cold dark matter. Moreover, the scalar space-space equation (2.20) together with the last of equations (2.16) tell us that, in absence of anisotropic stresses, Ψ and Φ coincide: $\Phi = \Psi$. The four scalar equations are easily comparable with equations (23a) to (23d) in [54].

2.4 The linearized Boltzmann equation

The Einstein equations alone are not sufficient and have to be complemented by a model which determines the form and the evolution of the energy-momentum tensor. The conservation equation (1.13) is valid only for a single uncoupled fluid (or for the total fluid). However, in a multispecies environment as the cosmological plasma we have to consider also possible interactions and hence we must follow a more complex approach.

The systematic way to deal with interactions is to work with the Boltzmann equation for each species. Within this formalism, the key object to work with is the *phase-space distribution function*, $f(\tau, \mathbf{x}, \mathbf{P})$, which is defined so that the quantity

$$\mathrm{d}N = f(\tau, \mathbf{x}, \mathbf{P})\, \mathrm{d}\mathbf{x}\, \mathrm{d}\mathbf{P} \tag{2.21}$$

represents, for an observer at $(\tau, \mathbf{x})$ and in a local inertial frame, the average number of particles in the volume element $\mathrm{d}\mathbf{x}\, \mathrm{d}\mathbf{P}$ around the point $(\mathbf{x}, \mathbf{P})$ in phase space. Note that this is a statistical approach: instead of dealing with the evolution of each individual particle, the focus is on the probability distribution in phase space and the key observables, like number density or energy of the system, are obtained by just integrating over the distribution function. The general expression which relates the energy-momentum tensor with the distribution function is

$$T_{\mu\nu} = \int \sqrt{-g}\, \mathrm{d}P_1\, \mathrm{d}P_2\, \mathrm{d}P_3\, \frac{P_\mu P_\nu}{P^0}\, f(\tau, \mathbf{x}, \mathbf{P}) \ . \tag{2.22}$$

The role of the Boltzmann equation is to determine how the distribution function of a given interacting species evolves. It takes the form

$$\frac{\mathrm{d}f}{\mathrm{d}\tau} = \mathcal{C}[f] \ , \tag{2.23}$$

where $\mathrm{d}f/\mathrm{d}\tau$ is the *Liouville term* and $\mathcal{C}[f]$ is the *collision term* and it is where all the complexity of the quantum field theory for particle physics enters.

In what follows, we assume to work in a local inertial frame, since the cross section appearing in the collisional term is a local quantity which is very well known in the flat Minkowskian space. This is mathematically realized by implementing the tetrads, which form a basis of four contravariant vectors for the tangent space of a spacetime point. So, it is important to stress that the energy-momentum tensor obtained by evolving the Boltzmann equation is the one in the local inertial frame and in principle one has to subsequently transform it to the one in the general coordinate frame, which is used in the Einstein equations. However, at first order in perturbation theory the EMTs in the local inertial frame and in the general coordinate frame coincide and therefore the tetrads formalism is not strictly necessary; at second order, instead, the transformation introduces additional terms which have to be included in the equations. We do not present the details of these calculations and an extensive discussion can be found in [70].

In such local inertial frame, we can express the 4-momentum of a particle as $P^\mu = (E, p\, n^i)$, where the spatial part has been separated in its magnitude, p, and its direction, n^i, satisfying $n_i n^i = 1$. With this parametrization, the distribution function reads $f = f(\tau, x^i, p, n^i)$. Then, the Boltzmann equation (2.23) can be conveniently written as

$$\frac{\partial f}{\partial \tau} + \frac{\partial f}{\partial x^i}\frac{\mathrm{d}x^i}{\mathrm{d}\tau} + \frac{\partial f}{\partial p}\frac{\mathrm{d}p}{\mathrm{d}\tau} + \frac{\partial f}{\partial n^i}\frac{\mathrm{d}n^i}{\mathrm{d}\tau} = \mathcal{C}[f] \ . \tag{2.24}$$

Projected Boltzmann equation

The Boltzmann equation is a partial differential equation which is in general really difficult to solve. The systematic way to proceed is then to project its positional ($\mathbf{x}$), angular ($\hat{\mathbf{n}}$) and momentum (p) dependence so that it becomes an ordinary differential equation, thus hugely simplifying the numerical computations.

For what concerns the momentum projection, it is useful to introduce the formalism of *beta-moments*. We define the β_n operator acting on a generic distribution F as

$$\beta_n[F] \equiv \frac{1}{\int \mathrm{d}p\, p^3 F^{(0)}} \int dp\, p^3 \left(\frac{p}{E}\right)^{n-1} F \ , \tag{2.25}$$

where $F^{(0)}$ is its background part. If now we introduce the beta-moments ${}_n\Delta$ of the distribution function f as

$$1 + {}_n\Delta(\tau, \mathbf{x}, \hat{\mathbf{n}}) \equiv \frac{1}{\int \mathrm{d}p\, p^3 f^{(0)}(\tau, p)} \int \mathrm{d}p\, p^3 \left(\frac{p}{E}\right)^{n-1} f(\tau, \mathbf{x}, p, \hat{\mathbf{n}}) \ , \tag{2.26}$$

it becomes clear that

$$\beta_n[f] = 1 + {}_n\Delta \ . \tag{2.27}$$

The β_n operator integrates out the dependence on p and defines an expansion in the powers of the dimensionless velocity of the particle, $\beta = p/E$. The great advantage of using this formalism is that it allows the treatment of relativistic and non-relativistic particles within the same framework. For relativistic (or massless) particles ($p/E = 1$), the beta-moments just reduce to what is called *brightness fluctuation* Δ; for non-relativistic particles ($p/E \ll 1$), instead, higher beta-moments are suppressed and hence only the very first ones really count, thus recovering the usual fluid treatment[1].

It remains to project the positional and directional dependence. It can be achieved through the Fourier transformation (which projects on plane waves) and the multipole

[1]To describe the evolution of a non-relativistic species like baryons and cold dark matter we just need the continuity equation (conservation of number density) and the Euler equation (conservation of momentum).

decomposition (which projects on spherical harmonics), respectively. Denoting with $\mathcal{F}_k$ and $L_{\ell m}$ their respective operators, we can write

$$\begin{aligned} {}_n\Delta_{\ell m}(\tau, \mathbf{k}) &\equiv (\mathcal{F}_k \circ L_{\ell m} \circ \beta_n)[f] \\ &= i^\ell \sqrt{\frac{2\ell+1}{4\pi}} \int \mathrm{d}^3x \, \mathrm{d}\Omega \, e^{-i\mathbf{k}\cdot\mathbf{x}} \, Y^*_{\ell m}(\hat{\mathbf{n}}) \, {}_n\Delta(\tau, \mathbf{x}, \hat{\mathbf{n}}) \ , \end{aligned} \tag{2.28}$$

where $\int \mathrm{d}\Omega = \int_0^\pi \sin\theta \, \mathrm{d}\theta \int_0^{2\pi} \mathrm{d}\phi$ denotes the integration over all the angles and $Y_{\ell m}$ are the spherical harmonics [2].

The evolution of ${}_n\Delta_{\ell m}$ is thus governed by the *projected Boltzmann equation*:

$$(\mathcal{F}_k \circ L_{\ell m} \circ \beta_n) \left[\frac{\mathrm{d}f}{\mathrm{d}\tau} - \mathcal{C}[f] \right] = 0 \ , \tag{2.30}$$

which, as we already mentioned, is no longer a partial differential equation in time, position, momentum and direction but just an ordinary differential equation in time[3].

How the beta-moments are related to the energy-momentum tensor can be derived from equation (2.22), that is

$$\begin{aligned} T^0_{\ 0} &= -\,\bar{\rho}\,(1 + {}_0\Delta_{00}) \ , \\ T^i_{\ i} &= -\,\bar{\rho}\,(1 + {}_2\Delta_{00}) \ , \\ i\xi^i_{[m]} T_{i0} &= -\,\frac{1}{3}\,\bar{\rho}\,{}_1\Delta_{1m} \ , \\ \chi^{ij}_{2,[m]} &= -\,\frac{2}{15}\,\bar{\rho}\,{}_2\Delta_{2m} \ . \end{aligned} \tag{2.31}$$

with $\bar{\rho} = \int \mathrm{d}\mathbf{p} \, E \, f^{(0)}$ being the background energy density, while $f^{(0)}$ is the unperturbed distribution function.

Parametrizing the EMT as in equation (2.14), it is possible to derive the relations with the fluid variables up to first order, which for fluids with equation of state $\omega = P/\rho = \text{constant}$ read

$$\begin{aligned} {}_0\Delta_{00} &= \delta \ , \\ {}_1\Delta_{1m} &= 3\,(\omega+1)\, i v_{[m]} \ , \\ 1 + {}_2\Delta_{00} &= 3\,\omega\,(1+\delta) \ , \\ {}_2\Delta_{2m} &= -\frac{15}{2}\,\frac{\Sigma_{[m]}}{\bar{\rho}} \ , \end{aligned} \tag{2.32}$$

[2]Spherical harmonics $Y_{\ell m}$ are a complete set of orthonormal functions on the unit sphere, defined as

$$Y_{\ell m} = \sqrt{\frac{2\ell+1}{4\pi}\frac{(\ell-m)!}{(\ell+m)!}} P^m_\ell(\cos\theta) e^{im\phi} \tag{2.29}$$

.

[3]Think, for example, of the action of the Fourier transformation on spatial derivatives: $\nabla f \to i\mathbf{k}f$ and $\nabla^2 f \to -k^2 f$.

where $v_{[m]}$ is the spherical projection of $v^i \equiv (p/E)n^i$ and $\delta \equiv (\rho - \bar{\rho})/\bar{\rho}$ is the density contrast.

It is now the moment to show the explicit form of the Boltzmann equation for each species, that is photons, neutrinos, baryons and cold Dark Matter.

2.4.1 Photons

We have already seen that for relativistic particles the beta-moments reduce to the brightness fluctuation, ${}_n\Delta = \Delta$. In order to have a more intuitive understanding of this quantity, let us consider the photon distribution function at equilibrium, which is the one of a *blackbody spectrum*:

$$f_\gamma = \left[\exp\left(\frac{p}{T(\tau)}\right) - 1\right]^{-1} , \tag{2.33}$$

where p is the photon momentum in the local inertial frame and T represents the CMB temperature. If we now consider a small *temperature fluctuation* $\Theta \equiv (T - \bar{T})/\bar{T}$ so that we get the substitution $T(\tau) \to \bar{T}(\tau)[1 + \Theta(\tau, \mathbf{x}, p, \hat{\mathbf{n}})]$ in equation (2.33), the Taylor expansion of f_γ around $\Theta = 0$ then reads

$$f_\gamma = f_\gamma^{(0)} - p\,\frac{\partial f_\gamma^{(0)}}{\partial p}\,\Theta + \mathcal{O}(\Theta^2) , \tag{2.34}$$

with $f_\gamma^{(0)}$ still having the blackbody shape as in (2.33), evaluated at the background temperature $\bar{T}(\tau)$. The brightness $\mathcal{I}$ is defined as

$$\mathcal{I} \equiv \int \mathrm{d}p\, p^2\, E\, f_\gamma . \tag{2.35}$$

Thus, the brightness fluctuation simply reads

$$\mathcal{I} = \bar{\mathcal{I}}\,(1 + \Delta) , \tag{2.36}$$

with $\bar{\mathcal{I}}$ being just the brightness obtained from $f_\gamma^{(0)}$. Up to first order, we simply have that[4] $\Delta = 4\Theta$, so it can equivalently be thought as the perturbation to the photon temperature, up to a factor of 4.

After having further projected in spherical harmonics and in plane waves as in equation (2.28), we define the brightness multipoles as

$$\mathcal{I}_m^\ell(\mathbf{k}) \equiv (\mathcal{F}_k \circ L_{\ell m} \circ \beta)[f_\gamma] = \Delta_{\ell m} . \tag{2.37}$$

[4]Integrating by parts $\mathcal{I} = \int \mathrm{d}p\, p^3\, f_\gamma$ and using $\partial f_\gamma/\partial p = -T/p\,\partial f_\gamma/\partial T$, we obtain that $(T/\bar{T})^4 = \mathcal{I}/\bar{\mathcal{I}}$ and hence $(1 + \Theta)^4 = 1 + \Delta$, which finally leads to $\Delta = 4\Theta$, at first order.

In what follows, we drop the $\mathbf{k}$ dependence and we also denote with $u^i \equiv iv^i$ the baryon velocity, so that all the imaginary factors in the equations are absorbed. The collision term accounts for the tight coupling to the baryons before recombination through Thompson scattering; after recombination, photons stream freely but still continue to transfer energy and momentum with matter. Photons are also polarized in the plane orthogonal to their propagation direction $\hat{\mathbf{n}}$ and hence two more types of brightness multipoles, $\mathcal{E}^\ell_m$ and $\mathcal{B}^\ell_m$, should be taken into account, for E-modes and B-modes respectively (the physics of CMB polarization is addressed in Chapter 3, while the Boltzmann equations for these two modes are shown and extensively described in [70]). We again focus on scalar perturbations, since we assume vanishing vector and tensor modes at linear level.

Finally, the scalar Boltzmann equations for the photon temperature multipoles are the following:

$$\left(\mathcal{I}^0_0\right)' = -\frac{k}{3}\,\mathcal{I}^1_0 - 4\,\dot{\Phi}\ , \tag{2.38}$$

$$\left(\mathcal{I}^1_0\right)' = -k\left(\frac{2}{5}\mathcal{I}^2_0 - \mathcal{I}^0_0\right) - 4k\Psi + \kappa'\left(4u_{[0]} - \mathcal{I}^1_0\right)\ , \tag{2.39}$$

$$\left(\mathcal{I}^2_0\right)' = -k\left(\frac{3}{7}\mathcal{I}^3_0 - \frac{2}{3}\mathcal{I}^1_0\right) + \kappa'\left(-\mathcal{I}^2_0 + \frac{1}{10}\left(\mathcal{I}^2_0 - \sqrt{6}\mathcal{E}^2_0\right)\right)\ , \tag{2.40}$$

$$\left(\mathcal{I}^\ell_0\right)' = -k\left(\frac{\ell+1}{2\ell+3}\mathcal{I}^{\ell+1}_0 - \frac{\ell}{2\ell-1}\mathcal{I}^{\ell-1}_0\right) - \kappa'\,\mathcal{I}^\ell_0\ , \quad \ell \geq 3\ . \tag{2.41}$$

In the above equations we have introduced the *Thomson scattering rate* $\kappa' = -\bar{n}_e\sigma_T a$, with $\bar{n}_e$ being the background free electron density and $\sigma_T = 6.652 \times 10^{-29}\,\mathrm{m}^2$ the Thomson cross section; all the terms containing κ' form the collision term. Note that adjacent multipoles are coupled to each other (the evolution of $\mathcal{I}^\ell_0$ is determined by $\mathcal{I}^{\ell-1}_0$ and $\mathcal{I}^{\ell+1}_0$ and this is true also for $m > 0$), hence implying an infinite hierarchy of equations (m modes instead do not couple at linear order, as already explained). However, monopoles of higher orders than the monopole ($l = 0$) and the dipoles ($l = 1$) are negligible, especially during the tight coupling to baryons, and start to become relevant only approaching to the photon decoupling; hence, generally this infinite hierarchy can be truncated at some $\ell_{\max}$. Note finally that the monopole, dipole and quadrupole equations (2.38)-(2.40) are equivalent and directly comparable to the continuity, Euler and shear equations for photons respectively, that is for δ_γ, θ_γ and σ_γ following the Ma & Bertschinger [54] notation (see Appendix A for more details).

2.4.2 Neutrinos

Neutrinos, which we now assume as massless [5], are governed by the same Boltzmann equations of photons; however, since they weakly interact with other particles, the collision term can be set to zero. Hence, defining with $\mathcal{N}_m^\ell$ the neutrino multipoles in the same way of $\mathcal{I}_m^\ell$, the Boltzmann equations are the following:

$$\left(\mathcal{N}_0^0\right)' = -\frac{k}{3}\mathcal{N}_0^1 - 4\,\dot{\Phi}\ , \tag{2.42}$$

$$\left(\mathcal{N}_0^1\right)' = -k\left(\frac{2}{5}\mathcal{N}_0^2 - \mathcal{N}_0^0\right) - 4k\Psi\ , \tag{2.43}$$

$$\left(\mathcal{N}_0^2\right)' = -k\left(\frac{3}{7}\mathcal{N}_0^3 - \frac{2}{3}\mathcal{N}_0^1\right)\ , \tag{2.44}$$

$$\left(\mathcal{N}_0^\ell\right)' = -k\left(\frac{\ell+1}{2\ell+3}\mathcal{N}_0^{\ell+1} - \frac{\ell}{2\ell-1}\mathcal{N}_0^{\ell-1}\right)\ , \quad \ell \geq 3\ . \tag{2.45}$$

As before, we have an infinite hierarchy of equations coupled in adjacent ℓ, which again can be safely truncated at some $\ell_{\max}$ (usually $\ell_{\max} = 3$).

2.4.3 Baryons

Baryons are treated as pressureless perfect fluid, hence being described only by their energy density and velocity. Within the formalism used so far, this means that the only beta-moments which survives are the $n = 0$ and $n = 1$ ones; we denote them with ${}_nb_m^\ell$. The Boltzmann equations for baryons then read

$$\left({}_0b_0^0\right)' = -\frac{k}{3}\,{}_1b_0^1 + 3\,\dot{\Phi}\ , \tag{2.46}$$

$$\left({}_1b_0^1\right)' = -\mathcal{H}\,{}_1b_0^1 + 3\,k\,c_s^2\,{}_0b_0^0 + 3\,k\,\Psi - r\kappa'\left(4u_{[0]} - \mathcal{I}_0^1\right)\ , \tag{2.47}$$

where $r = \bar{\rho}_\gamma/\bar{\rho}_b$ and c_s is the baryon speed of sound. Physically, they represent the continuity equation and the Euler equation, respectively. Note that the collision term is exactly the same, with opposite sign, of the one for the photon dipole $\mathcal{I}_0^1$, suitably weighted by the factor r: before recombination, in fact, baryons are tightly coupled to photons through Thomson scattering and hence the form of the collision term for the two species is the same; to ensure momentum conservation, however, they have opposite sign and a relative factor r, which accounts for the difference in energy density for baryons and photons.

[5] For the sole purpose of simplicity in the equation visual representation.

Tight-coupling approximation

Before recombination, photons and baryons are tightly coupled and the Thomson opacity is much larger than the expansion rate, that is $\kappa' \gg a'/a$. The Euler equations for photons and baryons hence become numerically difficult to solve, due to the large value of κ', leading to the necessity to find an alternative form for the equations during this regime.

The combination of equations (2.39) and (2.47) gives the following exact expression:

$$\begin{aligned}(1+r)\left({}_1b_0^1\right)' = &-\mathcal{H}\,{}_1b_0^1 + 3\,k\,c_s^2\,{}_0b_0^0 + (1+r)\,3\,k\,\Psi \\ &+ 3\,k\,r\left(\frac{1}{4}\mathcal{I}_0^0 - \frac{1}{10}\mathcal{I}_0^2\right) + r\left[\frac{3}{4}\left(\mathcal{I}_0^1\right)' - \left({}_1b_0^1\right)'\right] .\end{aligned} \tag{2.48}$$

The term $[(3/4)\,(\mathcal{I}_0^1)' - ({}_1b_0^1)']$ can be written as

$$\begin{aligned}\left({}_1b_0^1\right)' - \frac{3}{4}\left(\mathcal{I}_0^1\right)' = &\frac{2\,r}{1+r}\,\mathcal{H}\left({}_1b_0^1 - \frac{3}{4}\mathcal{I}_0^1\right) + \frac{\tau}{1+r}\Bigg[-\frac{a''}{a}{}_1b_0^1 \\ &- 3\,k\,\mathcal{H}\left(\frac{1}{2}\mathcal{I}_0^0 + \Psi\right) + 3\,k\left(c_s^2\left({}_0b_0^0\right)' - \frac{1}{4}\left(\mathcal{I}_0^0\right)'\right)\Bigg] + \mathcal{O}((1/\kappa')^2) .\end{aligned} \tag{2.49}$$

Substituting equation (2.49) in (2.48) provides the desired equation for $({}_1b_0^1)'$ during the tight-coupling regime.

The equation for $(\mathcal{I}_0^1)'$ is instead

$$\begin{aligned}\left(\mathcal{I}_0^1\right)' = &-\frac{1}{r}\left(\frac{4}{3}\left({}_1b_0^1\right)' + \frac{4}{3}\,\mathcal{H}\,{}_1b_0^1 - 4\,k\,c_s^2\,{}_0b_0^0\right) \\ &+ 2\,k\left(\frac{1}{2}\mathcal{I}_0^0 - \frac{1}{5}\mathcal{I}_0^2\right) + \frac{1+r}{r}\,4\,k\,\Psi .\end{aligned} \tag{2.50}$$

2.4.4 Cold Dark Matter

All the assumptions and statements made for baryons are valid also for cold Dark Matter. However, since it interacts with other particles only via gravity, the collision term is now zero. Then, denoting with ${}_nc_m^\ell$ its multipoles, we simply have

$$\left({}_0c_0^0\right)' = -\frac{k}{3}\,{}_1c_0^1 + 3\,\dot{\Phi} , \tag{2.51}$$

$$\left({}_1c_0^1\right)' = -\mathcal{H}\,{}_1c_0^1 + 3k\Psi . \tag{2.52}$$

2.5 Initial conditions for cosmological perturbations

In order to solve the system of Einstein and Boltzmann equations and compute observables of interest, we need to specify the initial conditions for the perturbations. They are usually defined deep in the radiation era, after neutrino decoupling. During this epoch, we have that $\mathcal{H} \sim \tau^{-1}$ and $\bar{\rho}_{\rm tot} \sim \bar{\rho}_\nu + \bar{\rho}_\gamma$, since baryons and CDM make a negligible contribution. The equations start to be integrated when a given mode k is well outside the horizon, that is $k\tau \ll 1$ (note that $k\tau$ is dimensionless), allowing to expand the equations for small $k\tau$.

There are two main classes of initial conditions: *adiabatic* and *isocurvature* ones. In the former case, the relative abundances of the different species are spatially constant, while in the latter case the relative abundances are allowed to vary, but in such a way that there is no net contribution to the curvature perturbation. Single-field inflation predicts adiabatic initial conditions and indeed CMB observations strongly support their dominant presence with respect to the isocurvature ones, whose fractional contribution is instead constrained to be below a few percent. For this reason, we now focus only on the adiabatic case, which is also the one always assumed in this thesis.

For adiabatic initial conditions, all the fluids (photons, neutrinos, baryons and cold Dark Matter) share a common velocity,

$$v_{\gamma[m]} = v_{\nu[m]} = v_{b[m]} = v_{c[m]} \ . \tag{2.53}$$

Moreover, the density contrasts $\delta = (\rho - \bar{\rho})/\bar{\rho}$ of each species are related as

$$\delta_\gamma \simeq \delta_\nu \simeq \frac{3}{4}\delta_b \simeq \frac{3}{4}\delta_c \ . \tag{2.54}$$

A way to explain this last expression is to look at the entropy perturbation $\mathbf{S} = \delta\Gamma/\Gamma$, where $\Gamma = T^3/n_m$ is the entropy per matter particle and n_m is the number density of matter particles. In fact, an alternative condition for the adiabatic case is to set $\mathcal{S} = 0$, which gives

$$\mathcal{S} = 3\frac{\delta T}{T} - \delta_m = \frac{3}{4}\delta_r - \delta_m = 0 \ , \tag{2.55}$$

since $\rho_r \propto T^4$ and hence we obtain equation (2.54).

Conditions (2.53) and (2.54) imply that we only need to find the initial conditions for the common velocity v and for the density perturbation of one fluid. Moreover, all vector and tensor modes ($m \neq 0$) are assumed to have vanishing initial conditions[6].

[6]Since in linear theory different m modes do not mix, this conditions implies that vector and tensor perturbations are never generated; this is not generally true at higher orders, when non-scalar modes can be present even from initial vanishing values.

The adiabatic initial conditions, at linear order, are the following:

$$\mathcal{I}_0^0 = \mathcal{N}_0^0 = -2\Psi \ , \quad {}_0b_0^0 = {}_0c_0^0 = \frac{3}{4}\mathcal{I}_0^0 = \frac{3}{4}\mathcal{N}_0^0 \ , \tag{2.56}$$

$$u_{[0]} = \frac{1}{2}\,k\tau\,\Psi \ , \tag{2.57}$$

$$\mathcal{N}_0^2 = \frac{2}{3}(k\tau)^2\Psi \ , \tag{2.58}$$

$$\Psi = -\frac{10\,\zeta}{15+4\Omega_\nu} \ , \quad \Phi = \left[1+\frac{2}{5}\Omega_\nu\right]\Psi \ , \tag{2.59}$$

where $\Omega_\nu = \bar{\rho}_\nu/\bar{\rho}_{\rm tot}$ and $u_{[0]} = iv_{[0]}$ is the variable associated to the common velocity. Since the equations we have introduced so far evolve dipoles rather then velocities, it is useful to remember, from equation (2.32), the relation between the dipole and the velocity of a given species, that is

$$\mathcal{I}_0^1 = \mathcal{N}_0^1 = 4\,iv_{[0]} \ , \tag{2.60}$$

$${}_1b_0^1 = {}_0c_0^1 = 3\,iv_{[0]} \ . \tag{2.61}$$

The quantity ζ is instead the *gauge-invariant curvature perturbation*, which at linear order is just $\zeta = -\mathcal{R}$ and

$$\mathcal{R} = \Phi + \frac{2}{3\mathcal{H}(\omega+1)}\left[\Phi' + \mathcal{H}\Psi\right] \ . \tag{2.62}$$

In the radiation dominated era ($\omega = 1/3$) and on superhorizon scales we simply have

$$\zeta = -\mathcal{R} = -\Phi - \frac{1}{2}\Psi \ . \tag{2.63}$$

The great advantage of using ζ is that, for adiabatic fluctuations, it is conserved on superhorizon scales at any perturbative order. This property provides a very convenient way to connect primordial fluctuations set up by inflation to the initial conditions for Ψ and Φ of our differential equations and allows ignoring all the complexity of the physics occurring between the end of inflation and the time the equations start being evolved.

Chapter 3

Cosmic Microwave Background

The detection and the analysis of the *cosmic microwave background* (CMB) surely represent one of the most important aspect of the development of modern cosmology. It was accidentally discovered in 1964 by radio engineers Penzias and Wilson [68], who detected an highly isotropic electromagnetic radiation at microwave frequencies which could not be associated with any known radio source or instrumental noise. It was soon clear that this signal represented a relic radiation of photons from the early Universe and therefore a strong hint to the hot Big-Bang model, which at the epoch was in contraposition to the steady state theory. According to the former model, in the early stages of the Universe all the species were in thermal equilibrium forming a unique hot and dense plasma; as the Universe cooled down due to its expansion, it was possible for different species to go out of equilibrium and freeze out, leaving only photons and electrons in thermal contact through Thomson scattering. As the temperature lowered, the electrons began to combine with protons to form hydrogen (*recombination*) and Thomson scattering started to lose efficiency, leaving the photons able to stream freely through the Universe. Since they were in thermal equilibrium, at *last scattering* (the process of decoupling happened in a quite short interval of redshift around $z \sim 1100$, so we usually refer to it as *last scattering surface*) the distribution of photons was the one of an almost perfect black body (Figure 3.1), whose intensity at a given temperature T and frequency ν is given by

$$I(T,\nu) = \frac{4\pi\hbar\nu^3}{c}\left[\exp\left(\frac{h\nu}{k_B T}\right) - 1\right]^{-1} \tag{3.1}$$

and its form almost preserved until today [1], whereas its temperature redshifted as $T(z) = T_0(1+z)$ due to the expansion of the Universe.

Despite its great isotropy, the spatial distribution of the CMB radiation presents a pattern of tiny anisotropies in temperature and polarization, of order of 10^{-5} and 10^{-6}

[1] Effects like Sunyaev-Zel'dovich and reionization slightly modify the CMB black body spectrum, as we will see.

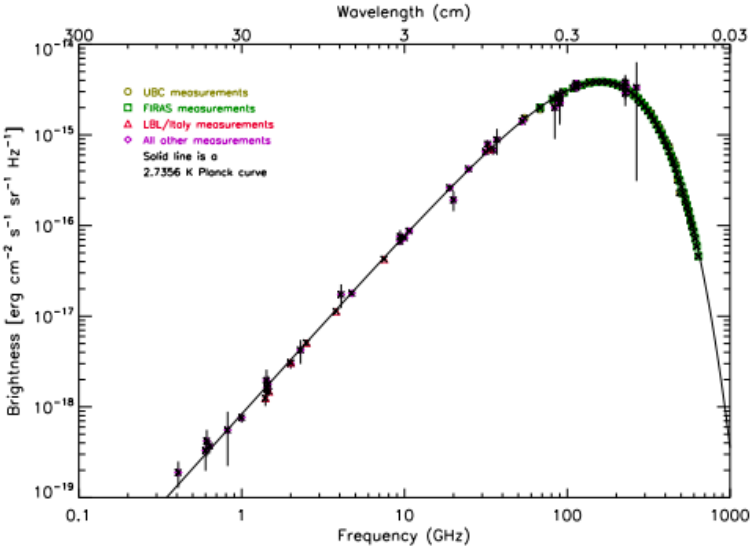

Figure 3.1: CMB black body spectrum as measured by FIRAS [82].

respectively, which are profoundly connected to the primordial density inhomogeneities necessary to feed structure formation. The precise measurement of these fluctuations would therefore provide strong experimental constraints to our cosmological models and in particular to the theory of inflation, which is currently the most powerful theoretical model for the generation of primordial perturbations.

The first measurement of CMB anisotropies came from the Cosmic Background Explorer (COBE) satellite in 1992, which detected a black body emission of $T = 2.726 \pm 0.005K$ [27] and provided the first map of the CMB radiation along with its anisotropy pattern. These measurements were then improved in 2003 by the NASA's Wilkinson Microwave Anisotropy Probe (WMAP) and more recently by ESA's *Planck* satellite, whose first results were published in 2013 and the final data release in 2018 [72].

3.1 The angular power spectrum

Fluctuations in the CMB radiation correspond to perturbations in the photon phase-space distribution, where the latter are governed by the Boltzmann equation with Thomson scattering as collision term. In the rest frame of the electron, the Thomson scattering does not change the photon momentum, implying that the perturbed photon phase-space distribution depends only on the direction of the photon momentum and not on its magnitude. If $\hat{\mathbf{n}}$ is the direction in the sky from which the photon is detected, it is customary

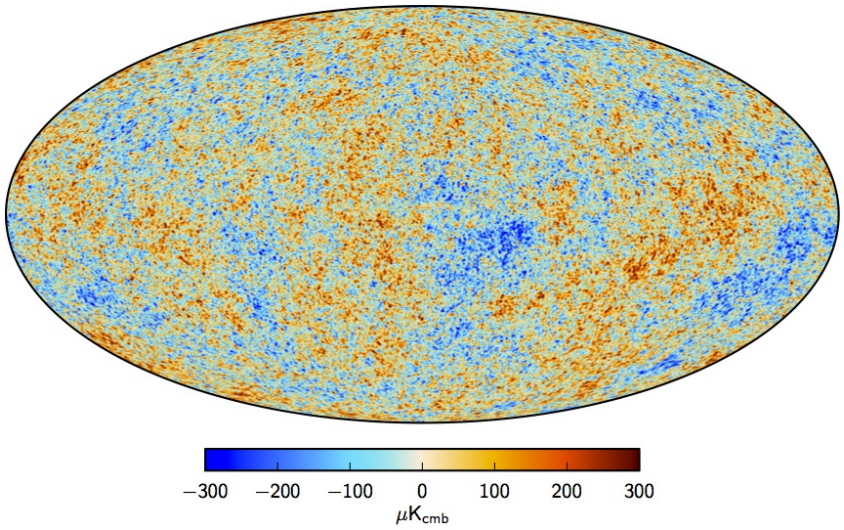

Figure 3.2: CMB temperature map at 5' resolution derived by *Planck* [62].

to introduce the brightness temperature perturbation

$$\Theta(\hat{\mathbf{n}}) \equiv \frac{\Delta T}{T}(\hat{\mathbf{n}}) \ , \tag{3.2}$$

which is of order of 10^{-5} for the CMB, as already mentioned [2]. Since we are dealing with a map projected on the sky, it is convenient to expand $\Theta(\hat{\mathbf{n}})$ in spherical harmonics Y_{lm}

$$\Theta(\hat{\mathbf{n}}) = \sum_{\ell=0}^{\infty} \sum_{m=-\ell}^{\ell} a_{\ell m} Y_{\ell m}(\hat{\mathbf{n}}) \ , \tag{3.3}$$

where $a_{\ell m}$ are the coefficients of the expansion and ℓ is the multipole index which is related to the inverse of the angular distance θ of two points in the sky

$$\ell \sim \frac{180^\circ}{\theta} \ . \tag{3.4}$$

This allows us to split the CMB maps in well-defined scales, which is quite convenient since different physical processes could affect different scales, as we will see. Using the orthonormality of the spherical harmonics, the coefficients $a_{\ell m}$ can be written as

$$a_{\ell m} = \int \Theta(\hat{\mathbf{n}}) Y^*_{\ell m}(\hat{\mathbf{n}}) \, \mathrm{d}\hat{\mathbf{n}} \ . \tag{3.5}$$

[2] To be more precise, we are neglecting the dipole term due to the motion of the Earth with respect to the last scattering surface reference frame, which is usually removed in CMB data.

Since the initial conditions set up by inflation are stochastic and therefore lead to stochastic coefficients, we are interested in their statistical properties. Homogeneity and isotropy of the Universe imply $\langle a_{\ell m} \rangle = 0$, while the two-point correlator takes the form

$$\langle a_{\ell m} a^*_{\ell' m'} \rangle = \delta_{\ell \ell'} \, \delta_{m m'} \, C_\ell \ , \tag{3.6}$$

where the quantity $C_\ell \equiv \langle |a_{\ell m}|^2 \rangle$ is the *angular power spectrum* of the CMB anisotropy. It is important to stress that the averages in the above formulas are *ensemble averages*, which means that these quantities are computed making averages on all the possible different realizations of the Universe. What we really observe is instead only one particular realization, thus once measured the coefficients a_{lm} the power spectrum can be estimated as

$$\hat{C}_\ell = \frac{1}{2\ell + 1} \sum_{m=-\ell}^{\ell} |a_{\ell m}|^2 \ , \tag{3.7}$$

where now with $\hat{C}_\ell$ we mean the observed quantity, in principle different from the theoretical one (C_ℓ). This introduces an unavoidable error which is called *cosmic variance*, given by

$$\Delta C_\ell = \sqrt{\frac{2}{2\ell + 1}} C_\ell \tag{3.8}$$

(under the assumption of Gaussian fluctuations, C_ℓ follows a χ^2 distribution) and it is dominant for small ℓ (*i.e.* for large scales, where indeed we have very few modes m to estimate C_ℓ).

The standard cosmological model and the standard models of single field slow roll inflation predict CMB fluctuations to be almost entirely Gaussian, with only very little non-Gaussian contributions well below the current experimental sensitivities. The Gaussian hypothesis implies that the two-point correlation function fully determines the statistical properties of the CMB anisotropies [3]. Using the equation (3.6), the two-point correlation function $C(\theta)$ can be expressed as

$$\begin{aligned} C(\theta) &= \langle \Theta(\hat{\mathbf{n}}_\mathbf{1}) \Theta(\hat{\mathbf{n}}_\mathbf{2}) \rangle \\ &= \sum_{\ell \ell'} \sum_{m m'} \langle a_{\ell m} a^*_{\ell' m'} \rangle Y_{\ell m}(\hat{\mathbf{n}}_\mathbf{1}) Y^*_{\ell' m'}(\hat{\mathbf{n}}_\mathbf{2}) \\ &= \sum_\ell C_\ell \sum_m Y_{\ell m}(\hat{\mathbf{n}}_\mathbf{1}) Y^*_{\ell m}(\hat{\mathbf{n}}_\mathbf{2}) \\ &= \sum_\ell \frac{2\ell + 1}{4\pi} \, C_\ell \, P_\ell(\cos\theta) \ , \end{aligned} \tag{3.9}$$

[3] In a Gaussian random field, all the n-point correlation functions with n odd vanish, while the n-even ones can be expressed in terms of the two-point correlation function.

where $\cos\theta = \hat{\mathbf{n}}_\mathbf{1} \cdot \hat{\mathbf{n}}_\mathbf{2}$ and $P_\ell(\cos\theta)$ are the Legendre polynomials, defined as

$$P_\ell(\cos\theta) = \frac{4\pi}{2\ell+1} \sum_{m=-\ell}^{\ell} Y_{\ell m}(\hat{\mathbf{n}}_\mathbf{1}) Y^*_{\ell m}(\hat{\mathbf{n}}_\mathbf{2}) \ . \tag{3.10}$$

It is useful to express the angular power spectrum C_ℓ in terms of the primordial perturbations. For this purpose, let us compute the temperature anisotropy in a generic spacetime point $(\mathbf{x}, \tau)$ as superposition of plane waves, that is

$$\begin{aligned} \Theta(\mathbf{x}, \hat{\mathbf{n}}, \tau) &= \int \frac{\mathrm{d}^3 k}{(2\pi)^3} \, e^{i\mathbf{k}\cdot\mathbf{x}} \, \Theta(\mathbf{k}, \hat{\mathbf{n}}, \tau) \\ &= \int \frac{\mathrm{d}^3 k}{(2\pi)^3} \, e^{i\mathbf{k}\cdot\mathbf{x}} \sum_{\ell=0}^{\infty} (-i)^\ell (2\ell+1) \, \Theta_\ell(\mathbf{k}, \tau) \, P_\ell(\hat{\mathbf{k}} \cdot \hat{\mathbf{n}}) \ , \end{aligned} \tag{3.11}$$

where we also used an expansion in series of Legendre polynomials. The coefficients Θ_ℓ depend on the initial perturbations and therefore we can factorize such dependence as

$$\Theta_\ell(\mathbf{k}, \tau) = \mathcal{R}(\mathbf{k}) \, \Theta_\ell(k, \tau) \ , \tag{3.12}$$

where $\mathcal{R}(\mathbf{k})$ is the curvature perturbation already introduced in the previous chapters and $\Theta_\ell(k, \tau)$ is the *photon transfer function*, *i.e.* the solution of the Boltzmann equation setting $\mathcal{R} = 1$ [4]. Using the expression (3.7) and the orthonormality of the spherical harmonics, we obtain the final result:

$$C_\ell = 4\pi \int \frac{\mathrm{d}k}{k} \, \Theta^2_\ell(k, \tau) \, \mathcal{P}_\mathcal{R}(k) \ , \tag{3.13}$$

where $\mathcal{P}_\mathcal{R}(k) = (k^3/2\pi) \, \mathcal{P}(k)$ is the (dimensionless) power spectrum of primordial curvature perturbation, defined through its two-point correlation function

$$\langle \mathcal{R}(\mathbf{k_1}) \mathcal{R}(\mathbf{k_2})^* \rangle = (2\pi)^3 \, \delta(\mathbf{k_1} + \mathbf{k_2}) \, \mathcal{P}(k) \ . \tag{3.14}$$

3.2 CMB multipoles

We shall now analyze more in details the features of the CMB angular power spectrum. In equation (3.3) the temperature perturbation is decomposed in a series of multipoles, each of them concerning different angular scales, for different values of ℓ. At the same time, temperature anisotropy can be sourced by different physical processes at different scales, so it is interesting to investigate deeper the characteristics of such multipoles and consequently better understand the form of the power spectrum shown in Figure 3.3.

[4] Note that the photon transfer function depends only on the magnitude of $\mathbf{k}$, since its evolution via Boltzmann equations does not depend on $\hat{\mathbf{k}}$.

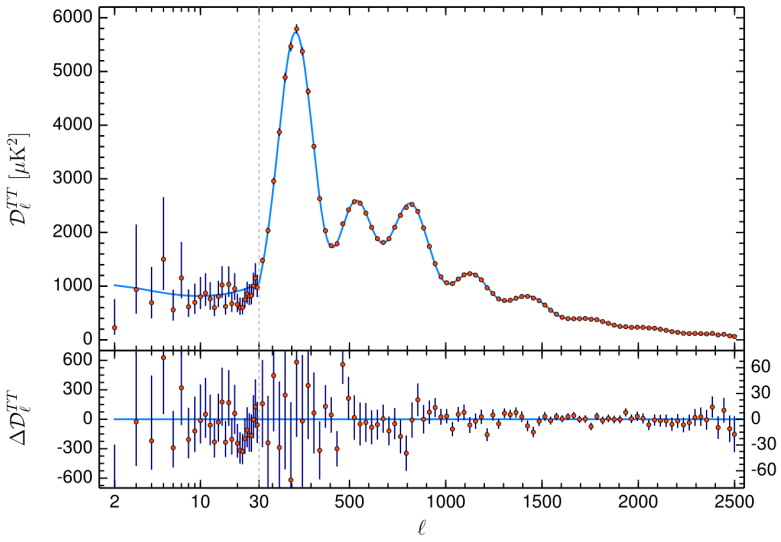

Figure 3.3: CMB temperature power spectrum expressed in bandpowers $D_l \equiv [\ell(\ell+1)/2\pi]C_l$ and residuals in the lower panel [72].

3.2.1 Monopole ($\ell = 0$)

The monopole component of the power spectrum, a_{00}, is simply related to the average temperature of the CMB radiation. Such term needs absolute temperature devices to be measured, like the FIRAS instrument on the COBE satellite, while more recent experiments are dedicated to differential measurements and therefore they are insensitive to such average quantities.

3.2.2 Dipole ($\ell = 1$)

The dipole anisotropy of the CMB was well known since the 1970s and it represents the largest contribution to temperature fluctuations. It is commonly interpreted as the relative motion of our galaxy with respect to the comoving frame in which the CMB radiation is isotropic. It is better to specify that this is not just a simple Doppler effect, since both the energy of the CMB photons seen in the direction of motion of the Earth and the interval of frequency dν are increased by the same factor and therefore the temperature (which is proportional to the energy per unit frequency) is not affected. The main two contributions of the dipole anisotropy are indeed the following:

- we collect a larger number of photons in the direction of motion with respect to the CMB reference frame and less in the opposite one, providing a variation factor for the temperature of $(1 + \frac{v}{c}\cos\theta)$ (where θ is the angle between the direction of

motion, with velocity v, and the direction of observation);

- there is an effect of aberration: the solid angle under which we observe the sky is reduced by a factor $(1 + \frac{v}{c}\cos\theta)^{-2}$ and therefore the flux increases by the inverse of this factor.

These effects together produce a factor of $(1 + \frac{v}{c}\cos\theta)^3$ for the intensity and therefore (using equation (3.1)) the temperature changes accordingly as

$$T = T_0\left(1 + \frac{v}{c}\cos\theta\right) . \tag{3.15}$$

Such variation corresponds to a perturbation of $\sim 10^{-3}$, from which, after subtracting the Earth's motion around the Sun, the Sun's motion around the galactic centre and the velocity of our galaxy with respect to the centroid of the Local Group, the relative motion of the latter with respect to the CMB rest frame can be estimated to be $\sim 600\,\mathrm{km\ s^{-1}}$ in the direction of Hydra-Centaurus.

In order to study the CMB anisotropies directly connected with the physics of the early Universe, the dipole moment has to be subtracted; however, it still plays an important role in cosmology, since it allows the identification of a "preferred" cosmological reference frame, which is the one where the dipole would vanish.

3.2.3 Higher-order multipoles ($\ell \geq 2$)

Temperature anisotropies at smaller scales (*i.e.* starting from the $\ell = 2$ quadrupole term) are mainly the result of the primordial density fluctuations in the early Universe, thus representing a powerful tool for cosmologists to obtain information from the otherwise inaccessible early epochs of the Universe and constrain their models. However, it is important not to forget that the CMB photons we detect on Earth, after decoupling from baryons, traveled across the Universe before reaching us, possibly being affected by different phenomena which may distort their initial features. This concept leads to a natural distinction of the anisotropies of the CMB: *primary* anisotropies, originated directly at last scattering surface, and *secondary* anisotropies, which take into account all the integrated effects occurring during the path of the photons from the decoupling moment to the Earth detection.

Temperature anisotropy is sourced mainly by three different contributions: photon energy density perturbations, gravitational potential which causes gravitational redshift and Doppler effect at last scattering surface. These effects can be better visualized in the following expression:

$$\Theta(\hat{\mathbf{n}}) = \left[\left(\frac{1}{4}\delta_\gamma + \Psi\right) + \hat{\mathbf{n}}\cdot\mathbf{v}\right]_{\mathrm{ls}} + \int_{\tau_{\mathrm{ls}}}^{\tau_0} (\Psi' + \Phi')\,\mathrm{d}\tau\ , \tag{3.16}$$

which well approximates the temperature anisotropy; $\delta_\gamma = (\rho_\gamma - \bar{\rho}_\gamma)/\bar{\rho}_\gamma$ is the photon density contrast and $\mathbf{v}$ is the velocity vector of the photon. The first three terms are evaluated at last scattering and take into account the contribution of the photon energy density, gravitational redshift and Doppler effect respectively. The factor $\frac{1}{4}$ multiplying δ_γ comes from the dependence of the energy density of a relativistic species on the fourth power of the temperature, implying the above factor between temperature and energy density perturbations. The combined effect of photon density and gravitational redshift (the terms inside the round brackets in (3.16)) is called *Sachs-Wolfe effect* (SW) [76] and it dominates at large scales (small ℓ). The last term, which is the conformal time integration of the sum of the conformal time derivatives of the gravitational potentials Ψ and Φ from last scattering ($\tau_{\rm ls}$) to the present time (τ_0), takes into account secondary effects coming from possible time varying gravitational potentials which CMB photons may encounter during their journey; it is known as *Integrated Sachs-Wolfe effect* (ISW) and is dominant at very large scales.

It is now the moment to understand why the CMB power spectrum in Figure 3.3 has this peculiar form, what are the relevant features it shows and what are the principal physical processes involved. For these purposes, it is convenient to analyze the power spectrum in three different regions, starting from the lowest ℓ's to the largest ones (so from large scales to small scales).

Sachs-Wolfe plateau

A critical scale which discriminates between two very different physics for the evolution of perturbations is the horizon at last scattering (or, more precisely, the Hubble radius), corresponding to $\ell \sim 100$. At larger scales, perturbations are driven only by gravity and therefore they do not evolve significantly. This implies that such fluctuations reflect directly their initial conditions and hence provide strong constraints to the inflation mechanism. As already mentioned, at these scales the Sachs-Wolfe effect is dominant, whereas the Doppler effect and ISW are negligible. We have already seen (Sec. 2.5) that for adiabatic initial conditions the monopoles of photons and matter are initially related by a factor of (3/4) and the same holds for the density contrasts, that is $\delta_m = (3/4)\,\delta_\gamma$. At the same time, at superhorizon scales in a matter-dominated Universe we have that $\delta_m = -2\Phi$ and $\Psi = \Phi$, leading to $\delta_\gamma = -(8/3)\,\Phi$. Therefore, from equation (3.16) we obtain the following result:

$$\Theta(\hat{\mathbf{n}}) \simeq \left(\frac{1}{4}\delta_\gamma + \Phi\right)_{\rm ls} \simeq \left(-\frac{2}{3} + 1\right)\Phi_{\rm ls} = \frac{1}{3}\Phi_{\rm ls}\ . \tag{3.17}$$

In this case the integral in equation (3.13) can be computed and, using the parametrization of the primordial power spectrum as in (1.74), $\mathcal{P}_\mathcal{R}(k) = A_{\rm s}(k/k_*)^{n_{\rm s}-1}$, and assuming a nearly scale invariant primordial spectrum ($n_{\rm s} \simeq 1$), we obtain that the angular power

spectrum is proportional to the primordial amplitude of perturbations,

$$C_\ell \propto \frac{1}{\ell(\ell+1)} A_{\rm s} \ , \tag{3.18}$$

leading to the plateau that we actually observe in the CMB power spectrum. This result represents a great success for the theory of inflation, since the latter predicts a nearly scale invariant spectrum for the primordial fluctuations; at the same time, inflation does not constrain the amplitude $A_{\rm s}$ of such perturbations, which is therefore estimated directly from CMB observations.

At very large scales ($\ell < 10$) ISW becomes relevant and its effect produces a rise above the plateau (the *ISW rise*); other effects can contribute at low ℓ's, but at these scales it becomes hard to disentangle them due to the dominance of the cosmic variance.

In general, inflation produces scalar, vector and tensor perturbations. Both vector (vorticity) and tensor (transverse traceless perturbation of the metric) modes decay rapidly with the expansion of the Universe unless sourced by exotic mechanisms as for example primordial magnetic fields and cosmic strings; however, outside the horizon tensor modes survive and can therefore contribute to temperature perturbations by making the expansion of space locally anisotropic. Nevertheless, such contributions are almost impossible to distinguish from other effects in temperature anisotropies and therefore the principal way to identify primordial gravitational waves from CMB data is polarization, as we will see.

Acoustic peaks

At scales smaller than the horizon at last scattering, perturbations were able to evolve causally and therefore their signature on the CMB anisotropy pattern reflects all the complexity of the physics occurring before decoupling (also the other interactions play now a role, not only gravity). As mentioned, before recombination photons and electrons were in thermal equilibrium and formed together a *baryon-photon fluid*[5]. Perturbations of baryonic matter were therefore unable to grow significantly, since any attempt of the baryons to collapse was in opposition to the high radiation pressure of the photons. On the contrary, dark matter was already decoupled from radiation and consequently its perturbations could grow and form potential wells. Then, in these potential wells *acoustic oscillations* were able to take place: baryons tried to follow dark matter and collapse, while photon pressure provided an opposite contribution and tried to prevent the collapsing of the baryon matter. This competition causes the system to oscillate around

[5]Protons do not actively participate to Thomson scattering with photons like electrons, due to their higher mass ($\sigma_T \propto 1/m^2$); however, they are kept tightly coupled to electrons through Coulomb scattering, $e^- + p^+ \rightleftharpoons e^- + p^+$. and therefore we can safely say that photons are tightly coupled to electrons and protons (tiny differences in velocity between the two baryonic components can however be relevant at higher perturbative orders and source primordial magnetic field, as we will see).

its equilibrium, with a frequency which depends on the sound speed, and led to time variations of the temperature. When photons and baryons decoupled at recombination, the temporal phases of these sound waves were frozen, leaving projected on the sky a series of peaks, which is what we actually observe in the power spectrum. In particular, the odd peaks correspond to waves which were maximally compressed at last scattering, while even peaks correspond to maximal rarefaction.

The peak structure reflects a strong dependence on the cosmological parameters and therefore it is characterized by a great constraining power. For example, the first peak occurs at the physical scale of the sound horizon, which does not depend very much on the cosmological parameters and can be computed; however, the angle subtended by this scale depends on the geometry of the Universe and the observation of the first peak at $l \sim 200$ is strongly in agreement with a spatially flat Universe. The relative heights between even and odds peaks is instead highly sensitive to the abundance of the baryon component: the peak structure is indeed an alternating sequence of compressions and rarefactions, which are driven by baryons and photon pressure respectively and hence changes in the baryon density would affect it. The oscillations also depend on the amount of dark matter which builds the potential wells and therefore from the peak heights with respect to the troughs we can estimate the dark matter density.

Silk damping

Oscillations in the power spectrum have not all the same strength but they are progressively damped at small scales. This effect, which is known as *Silk damping*, is mainly due to the fact that the photons and baryons do not form a perfectly coupled system, especially at small scales: photons diffuse from hotter regions to colder ones, dragging along also protons and electrons. This mechanism causes an averaging of the anisotropies at small scales and therefore a damping in the power spectrum.

We can roughly estimate the scale of the Silk damping by considering the mean free path of the photons which interact with electrons via Thomson scattering; the probability per unit time of a photon performing Thomson scattering is $n_e \sigma_T$, where n_e is the number density of the electrons, $\sigma_T = (8\pi/3)(\alpha/m_e)$ is the Thomson scattering cross section (with $\alpha = 1/137$ the fine-structure constant and m_e the mass of the electron). The mean time between collisions for the random walking photon in the local baryon rest frame is $t_c \sim (n_e \sigma_T)^{-1}$; the average number of steps in time t is $N = t/t_c$, thus the diffusion of a photon in the same time is $d \sim \sqrt{N} t_c \sim \sqrt{t t_c}$. The Silk scale is therefore [19]

$$a\, k_S^{-1} \simeq \left(\frac{t}{n_e \sigma_T} \right)^{1/2} , \tag{3.19}$$

which at the epoch of last scattering is estimated to be $k_S^{-1} \simeq 8\,\mathrm{Mpc}$.

Another effect which contributes to the damping comes from the fact that recombination is not an instantaneous process and therefore we should more correctly think at

the last scattering surface having a non-vanishing thickness. This produces a damping of anisotropies at scales smaller than the one corresponding to this thickness.

3.2.4 Secondary anisotropies

All the anisotropies described so far were produced directly at last scattering (primary anisotropies), but other processes occurring after the decoupling could in principle affect the CMB radiation, thus providing additional signals which are called secondary anisotropies [2]. Being able to describe and consequently identify them from CMB data, with very high precision measurements, can therefore provide a way to extract further information about the Universe at $z < 1000$. Unlike the primary anisotropies, secondary ones are generally non-Gaussian.

The most important secondary effects are the following:

- *Integrated Sachs-Wolfe effect (ISW)*: as already discussed, this effect is due to time-varying gravitational potentials encountered by the CMB photon along the line of sight; it is used to distinguish it in the *Early ISW*, which occurs immediately after the usual SW effect as there is still enough radiation even in a matter-dominated scenario and affects the first peak of the power spectrum, and the *Late ISW*, which (at linear order in density perturbations) is caused in the recent epoch by the presence of the dark energy and also (at fully non-linear order) by time-varying structures like clusters or voids (this last contribution is also known as Rees-Sciama effect) and is responsible of the rise of the plateau at very large scales;

- *Reionization*: around $z \sim 7$ the Universe underwent a process of re-ionization due to the formation of the first stars and luminous objects and the newly freed electrons scatter with photons increasing the optical depth τ. Due to this effect the amplitude of the CMB power spectra is proportional to $A_s\, e^{-2\tau}$, opening one of the most known degeneracy in the CMB cosmology. This can be broken using the effect that reionization has in polarization, that will be described in the following section;

- *Sunyaev-Zel'dovich effect*: free electrons of the hot intergalactic plasma in galaxy clusters can transfer energy to the CMB photons via inverse Compton scattering, leading to a distortion of the CMB black-body spectrum; this effect is dominant at the scale of galaxy clusters and superclusters and provides a great instrument for their identification;

- *Gravitational lensing*: the presence of structures along the line of sight to the last scattering surface deflects the photon path in a weak lensing effect; this induces a smoothing of the acoustic peaks due to the defocusing of the CMB maps and the generation of B mode polarization that we will see in the next section.

3.3 Polarization

CMB radiation is observed to be linearly polarized [35, 95]. Such polarization is generated by Thomson scattering of the quadrupole moment of the temperature fluctuation around recombination. It is at the level of $\sim 5\%$ of the temperature anisotropies and hence it was not detected soon. Its first measurement came only in 2002 from the DASI experiment and still today polarization measurements represent an experimental challenge. The precise analysis of the CMB polarization pattern is however of great importance for cosmologists, since it provides complementary information to those extracted from the temperature power spectrum and it is also able to break parameter degeneracies, thus contributing to constrain cosmological parameter and probe theoretical models.

Let us now briefly analyze the mechanism of polarization production from Thomson scattering of radiation with a quadrupole moment. The Thomson scattering cross section depends on the polarization as [17]

$$\frac{\mathrm{d}\sigma_T}{\mathrm{d}\Omega} \propto |\hat{\epsilon} \cdot \hat{\epsilon}'|^2 \ , \tag{3.20}$$

where $\hat{\epsilon}$ and $\hat{\epsilon}'$ are the incident and scattered polarization directions respectively. This implies that the target electron is induced to oscillate in the direction of the incident photon polarization and the scattered radiation is therefore polarized in the same direction, while its intensity peaks to the normal one. Assuming an isotropic radiation field, the net outgoing polarization would vanish, since orthogonal polarization states from incident directions separated by 90° would compensate each other. We need therefore a radiation field with a non-vanishing quadrupole moment, *i.e.* with a variation in temperature at 90°, which would produce a net linear polarization of the scattered radiation, as shown in Figure 3.4. However, in a tight coupling regime (*i.e.* when the Thomson scattering rate is high) the random motion of photons destroys any quadrupole moment and consequently any polarization. Even so, a quadrupole moment can form around recombination by the diffusion of photons.

The linear polarization pattern can be decomposed in the Q and U Stokes parameters, which are related to the polarization amplitude P and to the angle clockwise from north α as [35]

$$P = \sqrt{Q^2 + U^2} \ , \qquad \alpha = \frac{1}{2}\tan^{-1}\left(\frac{U}{Q}\right) \ , \tag{3.21}$$

while the circular polarization V is assumed to be zero. It is however more intuitive to have a more geometrical decomposition, given by splitting the polarization into a curl-free (the *E-modes*) and a divergence-free component (the *B-modes*). More explicitly, Q and U are not rotationally invariant in the plane perpendicular to $\hat{\mathbf{n}}$, like the temperature, but their combinations $Q \pm iU$ behave like a spin-2 quantity, namely, under a rotation by an angle ψ they transform as

$$(Q \pm iU)'(\hat{\mathbf{n}}) = \mathrm{e}^{\mp 2i\psi}(Q \pm iU)(\hat{\mathbf{n}}) \ . \tag{3.22}$$

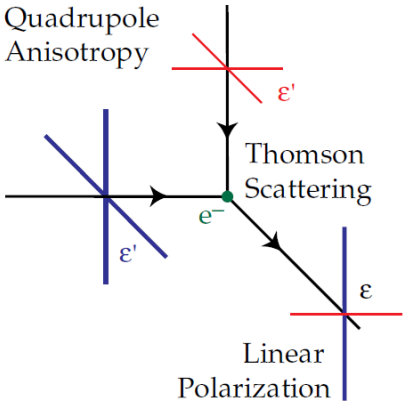

Figure 3.4: Generation of linear polarization from Thomson scattering of radiation with a quadrupole anisotropy. Blue and red lines represent hot and cold radiation, respectively [35].

We can therefore decompose them in spin-weighted spherical harmonics [95]:

$$(Q \pm iU)(\hat{\mathbf{n}}) = \sum_{\ell=0}^{\infty} \sum_{m=-\ell}^{\ell} a_{\ell m}^{(\pm 2)}\, Y_{\ell m}^{(\pm 2)}(\hat{\mathbf{n}})\,, \tag{3.23}$$

where $Y_{\ell m}^{(\pm 2)}$ are spin-(± 2) spherical harmonics. We then introduce the following convenient linear combinations

$$a_{\ell m}^{E} \equiv -\frac{1}{2}\left(a_{\ell m}^{(2)} + a_{\ell m}^{(-2)}\right) \tag{3.24}$$

$$a_{\ell m}^{B} \equiv i\,\frac{1}{2}\left(a_{\ell m}^{(2)} - a_{\ell m}^{(-2)}\right)\,, \tag{3.25}$$

to finally obtain the desired rotationally invariant quantities

$$E(\hat{\mathbf{n}}) = \sum_{\ell=0}^{\infty} \sum_{m=-\ell}^{\ell} a_{\ell m}^{E} Y_{\ell m}(\hat{\mathbf{n}})\,, \tag{3.26}$$

$$B(\hat{\mathbf{n}}) = \sum_{\ell=0}^{\infty} \sum_{m=-\ell}^{\ell} a_{\ell m}^{B} Y_{\ell m}(\hat{\mathbf{n}})\,. \tag{3.27}$$

The advantage of considering these quantities is that, whereas scalar perturbations source only E-modes, tensor ones produce both E-modes and B-modes, hence a detection of B-modes in the CMB polarization pattern provides a way to measure primordial gravitational waves and therefore to test inflation, which indeed predicts their existence. However, the expected signal within inflationary models still allowed by data is very weak,

making it necessary to have data cleaned to great accuracy from possible contamination, as the astrophysical signals, the foregrounds, or for example B-modes, which are also generated by gravitational lensing of E-modes; therefore such effects have to be carefully taken into account.

3.3.1 *TE*, *EE* and *BB* power spectra

Analogously to the case of the temperature anisotropy, it is possible to characterize the statistics of the CMB perturbations by defining their power spectra, either autospectra or cross-spectra. Out of all the possible 6 combinations, only 4 are non vanishing in the standard model,in fact the cross correlations BE and BT vanish because of the opposite parity of B with respect to E and T. Additionally to the two-point correlation function for the temperature (3.6), those for the polarizations are

$$\langle a^{E}_{\ell m} a^{E*}_{\ell' m'} \rangle = \delta_{\ell\ell'}\, \delta_{mm'}\, C^{EE}_{\ell} \ , \tag{3.28}$$

$$\langle a^{B}_{\ell m} a^{B*}_{\ell' m'} \rangle = \delta_{\ell\ell'}\, \delta_{mm'}\, C^{BB}_{\ell} \ , \tag{3.29}$$

$$\langle a^{T}_{\ell m} a^{E*}_{\ell' m'} \rangle = \delta_{\ell\ell'}\, \delta_{mm'}\, C^{TE}_{\ell} \tag{3.30}$$

and accordingly

$$C^{EE}_{\ell} = \frac{1}{2\ell+1} \sum_{m=-\ell}^{\ell} |a^{EE}_{\ell m}|^2 \ , \tag{3.31}$$

$$C^{BB}_{\ell} = \frac{1}{2\ell+1} \sum_{m=-\ell}^{\ell} |a^{BB}_{\ell m}|^2 \ , \tag{3.32}$$

$$C^{TE}_{\ell} = \frac{1}{2\ell+1} \sum_{m=-\ell}^{\ell} |a^{TE}_{\ell m}|^2 \ , \tag{3.33}$$

where just for a matter of notation we redefined $a^{T}_{\ell m} \equiv a_{\ell m}$.

In Figure 3.5 the EE power spectrum and the TE cross power spectrum are shown. They are both characterized by acoustic peaks due to the baryon-photon fluid oscillations, while the Sachs-Wolfe effect is absent for polarization and hence there is no plateau.
The TE one has a larger amplitude than the EE signal thanks to the correlation with the temperature and it can be positive or negative, since the polarization anisotropy comes from fluid velocity perturbations at last scattering and the latter can give positive or negative correlations with the temperature.
The peaks of the EE power spectrum are out of phase with those in the TT one, since polarization anisotropy is indeed sourced by fluid velocity. At $\ell < 10$, the observed excess signal arises from the Doppler shift during the reionization epoch and its amplitude gives additional information on when the first stars form.

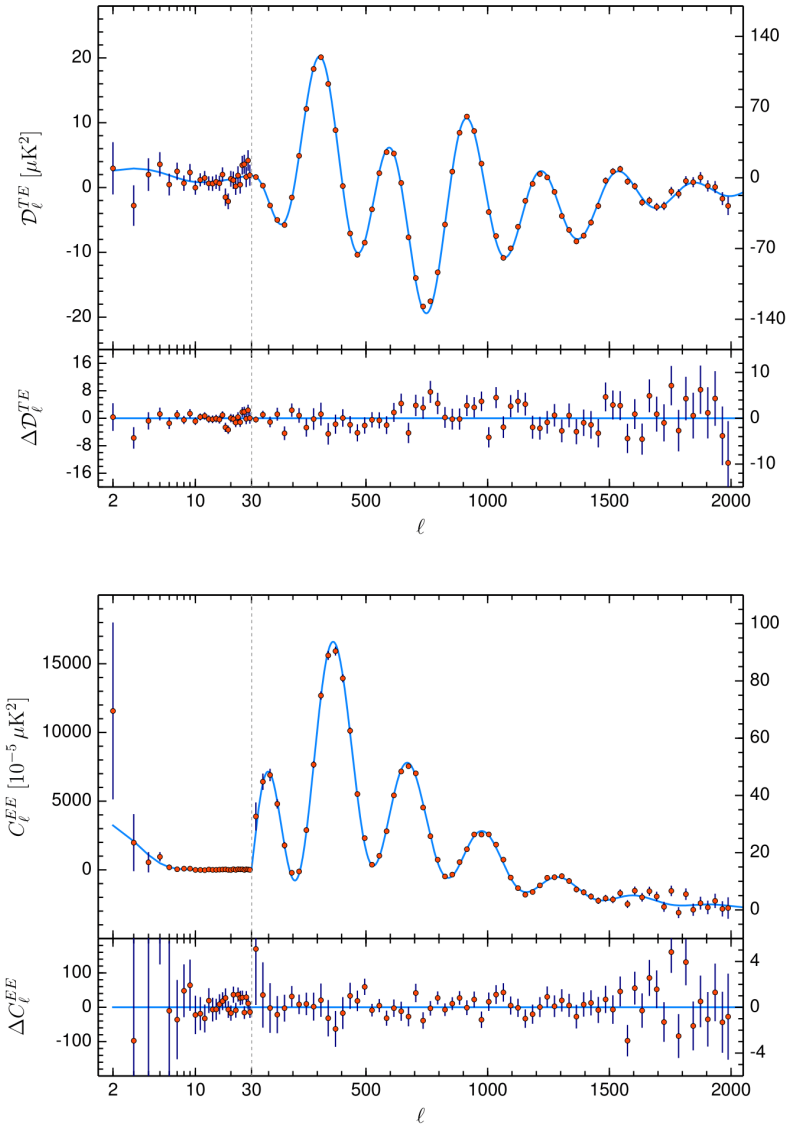

Figure 3.5: TE (*top*) and EE (*bottom*) power spectra and residuals in the lower panels [72].

Chapter 4

Second-order CMB

The linear cosmological perturbation theory, within the framework of general relativity, has been progressively developed in the last 40 years, reaching high levels of robustness and sophistication [3, 45, 67, 58, 54]. Describing the Universe with this first-order approximation proved to be a very successful approach and still allows performing predictions with an outstanding accuracy. Moreover, observations of the tiny CMB temperature fluctuations justify a linear treatment rather than higher-orders approaches, at least for most of the purposes. However, the focus of recent research is progressively shifting to the study of deviations from the standard picture, such as non-Gaussianity or non-adiabaticity. A second-order approach is then becoming an important opportunity to address these problems and gain further accuracy in the cosmological predictions. There are a lot of physical effects which a linear theory cannot predict [70]: a few examples are the generation of non-Gaussian signals in the CMB from the propagation of photons through an inhomogeneous Universe, spectral distortions due to the momentum transfer between photons and electrons through Compton scattering and generation of magnetic fields from vorticity at recombination. This last effect, in particular, is of particular interest for the purposes of this thesis. In fact, non-linear dynamics can generate vortical currents from the tiny difference between electron and proton velocity, then leading to a vortical electric field and, ultimately, to a magnetic field [34, 55]. Moreover, it has been recently proposed that the presence of primordial magnetic fields can induce small-scale non-linear baryon inhomogeneities which can considerably affect the recombination history and the average time of when it occurs [40]. These issues will be better explored in the next chapters.

The first study of relativistic cosmological perturbations at second order was performed by Tomita [89], who analyzed the growth of second-order density perturbations in synchronous gauge. Extensions to other gauges were then explored by Bruni et al. [13], Sonego and Bruni [83] and Matarrese et al. [56]. More recent works about second-order equations and gauge invariance can be instead found in [4, 71, 7, 59, 60].

As in Chapter 2, we mainly follow the notations and conventions of [70], where a

more detailed and complete discussion can be found.

4.1 Second-order perturbation theory

4.1.1 The formalism

The perturbative expansion (2.2) is now truncated at second order, so a generic cosmological field $X(t, \mathbf{x})$ now reads

$$X(t, \mathbf{x}) \simeq X^{(0)}(t) + \epsilon\, X^{(1)}(t, \mathbf{x}) + \epsilon^2\, X^{(2)}(t, \mathbf{x}) \ . \tag{4.1}$$

As in Chapter 2 we absorb the parameter ϵ into the definition of the perturbed variable, $\epsilon^n\, X^{(n)} \to X^{(n)}$, in order to improve the readability of the equations.

A generic function $f(X)$ is now expanded around $X^{(0)} \equiv \bar{X}$ as

$$f(X) \simeq f(\bar{X}) + \left(\frac{\partial f}{\partial X}\right)_{\bar{X}} (X - \bar{X}) + \frac{1}{2}\left(\frac{\partial^2 f}{\partial X^2}\right)_{\bar{X}} (X - \bar{X})^2 \tag{4.2}$$

and, after expanding $X \simeq X^{(0)} + X^{(1)} + X^{(2)}$, it can be rewritten order by order as

$$f(X)^{(0)} = f(\bar{X}) \ , \tag{4.3}$$

$$f(X)^{(1)} = \left(\frac{\partial f}{\partial X}\right)_{\bar{X}} X^{(1)} \ , \tag{4.4}$$

$$f(X)^{(2)} = \left(\frac{\partial f}{\partial X}\right)_{\bar{X}} X^{(2)} + \frac{1}{2}\left(\frac{\partial^2 f}{\partial X^2}\right)_{\bar{X}} X^{(1)} X^{(1)} \ . \tag{4.5}$$

Note that the expression for $f(X)^{(2)}$ contains a purely second-order part (the first term) and a quadratic part, which is formed by the product of two first-order perturbations (the second term).

4.1.2 The structure of equations at second order

Second-order equations can look quite intimidating at first sight, due to the appearance of numerous terms with respect to the linear case. However, it is possible to simplify the picture by noting the structure of equation (4.5). In fact, thanks to this property, any second-order equation can be always split in

- a *purely second-order part*, which is linear in the second-order perturbations;
- a *quadratic part*, which is composed of a product of couples of first-order perturbations.

Moreover, comparing equations (4.4) and (4.5), we see that the purely second-order part has the same structure of the linear one. Hence, a second-order equation can always be schematically represented as

$$\mathcal{G}^{(1)}\left[X^{(2)}\right] + \mathcal{S}\left[X^{(1)}X^{(1)}\right] = 0 \ , \tag{4.6}$$

where $\mathcal{G}^{(1)}$ is the first-order operator, *i.e.* the operator for which the linear equation is $\mathcal{G}^{(1)}[X^{(1)}] = 0$, and $\mathcal{S}$ represents the quadratic contribution, that is the product of first-order perturbations and acts as a time-dependent source term for the second-order structure. This peculiar property, which can be generalized at any perturbative order, hugely simplifies the treatment of higher-order equations: they always present the same structure of the linear equation, with in addition quadratic terms, whose evolution is however known from the equations at previous orders (which, in our case, are just the linear ones).

Despite this recursive structure of higher-order equations surely relieves the complexity of the non-linear framework, there are some issues which one has to face once he goes beyond linear theory; we shall now discuss some of them.

4.1.3 SVT decomposition and mode coupling

In Sec. 2.2.1 we introduced the projection vectors $\xi^{i}_{[m]}$ and matrices $\chi^{ij}_{2,[m]}$, with which we were able to decompose any generic spacetime tensor and consequently the Einstein and Boltzmann equations in scalar ($m = 0$), vector ($m = \pm 1$) and tensor ($m = \pm 2$) components, through what is known as SVT decomposition. Moreover, we saw that in linear theory these components never mix, that is we can always solve the equations separately for scalar, vector and tensor perturbations. This nice property, however, does not hold at second and higher orders and one cannot in principle decouple different azimuthal modes m. This issue comes directly from the non-linear nature of the quadratic sources, which allow different kind of modes to source each other (a few explicit examples will be shown in the next sections). Nevertheless, from a practical point of view, it is still possible to solve the second-order Einstein and Boltzmann equations separately for scalar, vector and tensor modes. In fact, the linear structure of the second-order equations is the same of the one of first-order equations and hence it is decoupled in m. The mixing of the different modes is all contained in the quadratic terms, which however can be previously computed by solving the linear equations, which in turn are decoupled in m; therefore, we are still always able to solve the equations separately for scalar, vector and tensor modes, even at second order.

The presence of quadratic terms introduces another kind of complexity to the second-order equations. In fact, when going to Fourier space, we have now to deal with the Fourier transform of products of first-order perturbations, which is not obtained by just applying the transformation to the two multiplying factors but is given by a convolution.

Let $A(\mathbf{x})B(\mathbf{x})$ be a generic quadratic term, its Fourier transform leads to the following convolution integral:

$$\begin{aligned}\mathcal{F}_{\mathbf{k}}[A(\mathbf{x})B(\mathbf{x})] &= \int \frac{\mathrm{d}\mathbf{k_1}}{(2\pi)^3}\, A(\mathbf{k_1})\, B(\mathbf{k}-\mathbf{k_1}) \\ &= \int \frac{\mathrm{d}\mathbf{k_1}\mathrm{d}\mathbf{k_2}}{(2\pi)^3}\, A(\mathbf{k_1})\, B(\mathbf{k_2})\, \delta(\mathbf{k}-\mathbf{k_1}-\mathbf{k_2})\ , \end{aligned} \tag{4.7}$$

where the Dirac delta $\delta(\mathbf{k}-\mathbf{k_1}-\mathbf{k_2})$ forces the three wavevectors $\mathbf{k}$, $\mathbf{k_1}$, $\mathbf{k_2}$ to form a triangle. The crucial thing to note is that the evolution of the wavemode $\mathbf{k}$ of a second-order perturbation is affected by the evolution of all other modes $\mathbf{k_1}$, which means that perturbations at different scales influence each other. This is completely different from the linear case, where all the modes $\mathbf{k}$ evolve independently, and such property of the non-linear theory is known as *mode coupling*.

In what follows, we will often denote with $A_1 \equiv A(\mathbf{k_1})$ and $B_2 \equiv B(\mathbf{k_2})$ the first-order perturbations appearing in the quadratic terms, while for the convolution integral we will adopt the notation

$$\mathcal{K}\{f\} \equiv \int \frac{\mathrm{d}\mathbf{k_1}\mathrm{d}\mathbf{k_2}}{(2\pi)^3}\, f(\mathbf{k_1},\mathbf{k_2})\, \delta(\mathbf{k}-\mathbf{k_1}-\mathbf{k_2})\ . \tag{4.8}$$

4.2 Second-order Einstein equations

It is now the moment to address the second-order Einstein equations, which take the form

$$\delta G^{\mu}{}_{\nu} = 8\pi G\, \delta T^{\mu}{}_{\nu}\ . \tag{4.9}$$

We then project them in their scalar, vector and tensor components in the same way of Sec. 2.3.

The form of the metric is still the one in equation (2.6), but now the metric perturbations are expanded as $X = X^{(1)} + X^{(2)}$; hence, its components up to second order read

$$g_{00} = -a^2(1 + 2\Psi^{(1)} + 2\Psi^{(2)})\ , \tag{4.10}$$

$$g_{0i} = g_{i0} = a^2\omega_i^{(2)}\ , \tag{4.11}$$

$$g_{ij} = a^2(1 - 2\Phi^{(1)} - 2\Phi^{(2)})\delta_{ij} + 2a^2\gamma_{ij}^{(2)}\ , \tag{4.12}$$

where now we can notice the appearance, at second order, of the vector and tensor perturbations, whose linear parts are assumed to be zero; for this reason, the second-order Einstein and Boltzmann equations will be written not only for scalar, but also for vector and tensor perturbations. Enforcing again the Newtonian gauge, we have that $\partial^i\omega_i = 0$ and $\partial^j\gamma_{ij} = 0$, which leads to 6 degrees of freedom (remember that γ_{ij} is

traceless by construction). The variables $\omega_i^{(2)}$ and $\gamma_{ij}^{(2)}$ are further decomposed in scalar, vector and tensor components through $\xi^i_{[m]}$ and $\chi^{ij}_{2,[m]}$, respectively, hence getting

$$\omega^{(2)}_{[m]} = \xi^i_{[m]}\,\omega_i^{(2)} \ , \quad \gamma^{(2)}_{[m]} = \chi^{ij}_{2,[m]}\,\gamma_{ij}^{(2)} \ . \tag{4.13}$$

The Newtonian gauge conditions, in Fourier space and aligning $\mathbf{k}$ along the zenith, then imply $\omega^{(2)}_{[0]} = 0$ and $\gamma^{(2)}_{[0]} = \gamma^{(2)}_{[\pm1]} = 0$.

Let us now focus on the energy-momentum tensor. Using the same parametrization in terms of fluid variables as in equation (2.14), its components, expanded up to second order, read

$$\begin{aligned}
T^0{}_0 &= -\rho - (\bar\rho + \bar P)V^iV_i \ , \\
T^i{}_0 &= -(\rho + P)(1+\Psi)V^i \ , \\
T^0{}_i &= (\rho + P)(1+\Psi+2\Phi)(V^i + \omega^i) \ , \\
T^i{}_j &= \delta^i{}_j P + \Sigma^i{}_j + (\bar\rho + \bar P)V^iV^j \ ,
\end{aligned} \tag{4.14}$$

where $V^i \equiv a\,U^i$, $\rho = \bar\rho + \delta\rho^{(1)} + \delta\rho^{(2)}$ and $P = \bar P + \delta P^{(1)} + \delta P^{(2)}$, the last two being the only quantities to possess a background value. We note that, at second order, the EMT components acquire also metric variables.

The SVT decomposition of the EMT, up to second order, leads to

$$\begin{aligned}
T^0{}_0 &= -\rho - (\bar\rho + \bar P)V^iV_i \ , \\
T^i{}_i &= 3P + (\bar\rho + \bar P)V_iV^i \ , \\
\xi^i_{[m]}T_{i0} &= -(\rho + P)(1+\Psi)V_{[m]} \ , \\
\chi^{ij}_{2,[m]}T_{ij} &= \Sigma_{[m]} + (\bar\rho + \bar P)\,(VV)_{[m]} \ ,
\end{aligned} \tag{4.15}$$

where $(VV)_{[m]} = \chi^{ij}_{2,[m]}V_iV_j$ and $V_{[m]} = \xi^i_{[m]}V_i$. Now we explicitly see the mixing of different azimuthal modes in the quadratic terms, such as the term $\Psi\,V_{[m]}$ which mixes the scalar potential Ψ with vector (for $m = \pm1$) or tensor (for $m = \pm2$) velocity perturbation $V_{[m]}$. We should finally remark that every quadratic term always involves the product of two first-order perturbations, hence Ψ, Φ and V^i are always meant to be first-order variables, in both (4.14) and (4.15).

We have now all the ingredients to write the Einstein equations at second order in perturbation theory, after having inserted the SVT decomposed components of the metric and the EMT in equation (4.9) and projected in Fourier space. In what follows, we omit the dependence on the wavemode $\mathbf{k}$ for the purely second-order quantities and also the order of perturbations, since any variable which appears alone in the equations is always a second-order one, while two perturbations which multiply each other are necessarily first-order variables. In doing the spherical decomposition, we align the wavemode $\mathbf{k}$ with the zenith. We also collect all the quadratic terms into the symbols $\mathcal{Q}$, in order to

clearly visualize the purely second-order structure of the equations (which we remember is the same of that of linear equations) and give their explicit expressions separately.

- Time-Time equation (TT):

$$6\mathcal{H}^2\Psi + 6\mathcal{H} + 2k^2\Phi + \mathcal{Q}_{\rm TT} = 8\pi G a^2\, \delta T^0{}_0 \ . \tag{4.16}$$

- TRace equation (TR):

$$6\ddot{\Phi} + \Psi(6\mathcal{H}^2 + 12\dot{\mathcal{H}}) + 6\mathcal{H}(\dot{\Psi} + 2\dot{\Phi}) + 2k^2(\Phi - \Psi) + \mathcal{Q}_{\rm TR} = 8\pi G a^2\, \delta T^i{}_i \ . \tag{4.17}$$

- Space-Time equations (ST):

$$-2k(\dot{\Phi} + \mathcal{H}\Psi) + \mathcal{Q}_{\rm ST[0]} = 8\pi G a^2\, (i\xi^i_{[0]}\delta T_{i0}) \ , \tag{4.18}$$

$$\frac{i}{2}\omega_{[\pm1]}(4\mathcal{H}^2 - 4\dot{\mathcal{H}} + k^2) + \mathcal{Q}_{\rm ST[\pm1]} = 8\pi G a^2\, (i\xi^i_{[\pm1]}\delta T_{i0}) \ . \tag{4.19}$$

- Space-Space equations (SS):

$$-\frac{2k^2}{3}(\Phi - \Psi) + \mathcal{Q}_{\rm SS[0]} = 8\pi G a^2\, (\chi^{ij}_{2,[0]} T_{ij}) \ , \tag{4.20}$$

$$-\frac{ik}{\sqrt{3}}(\dot{\omega}_{[\pm1]} + 2\mathcal{H}\omega_{[\pm1]}) + \mathcal{Q}_{\rm SS[\pm1]} = 8\pi G a^2\, (\chi^{ij}_{2,[\pm1]} T_{ij}) \ , \tag{4.21}$$

$$\ddot{\gamma}_{[\pm2]} + 2\mathcal{H}\dot{\gamma}_{[\pm2]} + k^2\gamma_{[\pm2]} + \mathcal{Q}_{\rm SS[\pm2]} = 8\pi G a^2\, (\chi^{ij}_{2,[\pm2]} T_{ij}) \ . \tag{4.22}$$

As in the linear case, the energy-momentum tensor is meant to be the sum of the EMTs of the single species, that is photons, neutrinos, baryons and cold Dark Matter. Note also that the four scalar equations have exactly the same structure of the first order ones (2.17)-(2.20), if the quadratic terms are set to zero.

The quadratic terms for the second-order Einstein equations, defined as

$$\begin{aligned} &\mathcal{Q}_{\rm TT} = a^2\, G^{0\,(1)(1)}_{\quad 0} \ , && \mathcal{Q}_{\rm TR} = a^2\, G^{i\,(1)(1)}_{\quad i} \ , \\ &\mathcal{Q}_{\rm ST[m]} = i\xi^i_{[m]}\, a^2\, G^{(1)(1)}_{i0} \ , && \mathcal{Q}_{\rm SS[m]} = \chi^{ij}_{2,[m]}\, a^2\, G^{(1)(1)}_{ij} \ , \end{aligned} \tag{4.23}$$

have the following explicit expressions:

$$\mathcal{Q}_{\rm TT} = -12\mathcal{H}^2\,\Psi_1\Psi_2 + (3\mathbf{k_1}\cdot\mathbf{k_2} + 4k_1^2 + 4k_2^2)\,\Phi_1\Phi_2 + 12\mathcal{H}\Phi_2'\,(\Phi_1 - \Psi_1) - 3\Phi_1'\Phi_2' \ ,$$

$$\begin{aligned}\mathcal{Q}_{\rm TR} = &-12\Psi_1\Psi_2(\mathcal{H}^2 + 2\mathcal{H}') + (k^2 + k_1^2 + k_2^2)\,\Psi_1\Psi_2 \\ &+ (3\mathbf{k_1}\cdot\mathbf{k_2} + 4k_1^2 + 4k_2^2)\,\Phi_1\Phi_2 + (2\mathbf{k_1}\cdot\mathbf{k_2} - 4k_2^2)\,\Phi_1\Psi_2 \\ &+ 12(\Phi_2'' + 2\mathcal{H}\Phi_2')\,(\Phi_1 - \Psi_1) - 6\Psi_2''\,(4\mathcal{H}\Psi_1 + \Phi_1') + 3\Phi_1'\Phi_2' \ ,\end{aligned}$$

$$\mathcal{Q}_{{\rm ST}[m]} = 2k_{1[m]}\left[2\mathcal{H}\Psi_1\,(\Psi_2 - \Phi_2) - 2\Phi_1\Phi_2' - 4\Phi_1'\Phi_2 + \Psi_1\Phi_2'\right] \ ,$$

$$\mathcal{Q}_{{\rm SS}[m]} = (k_1k_2)_{[m]}\left[2\Phi_1\Psi_2 - 3\Phi_1\Phi_2 - \Psi_1\Psi_2\right] + (k_1k_1)_{[m]}\left[2\Psi_1\Phi_2 - 4\Phi_1\Phi_2 - 2\Psi_1\Psi_2\right] \ . \tag{4.24}$$

The wavemodes $\mathbf{k_1}$ and $\mathbf{k_2}$ are dummy variables which are integrated out by the convolution integral.

4.3 Second-order Boltzmann equations

We remind that the Boltzmann equation for the different species completes the information given by the Einstein equations, accounting for interactions among particles and providing the evolution of the EMTs. It mathematically determines how the distribution function f of a given species changes in the phase space, according to

$$\frac{{\rm d}f}{{\rm d}\tau} = \mathcal{C}[f] \ , \tag{4.25}$$

where the collision term $\mathcal{C}[f]$ encodes the information about the interactions in which the species is involved.

At second order, a lot of extra quadratic terms appear, introducing additional effects which are absent at linear order. In fact, let us rewrite the Boltzmann equation in the form of (2.24),

$$\frac{\partial f}{\partial\tau} + \frac{\partial f}{\partial x^i}\frac{{\rm d}x^i}{{\rm d}\tau} + \frac{\partial f}{\partial p}\frac{{\rm d}p}{{\rm d}\tau} + \frac{\partial f}{\partial n^i}\frac{{\rm d}n^i}{{\rm d}\tau} = \mathcal{C}[f] \ . \tag{4.26}$$

If we consider the photon distribution function, we have that the left hand side of the above equation (the Liouville term) contains all the key effects which produce the observed CMB anisotropy. The first two terms (*free streaming*) account for the propagation of perturbations from small to large multiples; at higher order, they also include gravitational time delay effects. The third term (*redshift*) encodes, at background level, the redshifting of photons and, at higher orders, the SW, ISW and Rees-Sciama effects. The

fourth term (*lensing*) vanishes at linear order, while at higher order describes small-scale gravitational lensing.

As in Chapter 2, we use the formalism of beta-moments, defined through equation (2.26), namely

$$1 + {}_n\Delta(\tau, \mathbf{x}, \hat{\mathbf{n}}) \equiv \frac{1}{\int \mathrm{d}p\, p^3 f^{(0)}(\tau, p)} \int \mathrm{d}p\, p^3 \left(\frac{p}{E}\right)^{n-1} f(\tau, \mathbf{x}, p, \hat{\mathbf{n}}) \ , \tag{4.27}$$

and the β_n operator is defined as $\beta_n[f] = 1 + {}_n\Delta$. Further projections in Fourier and multipole spaces lead to

$$\begin{aligned} {}_n\Delta_{\ell m}(\tau, \mathbf{k}) &\equiv (\mathcal{F}_k \circ L_{\ell m} \circ \beta_n)[f] \\ &= i^\ell \sqrt{\frac{2\ell+1}{4\pi}} \int \mathrm{d}^3x\, \mathrm{d}\Omega\, e^{-i\mathbf{k}\cdot\mathbf{x}}\, Y^*_{\ell m}(\hat{\mathbf{n}})\, {}_n\Delta(\tau, \mathbf{x}, \hat{\mathbf{n}}) \ . \end{aligned} \tag{4.28}$$

The projected Boltzmann equation then reads

$$(\mathcal{F}_k \circ L_{\ell m} \circ \beta_n) \left[\frac{\mathrm{d}f}{\mathrm{d}\tau} - \mathcal{C}[f]\right] = 0 \ , \tag{4.29}$$

which, as already explained in Chapter 2, is remarkably easier to solve than the original one.

The beta-moment formalism has the great merit of describing relativistic (photons and neutrinos) and non-relativistic (baryons and CDM) species in the same way, since the former case is recovered by just setting $n = 1$ ($p/E = 1$), while the latter is in agreement with the fact that only the first moments are relevant ($p/E \ll 1$), as one can see in equation (4.27). Following the same notations as in (2.32), the relations with the fluid variables, up to second order, for fluids with equation of state $\omega = P/\rho =$ constant are the following:

$$\begin{aligned} {}_0\Delta_{00} &= \delta + (\omega+1)\, v^i v_i \ , \\ {}_1\Delta_{1m} &= 3\,(\omega+1)\, i v_{[m]}\, (1+\delta) \ , \\ 1 + {}_2\Delta_{00} &= 3\,\omega\,(1+\delta) + (\omega+1)\, v^i v_i \ , \\ {}_2\Delta_{2m} &= -\frac{15}{2}\left[\frac{\Sigma_{[m]}}{\bar{\rho}} + (\omega+1)\,(vv)_{[m]}\right] \ , \end{aligned} \tag{4.30}$$

where $(vv)_{[m]} = \chi^{ij}_{2,[m]} v_i v_j$. The quadratic terms represent the Lorentz boosts that brings the observer (which is chosen to be at constant spatial coordinates) to be at rest with the fluid, since ρ and P are defined in the comoving frame of the fluid. The relation $P = \omega\rho$, up to second order, reads

$$P(\rho) = \bar{\rho}\left[\omega + \delta\, c_s^2 + \frac{\rho}{2}\frac{\partial c_s^2}{\partial \rho}\,\delta^2\right] \ . \tag{4.31}$$

We can now express the second-order Boltzmann equations for photons, neutrinos, baryons and CDM. As already did for the Einstein equations and for the same reason, we drop the the suffix of the perturbative order.

4.3.1 Photons

Following the same arguments as in Sec. 2.4.1, the photon distribution function is now expanded up to second order as

$$f_\gamma = f_\gamma^{(0)} - p\,\frac{\partial f_\gamma^{(0)}}{\partial p}\,\Theta + \left(\frac{p^2}{2}\frac{\partial^2 f_\gamma^{(0)}}{\partial p^2} + \frac{\partial f^{(0)}}{\partial p}\right)\Theta^2 \,, \tag{4.32}$$

where now $\Theta = \Theta^{(1)} + \Theta^{(2)}$. The relation between the brightness perturbation Δ and the temperature fluctuation Θ, at second order, is not just $\Delta = 4\Theta$, but reads

$$\Delta = 4\,\Theta + 6\,\Theta\Theta \quad \Longleftrightarrow \quad \Theta = \frac{1}{4}\Delta - \frac{3}{32}\Delta\Delta \,. \tag{4.33}$$

We denote again with $\mathcal{I}_m^\ell(\mathbf{k}) = (\mathcal{F}_k \circ L_{\ell m} \circ \beta)[f_\gamma]$ the brightness multipoles for photons, we drop the $\mathbf{k}$ dependence in the purely second-order terms and we define $\tilde{\omega}_i \equiv i\omega_i$ and $u^i \equiv iv^i$ (relative to baryons), in order to absorb the imaginary factors. For the expansion in spherical harmonics, the wavemode $\mathbf{k}$ is chosen to be aligned with the zenith. For what concerns the quadratic terms, instead, we group them in $L_{\ell m}\big[\mathcal{Q}_\mathcal{I}^L\big]$ and $L_{\ell m}\big[\mathcal{Q}_\mathcal{I}^\mathcal{C}\big]$, for the Liouville and collision terms respectively.

The second-order Boltzmann equation for photons then reads

$$\begin{aligned}
&\big(\mathcal{I}_m^\ell\big)' + k\big(A_m^\ell\,\mathcal{I}_m^{\ell+1} - B_m^\ell\,\mathcal{I}_m^{\ell-1}\big) - \delta_{\ell 0}\,4\,\Phi' \\
&\qquad - 4\delta_{\ell 1}\left(\delta_{m0}\,k\,\Psi - \delta_{m1}\,\tilde{\omega}_{[1]}'\right) - \delta_{\ell 2}\,\delta_{m2}\,4\,\gamma_{[m]}' + L_{\ell m}\big[\mathcal{Q}_\mathcal{I}^L\big] \\
&\qquad = \kappa'\big(-\mathcal{I}_m^\ell + \delta_{\ell 0}\,\mathcal{I}_0^0 + \delta_{\ell 1}\,4\,u_{[m]} + \delta_{\ell 2}\,\Pi_m\big) + L_{\ell m}\big[\mathcal{Q}_\mathcal{I}^\mathcal{C}\big] \,,
\end{aligned} \tag{4.34}$$

where we have defined

$$\Pi_m = \frac{1}{10}\left(\mathcal{I}_m^2 - \sqrt{6}\,\mathcal{E}_m^2\right) \,, \tag{4.35}$$

and $\mathcal{E}_m^\ell$ are the multipoles associated to the E-mode polarization (for the second-order Boltzmann equations of the E-modes and B-modes, see [70]). The quantities A_m^ℓ and B_m^ℓ are just numerical coefficients, defined as

$$A_m^\ell = \frac{\sqrt{(\ell+1)^2 - m^2}}{2\ell+3} \,, \quad B_m^\ell = \frac{\sqrt{\ell^2 - m^2}}{2\ell - 1} \,. \tag{4.36}$$

It is possible to check that the Boltzmann equations for $m = 0$ and with vanishing quadratic sources coincides with the one given in Sec. 2.4.1 (equations (2.38)-(2.41)),

which is the direct consequence of having the purely second-order structure equal to the one of linear equations; it also implies that m modes are not mixed without quadratic terms (but this would not be true anymore if we choose the wavemode $\mathbf{k}$ not aligned with the polar axis).

The quadratic terms are a convolution integral over $\mathbf{k_1}$ and $\mathbf{k_2}$. In what follows, the expressions we will give are meant to be the kernel of this convolution and omit the sign of integration over the two dummy variables and the Dirac delta $\delta(\mathbf{k}-\mathbf{k_1}-\mathbf{k_2})$ (see equation (4.8)). We also assume that in any product the first variable is a function of $\mathbf{k_1}$, while the second one is a function of $\mathbf{k_2}$. We then introduce the indices m_1 and $m_2 = m - m_1$ and implicitly assume a sum over $m_1 = -1, 0, +1$. The expressions for the coupling coefficients C and R can be found in Appendix B.

The expressions of the quadratic sources for the Liouville and collision terms, respectively, are

$$\begin{aligned} L_{\ell m}\big[\mathcal{Q}^L_{\mathcal{I}}\big] =& \sum_{\pm} \pm(\Psi+\Phi)\, k_2^{[m_2]} \mathcal{I}^{\ell\pm1}_{m1}\, C^{\pm,\ell}_{m_1 m} \\ &+ 4\bigg[-\Phi'\,\mathcal{I}^{\ell}_{m} + \sum_{\pm} \pm k_1^{[m_2]}\,\Psi\,\mathcal{I}^{\ell\pm1}_{m_1}\, C^{\pm,\ell}_{m_1 m} - \delta_{\ell 0}\, 2\,\Phi'\Phi - \delta_{\ell 1}\, k_1^{[m]}\,\Psi\,(\Phi-\Psi)\bigg] \\ &+ \sum_{\pm} \pm k_1^{[m_2]}\,(\Psi+\Phi)\,\mathcal{I}^{\ell\pm1}_{m_1}\, R^{\pm,\ell}_{m_1 m}\ , \end{aligned} \tag{4.37}$$

$$\begin{aligned} L_{\ell m}\big[\mathcal{Q}^{\mathcal{C}}_{\mathcal{I}}\big] =& \left(\Psi + \delta_b + \frac{x_e^{(1)}}{\bar{x}_e}\right)\mathcal{C}_{\ell m}\big[\mathcal{I}\big] + \kappa'\, u^{[m_2]}\bigg\{ \sum_{\pm} \mp \mathcal{I}^{\ell\pm1}_{m_1}\, C^{\pm,\ell}_{m_1 m} \\ &+ \delta_{\ell 0}\left(2\,\mathcal{I}^1_{m_1} - 4\,u^{m_1}\right) C^{+.0}_{m_1 m} + \delta_{\ell 1}\, 3\,\mathcal{I}^0_{m_1}\, C^{-,1}_{m_1 m} \\ &+ \delta_{\ell 2}\left(7\,u^{[m_1]} - \frac{1}{2}\mathcal{I}^1_{m_1}\right) C^{-,2}_{m_1 m} + \delta_{\ell 3}\, 5\,\Pi_{m_1}\, C^{-,3}_{m_1 m}\bigg\}\ . \end{aligned} \tag{4.38}$$

The quantities $\bar{x}_e$ and $x_e^{(1)}$ are the background and first-order ionization fraction, for which the density of free electrons n_e is $n_e = N_e\, x_e$, with N_e being the density of all electrons. The quadratic Liouville term (equation (4.37)), is written in such a way that the free-streaming, redshift and lensing contributions are contained in the first, second and third lines, respectively.

4.3.2 Neutrinos

As in the linear case, (massless) neutrinos obey the same Boltzmann equation, with the only difference of having vanishing collision term. Using the same definitions and conventions for the case of photons and denoting with $\mathcal{N}^\ell_m$ the multipoles of neutrinos,

it is straightforward to write

$$\begin{aligned}\big(\mathcal{N}^\ell_m\big)' + k\big(A^\ell_m\,\mathcal{N}^{\ell+1}_m - B^\ell_m\,\mathcal{N}^{\ell-1}_m\big) - \delta_{\ell 0}\,4\,\Phi' \\ - 4\delta_{\ell 1}\left(\delta_{m0}\,k\,\Psi - \delta_{m1}\,\tilde{\omega}'_{[1]}\right) - \delta_{\ell 2}\,\delta_{m2}\,4\,\gamma'_{[m]} + L_{\ell m}\big[\mathcal{Q}^L_{\mathcal{N}}\big] = 0\ .\end{aligned}$$

The quadratic Liouville term reads

$$\begin{aligned}L_{\ell m}\big[\mathcal{Q}^L_{\mathcal{N}}\big] =& \sum_{\pm} \pm(\Psi+\Phi)\,k_2^{[m_2]}\mathcal{N}^{\ell\pm1}_{m1}\,C^{\pm,\ell}_{m_1 m} \\ &+ 4\Bigg[-\Phi'\,\mathcal{N}^\ell_m + \sum_{\pm}\pm k_1^{[m_2]}\,\Psi\,\mathcal{N}^{\ell\pm1}_{m_1}\,C^{\pm,\ell}_{m_1 m} - \delta_{\ell 0}\,2\,\Phi'\Phi - \delta_{\ell 1}\,k_1^{[m]}\,\Psi\,(\Phi-\Psi)\Bigg] \\ &+ \sum_{\pm}\pm k_1^{[m_2]}\,(\Psi+\Phi)\,\mathcal{N}^{\ell\pm1}_{m_1}\,R^{\pm,\ell}_{m_1 m}\ .\end{aligned} \tag{4.39}$$

4.3.3 Baryons

For baryons, being non-relativistic and treated as pressureless perfect fluid, the only beta-moments which survive are the $n=0$ and $n=1$ ones. At second order, denoting them with ${}_nb^\ell_m$, their evolution is governed by the following Boltzmann equations:

$$\big({}_0b^0_0\big)' = -\,\mathcal{H}{}_2b^0_0 - \frac{k}{3}{}_1b^1_0 + 3\Phi' - (L_{00}\circ\beta_0)\big[\mathcal{Q}^L_b\big] - r\,\mathcal{C}\big[\mathcal{I}\big]_{00}\ , \tag{4.40}$$

$$\begin{aligned}\big({}_1b^1_m\big)' =& -\,\mathcal{H}_1b^1_0 + k\left(B^1_m\,{}_2b^0_0 - A^1_m\,{}_2b^2_m\right) - \big(L_{1m}\circ\beta_1\big)\big[\mathcal{Q}^L_b\big] \\ &+ 3\,\delta_{m0}\,k\,\Psi - 3\,\delta_{m1}\left(\tilde{\omega}'_{[1]} + \mathcal{H}\,\tilde{\omega}_{[1]}\right) - r\,\mathcal{C}\big[\mathcal{I}\big]_{1m}\ ,\end{aligned} \tag{4.41}$$

where $r=\bar{\rho}_\gamma/\bar{\rho}_b$ and $\mathcal{C}\big[\mathcal{I}\big]_{\ell m}$ is the collision term for the photons (the right hand side of equation (4.34)).

Note that in the above equations we should also know the values of ${}_2b^0_0$ and ${}_2b^2_m$, *i.e.* the evolution of the $n=2$ moment would be needed to. However, since baryons are assumed to be a perfect fluid, the anisotropic stress vanishes; hence, from equation (4.30), we see that we are allowed to simply set

$${}_2b^0_0 = v^i v_i \quad\text{and}\quad {}_2b^2_m = -\frac{15}{2}\,(vv)_{[m]}\ . \tag{4.42}$$

Thus, since the velocities forming the quadratic terms are already known from the first-order equations, we do not really need any higher moment than $n=1$.

The expressions for the quadratic Liouville terms are the following:

$$(L_{00}\circ\beta_0)\big[\mathcal{Q}^L_b\big] = \mathbf{k_1}\cdot\mathbf{k_2}\,(\Psi-\Phi)\,v + k_2^2\,(\Phi+\Psi)\,v + 3\,\Phi'(\delta_b + 2\,\Phi)\ , \tag{4.43}$$

$$(L_{1m}\circ\beta_1)\big[\mathcal{Q}^L_b\big] = 3\,k_1^{[m]}\,(\delta_b\Psi - 4v\,\Phi' + \Phi\Psi) - 3\,\Psi\Psi\,(k_1^{[m]} + k_2^{[m]})\ . \tag{4.44}$$

4.3.4 Cold Dark Matter

Cold Dark Matter behaves like baryons and hence is governed by the same equations, but since it interacts only gravitationally with other species, the collision term is now zero.

Thus, denoting with ${}_nc_m^\ell$ its multipoles, we simply have

$$\left({}_0c_0^0\right)' = -\,\mathcal{H}\,{}_2c_0^0 - \frac{k}{3}\,{}_1c_0^1 + 3\Phi' - \left(L_{00}\circ\beta_0\right)\left[\mathcal{Q}_c^L\right] \,, \tag{4.45}$$

$$\begin{aligned}\left({}_1c_m^1\right)' = &-\,\mathcal{H}\,{}_1c_0^1 + k\left(B^1_{m\,2}c_0^0 - A^1_{m\,2}c_m^2\right) - \left(L_{1m}\circ\beta_1\right)\left[\mathcal{Q}_c^L\right] \\ &+ 3\,\delta_{m0}\,k\,\Psi - 3\,\delta_{m1}\left(\tilde{\omega}'_{[1]} + \mathcal{H}\,\tilde{\omega}_{[1]}\right) \,,\end{aligned} \tag{4.46}$$

with the quadratic part being the same of that of baryons.

4.4 Initial conditions for second-order perturbations

We assume adiabatic initial conditions for scalar modes ($m = 0$) and vanishing initial conditions for vector and tensor ones ($m \neq 0$). As in the linear case, all the fluids share a common velocity field, $v_{[0]}$, but now the relation between the energy density contrasts of the different species up to second order reads

$$\delta_m = \frac{3}{4}\delta_r - \frac{3}{16}\delta_r^2 \quad \Longleftrightarrow \quad \delta_r = \frac{4}{3}\delta_m + \frac{4}{9}\delta_m^2 \,. \tag{4.47}$$

with δ_r referring to either δ_γ or δ_ν, and δ_m to either δ_b or δ_c. It should be remarked that now we mean $\delta = \delta^{(1)} + \delta^{(2)}$ and $\delta^2 = \delta^{(1)}\delta^{(1)}$.

Thus, the adiabatic initial conditions for the cosmological perturbations up to second order are the following:

$$\mathcal{I}_0^0 = \mathcal{N}_0^0 = -2\,\Psi + 4\,\Psi\Psi \,, \quad {}_0b_0^0 = {}_0c_0^0 = \frac{3}{4}\left(\mathcal{I} - \frac{1}{4}\mathcal{I}_0^0\mathcal{I}_0^0\right) \,, \tag{4.48}$$

$$u_{[0]} = \left\{2\,\frac{k}{\mathcal{H}}\left[\Psi - \frac{\mathcal{Q}_{\mathrm{ST}[0]}}{2k\mathcal{H}}\right] - u_{[0]}\left(3\,\Omega_m\,\delta_m + 4\Omega_r\,\delta_r\right)\right\}\frac{1}{3\,\Omega_m + 4\,\Omega_r} \,, \tag{4.49}$$

$$\mathcal{I}_0^2 = -10\,(vv)_{[0]} \,, \quad \mathcal{N}_0^2 = \frac{2}{3}\,(k\tau)^2\,\Psi + \mathcal{Q}_{\mathcal{N}_2} \,, \tag{4.50}$$

$$\left[1 + \frac{4}{15}\,\Omega_\nu\right]\Psi = \frac{2}{3}\left[-\,\zeta + \frac{1}{2}\,\Psi^2 - \Phi^2 + \mathcal{Q}^B\right] \,, \tag{4.51}$$

$$\Phi = \left[1 + \frac{2}{5}\,\Omega_\nu\right]\Psi - \mathcal{Q}^B \,, \tag{4.52}$$

where $u_{[0]} = i\, v_{[0]}$, $\Omega_r = \Omega_\gamma + \Omega_\nu$, $\Omega_m = \Omega_b + \Omega_c$ and

$$\mathcal{Q}_{\mathcal{N}_2} \equiv (k\tau)^2 \left(\frac{4}{3}\,\Psi^2 - \frac{1}{3}\,\frac{L_{10}\big[\mathcal{Q}^L_{\mathcal{N}}\big]}{k} - \frac{1}{2}\,\frac{L_{20}\big[\mathcal{Q}^L_{\mathcal{N}}\big]}{k^2\tau} \right) , \tag{4.53}$$

$$\mathcal{Q}^B \equiv \frac{3}{2k^2}\,\mathcal{Q}_{\mathrm{SS}[0]} - \frac{3}{5}\frac{1}{(k\tau)^2}\left[\Omega_\gamma\,\mathcal{I}^2_0 + \Omega_\nu\,\mathcal{Q}_{\mathcal{N}_2}\right] . \tag{4.54}$$

Since the Boltzmann equations given in the previous sections evolve the dipoles and not the velocities, we give the expressions for the former in terms of the common velocity field $v_{[0]}$, that is

$$\mathcal{I}^1_0 = \mathcal{N}^1_0 = 4\,i\left(v_{[0]} + \delta_r\, v_{[0]}\right) , \tag{4.55}$$

$${}_1b^1_0 = {}_1c^1_0 = 3\,i\left(v_{[0]} + \delta_m\, v_{[0]}\right) . \tag{4.56}$$

The expression for the gauge-invariant curvature perturbation ζ up to second order is

$$\zeta = -\mathcal{R} - \mathcal{R}^2 , \tag{4.57}$$

with

$$\mathcal{R} = \Phi + \frac{2}{3\mathcal{H}(\omega+1)}\left[\Phi' + \mathcal{H}\,\Psi - 4\,\mathcal{H}\,\Psi^2 - \frac{\Phi'^2}{\mathcal{H}} - 4\,(\Psi-\Phi)\,\Phi'\right] \tag{4.58}$$

$$+ (1+3\,c_s^2)\left[\frac{\delta}{3\,(\omega+1)}\right]^2 + \frac{4}{3\,(\omega+1)}\,\delta\,\Phi , \tag{4.59}$$

where the density contrast δ, ω and the sound of speed c_s^2 refer to the total fluid. In the radiation dominated era and on superhorizon scales we simply have

$$\zeta = -\Phi - \frac{1}{2}\,\Psi + \frac{1}{2}\,\Psi^2 - \Phi^2 . \tag{4.60}$$

4.5 The code, SONG

In order to implement all the formalism and equations introduced so far and compute the non-liner effects on the CMB observables, we make use of the numerical code SONG (**S**econd **O**rder **N**on-**G**aussianity)[1] [70, 69]. It is a second-order Boltzmann code, which solves the Einstein and Boltzmann equations up to second order in the cosmological perturbations. The advantage of this code is its ability to provide predictions for additional observables which do not exist at linear order, such as

- the intrinsic bispectrum of the CMB (*i.e.* the three-point function of temperature anisotropy),

[1] SONG is open-source and available on the website https://github.com/coccoinomane/song.

- the angular power spectrum of spectral distortions,
- the angular power spectrum of B-mode polarization,
- the power spectrum of the magnetic fields generated at recombination.

It is written in C, it is OpenMP parallelized and its structure is based on that of the first-order Boltzmann code CLASS [52, 9]; in particular, it inherits its philosophy, which is to provide an easy-to-use interface and a modular internal structure. It is also based on the principle of encapsulation, so that the code has to be modified only in a few localized portions of the source files if you want to add some feature in it.

SONG implements the formalism of beta-moments, which has been introduced in Chapter 2 and has the great advantage of treating both relativistic and non-relativistic fluids in a unified framework. Thus, the notations and the equations implemented in the code are almost the same of those presented in this thesis; however, it is worth to mention at least a couple of differences. First of all, the quadratic sources in SONG are symmetrized with respect to the exchange of $\mathbf{k_1}$ and $\mathbf{k_2}$, since they are dummy variables and there is not a unique way to express these terms. Secondly, the Einstein equations which are actually evolved in the code are just four, that is the time-time and the scalar, vector and tensor space-space equations, which evolve Φ, Ψ, $\omega_{[1]}$ and $\gamma_{[2]}$, respectively. In fact, using the Newtonian gauge conditions ($\omega_{[0]} = \gamma_{[0]} = \gamma_{[\pm1]} = 0$) and the fact that $\omega_{[-1]} = -\omega_{[1]}$ and $\gamma_{[-2]} = \gamma_{[2]}$, we have that only four of the ten Einstein equations are actually independent.

4.5.1 Setting up of the standard code

For the purposes of this thesis and its follow up with future studies, we needed a code that was capable of computing the angular power spectrum for CMB anisotropies up to second order, in order to then create a dedicated extension of the code to include the magnetic contributions to the equations, that we will see in the next chapters. Together with the second order perturbations the code SONG has also an additional interesting feature, that is the generation of weak magnetic fields from second order perturbations through the Harrison mechanism (see Sec. 5.2.3). This feature although not involved in the current work will be important for the future developments. Unfortunately the original code was partitioned into different branches which evolved independently over time, making each branch not suitable for our purposes. The *master* branch actually includes the Harrison mechanism, but it does not provide in output the power spectrum neither for the magnetic field, nor for matter. After exploring and testing all the different branches we identified the branch *spectra2_pks* as the most optimal one for our scope, since it provides both the second-order angular spectra and the magnetic power spectrum through the Harrison mechanism. The branch by construction was not capable of providing the second-order perturbations together with the magnetic spectrum; we

therefore extended it in order to provide both the results. The new extended code has been then extensively tested in the ΛCDM framework.

4.6 Second-order *TT*, *EE* and *TE* spectra for ΛCDM and magnetic power spectrum

We present now the second-order TT, EE and TE spectra for the CMB anisotropy for the ΛCDM model (Figure 4.1 and Figure 4.2), together with the magnetic power spectrum generated through the Harrison mechanism, obtained with SONG. In particular, we assumed adiabatic initial conditions and vanishing primordial non-Gaussianity, which means that the transfer function of the gauge-invariant curvature perturbation ζ is set to zero. This implies that the second-order perturbations are initially sourced only by the quadratic terms in the first-order ones.

Our results are based on the Planck 2018 results [72]; in particular, we set

$$\begin{aligned} &\Omega_b h^2 = 0.02237 \ , && \Omega_c h^2 = 0.120 \ , \\ &\tau = 0.0544 \ , && H_0 = 67.36 \text{ km s}^{-1} \text{ Mpc}^{-1} \ , \\ &A_\mathrm{s} = 2.1 \times 10^{-9} \ , && n_\mathrm{s} = 0.9649 \ . \end{aligned} \tag{4.61}$$

We can note that for the temperature power spectrum the relative second-order contribution becomes progressively important at small scales, but still highly subdominant.

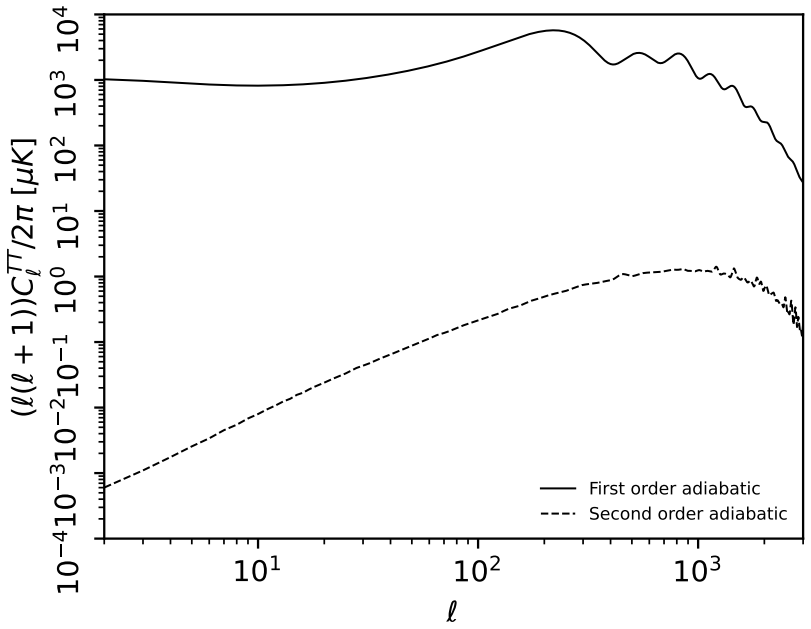

Figure 4.1: First-order (solid line) and second-order (dashed line) temperature spectra obtained with SONG.

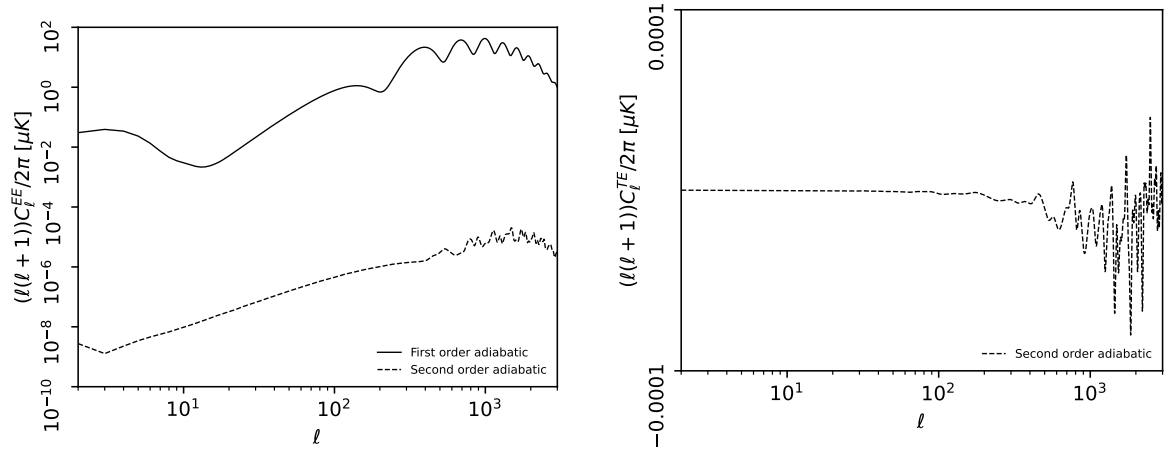

Figure 4.2: First-order (solid line) and second-order (dashed line) EE spectra (*left*) and second-order TE spectrum (*right*) obtained with SONG.

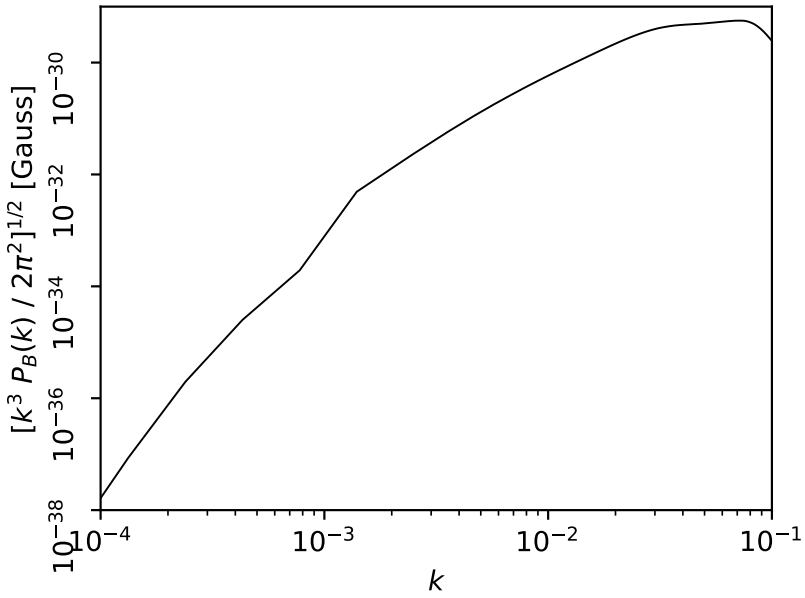

Figure 4.3: Magnetic power spectrum generated through the Harrison mechanism and obtained with SONG.

Chapter 5

Primordial Magnetic Fields

Magnetic fields are everywhere in the Universe at all scales probed so far, from planets and stars to galaxies [47, 8] and galaxy clusters [10, 31, 16] with hints of their presence on larger structures as voids [61, 88, 91] and filaments [30, 12, 90] . The Earth displays a dipolar magnetic field of about a Gauss, together with several other solar system planets and the Sun. In 1949, data on polarized star emission showed the presence of a diffuse magnetic field in our Galaxy, suggesting for the first time the existence of magnetic fields at such large scales. Also nearby spiral galaxies host magnetic fields of few or tens μG and with coherence lengths of the order of the galactic scales; moreover, the magnetic field presents the same spiral pattern and is aligned with the rotation direction. Magnetic fields of similar strengths are also present in elliptic galaxies, but in this case they are randomly distributed and possess coherence lengths smaller than the galactic scale. Observations of distant quasars, instead, showed the existence of magnetic fields also in higher redshift galaxies, with similar properties to that of low redshift ones. Also in cluster of galaxies, magnetic fields of a few μG are detected, with correlation on Mpc scales, and even in voids of the intergalactic medium weak magnetic fields of $\sim 10^{-16}$ G seem to be present.

The rapid growth of precision reached by recent experiments makes it increasingly difficult to ignore the presence of such magnetic fields, which are then progressively acquiring importance in the astrophysical and cosmological researches. In particular, the main subject of study about magnetic fields is about their generation and evolution. In fact, although a great amount of data strongly fixes the status of magnetic fields in the astrophysical context, their origin is still an open question. Since magnetic fields of $\sim \mu$G would have dramatically affected the process of structure formation, they must have originated from the amplification of smaller pre-existing fields. Compression from gravitational collapse and dynamos are the main two mechanisms which are able to amplify initial seed magnetic fields.

Such magnetic seeds can have an astrophysical or cosmological origin for reviews on the cosmic magnetism see [84, 21, 94, 93]. In the first case, they can be provided by small-

scales objects like stars in galaxies or AGN in clusters of galaxies; however, the resulting magnetic fields would have too small coherence lengths and too low amplitudes to be compatible with the observed large scales magnetic field. The other possibility is instead to have a cosmological origin for the magnetic seeds; in this case, both the coherence lengths and amplitudes can be comparable to the observed ones after amplification.

This scenario implies the existence of magnetic fields generated prior to recombination called *primordial magnetic fields* (PMFs). The generation of such fields implies the involvement of non-standard fundamental physics in the early Universe, as we will see in this chapter. This makes the PMFs existence and characteristics a non conventional observational window on the physics of the early Universe and for this reason is crucial to investigate their nature. Luckily, PMFs affect all the cosmological observables, leaving peculiar imprints that allow constraining their characteristics with cosmological data. The overall agreement between different probes from the CMB is currently of few nGauss on a Mpc scale [62, 66].

5.1 Generation of PMFs

Assuming the existence of these primordial seeds, whose subsequent amplification leads to the observed magnetic fields, does not solve completely the problem, since a mechanism which explains the generation of such primordial magnetic fields is still necessary. There are two main classes of generation mechanisms: inflationary and post inflationary ones.

5.1.1 Post inflationary mechanisms

This class of generation mechanisms is associated with phase transitions, like the electroweak (EW) or the QCD one. The main problem for these kind of processes however is that the generated magnetic fields suffer from too small coherence length, which has to be smaller than the Hubble radius at that epoch. Processes of inverse cascade can help to increase such correlation lengths, but it requires an helical component in the field (thanks to its conservation). Another issue is due to the fact that the optimal phase transition which can generates magnetic fields is the first order one, which is currently disfavoured. The idea behind such transitions is that bubbles of the new phase nucleate through the old phase environment, then expand and eventually collide until the whole volume is entirely occupied by the new phase. This mechanism provides non-equilibrium conditions which can possibly sustain processes like baryogenesis and leptogenesis, which in turn could lead to the generation of magnetic fields; such fields can then be amplified by turbulence, which is generated from the violent collisions of the bubbles. As already said, first order phase transitions are the optimal ones for the magnetic field generation, but both the EW and QCD phase transitions seem to be second order ones; however, there are some conditions under which this is not generally true. QCD phase transitions,

for example, could be first order if the lepton chemical potential is sufficiently large (and still within allowed values) [78]. Also the EW transition can be first order in some supersymmetric extensions of the standard model, like the MSSM [33, 37]. Post-inflationary PMFs have the peculiar characteristics of having a spectral index even and equal or greater than 2 [15].

5.1.2 Inflationary mechanisms

Contrary to the post inflationary scenarios, inflation provides the ideal conditions for the generation of primordial magnetic fields with large correlation lengths. In fact, the exponential stretching of wave modes due to the accelerated expansion during inflation can provide such fields with large coherence lengths. Moreover, vacuum fluctuations of the electromagnetic field can be excited when a mode is still inside the Hubble radius and then transformed to classical fluctuations once became superhorizon.

There is however a problem with this scenario, which is related to conformal invariance of the standard electromagnetic action. In fact, under a conformal transformation $g^*_{\mu\nu} = \Omega^2\, g_{\mu\nu}$, the electromagnetic action is not affected, that is $S \to S^* = S$ (for the explicit form of the action see Sec. 5.2). Furthermore, it can be noted that the FLRW metric is conformally flat, which means that it can be written as $g_{\mu\nu} = \Omega^2\, \eta_{\mu\nu}$, with $\eta_{\mu\nu}$ being the flat Minkowski metric. It can be proven that it is always possible to transform the electromagnetic waves and the Maxwell equations into their flat versions; this in turn implies that it is not possible to amplify an electromagnetic wave fluctuation in a FLRW spacetime and hence the field always decays with expansion as $1/a^2(t)$. We would then obtain PMFs with too small amplitudes to be the seeds for large scale magnetic fields and the only way to avoid this issue is to break conformal invariance. Such breaking can be achieved by involving in the inflationary mechanism some physical processes, such as coupling to scalar fields like the inflaton and the dilaton, extradimensions, coupling to pseudo-scalar field like the axion, having charged scalar fields and so on. Allowing for the breaking of conformal invariance, it is then possible to obtain the amplification of electromagnetic waves as the Universe expands. After the end of inflation, the process of reheating leads to the production of charged particles and hence to a huge increase in the plasma conductivity, which in turn makes the electric fields disappear and the magnetic fields get frozen in.

The best way we have to discriminate between inflationary and post inflationary scenarios and to constrain the properties of PMFs is to investigate cosmological observables, in particular CMB anisotropies in temperature and polarization. In fact, the presence of such primordial fields has a strong impact on the evolution of cosmological perturbations and hence leaves several imprints on CMB data, which can then be used as a powerful tool for the study of PMFs. Before going into these details, let us now see some general

features of the formulation of electrodynamics in a general curved spacetime and, in particular, in our Universe. We will mostly follow the notations of [85].

5.2 Electrodynamics in the expanding Universe

Electrodynamics in a generic curved spacetime is described by the following electromagnetic action:

$$S = -\int \mathrm{d}^4x\,\sqrt{-g}\,\frac{F_{\mu\nu}F^{\mu\nu}}{16\,\pi} + \int \mathrm{d}^4x\,\sqrt{-g}\,A_\mu J^\mu\ , \tag{5.1}$$

where A_μ is the electromagnetic 4-potential, J^μ is the 4-current density and $F_{\mu\nu} = A_{\nu;\mu} - A_{\mu;\nu} = A_{\nu,\mu} - A_{\mu,\nu}$ is the electromagnetic field tensor. From the variational principle we obtain the source dependent part of the Maxwell equations, while from the definition of $F_{\mu\nu}$ we get the source free part. They read

$$F^{\mu\nu}{}_{;\nu} = 4\pi\,J^\mu\ , \tag{5.2}$$

$$F_{[\mu\nu;\gamma]} = F_{[\mu\nu,\gamma]} = 0\ , \tag{5.3}$$

where with the square brackets we mean adding terms with cyclic permutations of the indices contained by them. It is useful to define the dual tensor ${}^*F = (\epsilon^{\mu\nu\alpha\beta}/2)\,F_{\alpha\beta}$, where $\epsilon^{\mu\nu\alpha\beta} = \mathcal{A}^{\mu\nu\alpha\beta}/\sqrt{-g}$ is the total antisymmetric Levi-Civita tensor and $\mathcal{A}^{\mu\nu\alpha\beta}$ is the total antisymmetric symbol such that $\mathcal{A}^{0123} = 1$ and ±1 for even or odd permutations of (0,1,2,3), respectively.

In flat spacetime, the electric components E^i and the magnetic ones B^i are directly related to the 6 independent components of $F^{\mu\nu}$ as

$$F^{0i} = E^i\ ,\quad F^{12} = B^3\ ,\quad F^{23} = B^1\ ,\quad F^{31} = B^2\ . \tag{5.4}$$

In a general curved spacetime, instead, we need first to isolate a time direction, which can be done by choosing a family of observer who measure the electromagnetic field and whose 4-velocity is $U^\mu = \mathrm{d}x^\mu/\mathrm{d}s$, with $U^\mu U_\mu = -1$. We can then define the projection tensor $h_{\mu\nu} = g_{\mu\nu} + U_\mu U_\nu$, which projects into the 3-space orthogonal to U^μ. The metric for these particular observers takes the form

$$\mathrm{d}s^2 = -(U_\mu\,\mathrm{d}x^\mu)^2 + h_{\mu\nu}\,\mathrm{d}x^\mu\mathrm{d}x^\nu\ . \tag{5.5}$$

The electric and magnetic fields can then be expressed as the 4-vectors E_μ and B_μ, respectively, which are defined as

$$E_\mu = F_{\mu\nu}\,U^\nu\ ,\quad B_\mu = \frac{1}{2}\,\epsilon_{\mu\nu\alpha\beta}\,U^\nu\,F^{\alpha\beta} = {}^*F_{\mu\nu}\,U^\nu\ . \tag{5.6}$$

One can check that $E_\mu\,U^\mu = B_\mu\,U^\mu = 0$, which means that both E_μ and B_μ are effectively 3-vectors in the 3-space orthogonal to U^μ.

The Maxwell equations can be decomposed into timelike and spacelike parts using U^μ and $h_{\mu\nu}$. For this purpose, let us define the spatial projection of the covariant derivative as $D_\beta B^\alpha = h^\mu_{\ \beta}\, h^\alpha_{\ \nu}\, B^\nu_{\ ;\mu}$, and split the covariant velocity gradient tensor, $U_{\alpha;\beta}$, as

$$U_{\alpha;\beta} = \frac{1}{3}\,\Theta\, h_{\alpha\beta} + \sigma_{\alpha\beta} + \omega_{\alpha\beta} - \dot{U}_\alpha\, U_\beta \ . \tag{5.7}$$

In the above equation, $\Theta = U^\alpha_{\ ;\alpha}$ is the expansion scalar, $\sigma_{\alpha\beta}$ is the (symmetric, traceless and purely spatial) shear tensor, $\omega_{\alpha\beta}$ is the vorticity and $\dot{U}_\beta = U^\alpha\, U_{\beta;\alpha}$ is the acceleration of the observer. Another useful quantity to define is the vorticity vector $\omega_\nu = -\omega_{\alpha;\beta}\,\epsilon^{\alpha\beta\mu\nu}\, U_\mu/2$. Finally, the timelike and spacelike projections of both equations (5.2) and (5.3) read

$$D_\beta B^\beta = 2\,\omega^\beta\, E_\beta \ , \tag{5.8}$$

$$h^\kappa_{\ \alpha}\dot{B}^\alpha = \left[\sigma^\kappa_{\ \beta} + \omega^\kappa_{\ \beta} - \frac{2}{3}\,\Theta\,\delta^\kappa_{\ \beta}\right] B^\beta - \bar{\epsilon}^{\,\kappa\mu\nu}\,\dot{U}_\mu\, E_\nu - \mathrm{Curl}(E^\kappa) \ , \tag{5.9}$$

$$D_\beta E^\beta = 4\pi\,\rho_q - 2\,\omega^\beta\, B_\beta \ , \tag{5.10}$$

$$h^\kappa_{\ \alpha}E^\alpha = \left[\sigma^\kappa_{\ \beta} + \omega^\kappa_{\ \beta} - \frac{2}{3}\,\Theta\,\delta^\kappa_{\ \beta}\right] E^\beta + \bar{\epsilon}^{\,\kappa\mu\nu}\,\dot{U}_\mu\, B_\nu + \mathrm{Curl}(B^\kappa) - 4\pi\, j^\kappa \ . \tag{5.11}$$

Here we have defined $\dot{B}^\alpha = U^\beta\, B^\alpha_{\ \beta}$, $\mathrm{Curl}(E^\kappa) = \bar{\epsilon}^{\,\kappa\beta\nu}\, E_{\nu;\beta}$ with $\bar{\epsilon}^{\,\kappa\beta\nu} = \epsilon^{\kappa\beta\nu\mu}\, U_\mu$ being the 3-dimensional fully antisymmetric tensor; finally, $\rho_q = -J^\mu\, U_\mu$ and $j^\kappa = J^\nu\, h^\kappa_{\ \mu}$ are respectively the charge and 3-current densities as perceived by the observer with 4-velocity U^μ. Note that in the equation (5.8) the term $2\,\omega^\beta\, E_\beta$ acts as an effective magnetic charge, which is generated by the vorticity related to the motion of the observer. We complete the set of equations by giving the generalized relativistic Ohm's law, that is

$$J^\alpha = \rho_q\,\omega^\alpha + \sigma\, E^\alpha \ , \tag{5.12}$$

where σ is the conductivity of the fluid and all the quantities are measured in its rest frame (ω^α is the mean 4-velocity of the fluid and $E^\alpha = F^{\alpha\beta}\,\omega_\beta$).

We now have all the ingredients to consider the particular case of the flat FLRW spacetime. The observer that we now consider is the fundamental one of the FLRW metric, which has $U^\alpha = (1,0,0,0)$. Hence, we also get $\dot{U}^\alpha = 0$, $\omega_{\alpha\beta} = 0$, $\sigma_{\alpha\beta} = 0$ and $\Theta = 3\,\dot{a}/a$. With all these simplifications, Maxwell equations now take the form

$$\frac{\partial B^i}{\partial x^i} = 0 \ , \qquad \frac{1}{a^3}\frac{\partial}{\partial t}\left[a^3\, B^i\right] = -\frac{1}{a}\,\epsilon^*_{ilm}\frac{\partial E^m}{\partial x^l} \ , \tag{5.13}$$

$$\frac{\partial E^i}{\partial x^i} = 4\pi\,\rho_q \ , \qquad \frac{1}{a^3}\frac{\partial}{\partial t}\left[a^3\, E^i\right] = \frac{1}{a}\,\epsilon^*_{ilm}\frac{\partial B^m}{\partial x^l} - 4\pi\, j^i \ , \tag{5.14}$$

with ϵ^*_{ijk} being the usual 3-dimensional fully antisymmetric symbol, such that $\epsilon^*_{123} = 1$.

Let us consider the case of no peculiar velocity ($\omega^\alpha = U^\alpha$) and infinite conductivity ($\sigma \to \infty$), which are realistic conditions for the plasma in the Universe. Then, from the Ohm's law (5.12) we have $E^\alpha = 0$ and hence, from the second of equations (5.13), $B^i \propto 1/a^3$. This is however in contrast with the idea that in flat spacetime and in a highly conductive fluid, the magnetic flux through a comoving surface with the fluid itself is constant; thus, since in an expanding Universe the proper surface increases as $a^2(t)$, we would expect that $B^i \propto 1/a^2$ as the Universe expands. This apparent contradiction comes from the fact that the magnetic and electric fields considered so far are defined on the coordinate basis, that are the ones for which the metric is of the FLRW form. Let us instead refer the EM components to the local inertial frame, which is the one that laboratory measurements would use. This can be done by projecting them into the four orthonormal vectors $\mathbf{e}_{(a)}$ ($a = 0, 1, 2, 3$), which satisfy the relation $g_{\mu\nu} e^\mu_{(a)} e^\nu_{(b)} = \eta_{ab}$. In the frame defined by the tetrads, the metric assumes locally the form of the flat Minkowski one, $\eta_{\mu\nu}$. It can be proven [85] that the projected components of the magnetic field along the four tetrads, that is $\bar{B}^a = g_{\mu\nu}\, B^\mu\, e^{\nu(a)} = B^\mu\, e^{(a)}_\mu$, scale as $\bar{B}^i = \bar{B}_i \propto 1/a^2$, which is exactly what we would expect from the the flux freezing. Thus, such frame seems to be the most natural one to express the *physical* components of the magnetic field. A similar argument holds also for the electric field.

If we now define the vectors $\mathbf{B} \equiv (\bar{B}^1, \bar{B}^2, \bar{B}^3)$, $\mathbf{E} \equiv (\bar{E}^1, \bar{E}^2, \bar{E}^3)$ and $\mathbf{J} \equiv (\bar{j}^1, \bar{j}^2, \bar{j}^3)$, together with the comoving variables

$$\mathbf{B}^* = a^2\, \mathbf{B}\ , \quad \mathbf{E}^* = a^2\, \mathbf{E}\ , \quad \rho_q^* = a^3\, \rho_q\ , \quad \mathbf{J}^* = a^3\, \mathbf{J}\ , \tag{5.15}$$

the Maxwell equations become

$$\begin{aligned} \nabla \cdot \mathbf{B}^* &= 0\ , \\ \nabla \cdot \mathbf{E}^* &= 4\pi\, \rho_q^*\ , \\ \nabla \times \mathbf{E}^* &= -(\mathbf{B}^*)'\ , \\ \nabla \times \mathbf{B}^* &= 4\pi\, \mathbf{J}^* + (\mathbf{E}^*)'\ , \end{aligned} \tag{5.16}$$

while the Ohm's law reads

$$\mathbf{J}^* = \rho_q^*\, \mathbf{v} + \sigma^*\, (\mathbf{E}^* + \mathbf{v}^* \times \mathbf{B}^*)\ , \tag{5.17}$$

with $\sigma^* = a\, \sigma$. Note that we are now referring the equations to the conformal time τ and to the comoving spatial coordinates x^i. The interesting result is that the above equations are exactly the same of those in flat spacetime, which is also a consequence of conformal invariance of electrodynamics.

5.2.1 The induction equation

The combination of the Ohm's law with the Maxwell equations leads to an evolution equation for the magnetic field, which is called *induction equation* and reads

$$\frac{\partial \mathbf{B}^*}{\partial \tau} = \nabla \times \left[\mathbf{v} \times \mathbf{B}^* - \eta^* \nabla \times \mathbf{B}^* \right] , \tag{5.18}$$

with $\eta^* \equiv (4\pi\,\sigma^*)^{-1}$ being the magnetic diffusivity.

We can notice that in absence of resistivity ($\eta = 0$) and with no peculiar velocities ($\mathbf{v} = 0$), the magnetic field defined in the local inertial frame just decays as $\mathbf{B} \propto 1/a^2$. In the general case, instead, the two terms in the right hand side of the induction equation affect the evolution of the magnetic field; in particular, it is possible to identify two different regimes, which are valid when one term dominates the other and vice versa.

- *Magnetic flux freezing.* In the high conductivity limit $\eta \to 0$, the only term which contributes to the evolution of the magnetic field is $\mathbf{v} \times \mathbf{B}^*$, also known as induction term. In this case, the magnetic flux through a surface which is moving with the fluid stays constant.

- *Magnetic diffusion.* In the opposite limit, that is $\mathbf{v} = 0$, for a constant η^* the induction equations reduces to the diffusion equation

$$\frac{\partial \mathbf{B}^*}{\partial \tau} = \eta^* \nabla^2 \mathbf{B}^* \ . \tag{5.19}$$

  Hence, the field $\mathbf{B}^*$ decays on the comoving diffusion timescale $\tau_d \sim L^2/\eta^*$, where L is the typical comoving scale for the variation of the magnetic field.

All the intermediate cases are characterized by the magnetic Reynolds number, which quantifies how much the induction term dominates the diffusion term and it is defined as

$$R_{\rm m} = \frac{v\,L}{\eta^*} = \frac{v\,l}{\eta} \ . \tag{5.20}$$

Here, v is the typical fluid velocity on the comoving scale L, while $l = a\,L$ is the proper scale. For $R_{\rm m} \to \infty$ we recover the high conductivity scenario, while for $R_{\rm m} \to 0$ we obtain the magnetic diffusion case.

5.2.2 Magnetic helicity

An important quantity characterizing magnetic fields is the magnetic helicity, which is defined as

$$H = \int_V {\rm d}^3\mathbf{r}\, \mathbf{A} \cdot \mathbf{B} \tag{5.21}$$

where V is a proper closed volume and $\mathbf{B} = \nabla_{\mathbf{r}} \times \mathbf{A}$ (the definition of helicity is the same if comoving quantities were used). It intuitively quantifies how much non-overlapping field lines are linked and twisted. An important property of helicity is that, under many astrophysical conditions with $R_{\rm m}$ large, it is almost conserved even in presence of magnetic energy dissipation. Magnetic helicity is also crucial for the evolution of post inflationary PMFs, since they require its conservation to activate the inverse cascade mechanism which in turn increases their correlation length, as already mentioned in Sec. 5.1.1.

The presence and the relative importance of helical components into PMFs is still a subject of intense study. Such contribution would lead to different imprints on the CMB power spectra, which therefore provide the best way to constrain magnetic helicity so far [62]. However, helicity is a parity violating property: this would imply, together with many other deep implications for fundamental physics, the presence of non-vanishing odd cross-correlators *TB* and *EB* for CMB anisotropy, hence providing an extraordinary opportunity for future experiments to constrain the presence and properties of helical PMFs.

5.2.3 The Harrison mechanism

The induction equation (5.18) admits the solution $\mathbf{B} = 0$, which means that if a magnetic field vanishes at some initial time, it will never be generated. There is however a mechanism, proposed for the first time by Harrison in 1970 [34], through which a initially vanishing magnetic field can be generated. It is based on the vortical velocity difference between electrons and protons, which induces an electric field with a non-vanishing curl and hence, through the Maxwell equations, a magnetic field can be generated. Although the resulting magnetic fields would be too weak to justify the observed large-scale magnetic fields, it is worth mentioning it, especially for the purposes of this thesis and more in general for possible future studies of primordial magnetic field. Harrison considered the case of the differential rotation of electrons and ions in a protogalaxy, but this mechanism is now reinterpreted in a more general framework. Let us consider the multicomponent fluid formed by photons, electrons and protons. Before recombination. photons and electrons are tightly coupled through Thomson scattering, but also electrons and protons can be considered tightly coupled through Compton scattering. However, a tiny difference in the velocities of protons and electrons arises from the difference in the strength of these interactions and in the mass of the two species, leading to vortical currents and magnetic fields. This effect is appreciable only at non-linear order and this is why the Harrison mechanism should be considered for a fully non-linear treatment of primordial magnetic fields in the cosmological plasma (and hence for this thesis, which computes a first step in this direction). At first order, in fact, vector perturbations are zero after inflation, at least in the standard model; at second order, however, vector modes can be sourced by scalar cosmological perturbations and therefore vortical currents can be generated.

The original version of SONG implements the generation of magnetic fields around recombination through the Harrison mechanism, up to second order. In particular, the evolution equation for the field is given by [24, 25]

$$(a^2 B^i)' = -a^2 \, \epsilon^{ijk} \, \partial_j [(1 + \Phi - \Psi) \, E_k] \, , \tag{5.22}$$

where all the quantities are evaluated in the local inertial frame. The electric field is the one generated by the vortical currents induced by protons and electrons and has to be calculated at least up to second order to give a non-vanishing result in equation 5.22 [1]. This is one of the reasons of having chosen this code, because it might be suitable for a future fully non-linear treatment of PMFs, since this mechanism may be used to drive the evolution of the magnetic field at second order in perturbations.

[1] In fact, at linear order we have only scalar perturbations and therefore $E_i \propto \partial_i \Phi$, which would imply a zero right hand side of equation 5.22 and a decay of the magnetic field just as $1/a^2$.

Chapter 6

Primordial Magnetic Fields and CMB anisotropy

PMFs offer an extraordinary observational window to study the early Universe, test its physics and possibly open the way at new exotic phenomena. Detecting and measuring primordial fields and constraining their properties could, for example, provide strong constraints to inflation and the possibility to discriminate between different models. Fortunately, the presence of PMFs has a strong impact on several cosmological observables, leading to a wide range of possibilities to constrain their properties. A lot of information can be extracted, for example, from the imprints of PMFs on Big-Bang nucleosynthesis (BBN) [44, 18, 29, 43, 53] and on large-scale structure (LSS) [87, 42, 23, 63, 48, 14, 57, 77]. In particular, such observational windows allow the identification of upper bounds on the strength of the PMF; an upper limit of $\sim 0.1\,\mu$G was found from BBN [32, 43] and of ~ 10 nG from LSS [5]. Another way to constrain PMFs come from the study of the thermal spectrum of the CMB radiation. The presence of such primordial fields can indeed induce spectral distortions through the injection of dissipated magnetic energy via damping processes [49].

A crucial role in the investigation of PMFs is however played by the CMB anisotropies. Most of the more robust constraints we have so far come indeed from the analysis of CMB data, which provide one the best opportunities to acquire information about the origin and characteristics of PMFs, together with their possibility to be the seeds of the large-scale magnetic fields we observe today. An extensive and detailed discussion about PMF constraints from combined analyses of CMB temperature and polarization anisotropies is found at [62].

There are mainly two way to model a PMF:

- as a *homogeneous field*, which however cannot be included in a homogeneous and isotropic model since it breaks isotropy, but it has to be described in the framework of an anisotropic cosmological model;

- as a *stochastic background* (SB), which can be described within the FLRW metric and is modelled as a fully inhomogeneous component of the cosmological plasma, *i.e.* its energy density and anisotropic stress do not contribute at background level and its energy-momentum tensor components are treated on the same footing of first-order cosmological perturbations.

In this thesis we assume a SB of PMF, which is also the most used model in the literature.

6.1 Stochastic background of PMF

As already said, for SB of PMF the contribution of its energy density and anisotropic stress can be neglected at homogeneous level. The PMF EMT components contribute, indeed, at the same level of first-order perturbations. At linear order, PMFs evolve like a stiff source, which means that we can ignore the back-reaction of gravity onto the PMFs. Moreover, prior to the recombination we can safely consider the case of infinite conductivity, in which case the induced electric field is zero. Within this limit, the magnetic field just dilutes as $\mathbf{B}(\mathbf{x},\tau) = \mathbf{B}(\mathbf{x})/a(\tau)^2$, with $\mathbf{B}(\mathbf{x})$ being the comoving field (the $\mathbf{B}^*$ of Chapter 5, but now we drop the asterisk to avoid a heavy notation). These conditions allow working in first approximation within the ideal magneto-hydrodynamics (MHD); however, at small scales the magnetic field undergoes non-trivial dynamics and the aforementioned assumptions of ideal MHD cannot hold anymore. In our work, we lay the foundation of a complete treatment that includes all these non-linear and non-ideal MHD effects, which may be crucial, as we will see, for the physics of recombination [40], and in general for acquiring further predictive power.

As a first approximation (as it is usually done) we will focus on non-helical PMFs.

6.1.1 Statistics of PMF

The non-helical SB of PMF is modelled with a power-law power spectrum, defined through the two-point correlation function in Fourier space

$$\left\langle B_i(\mathbf{k})\, B_j^*(\mathbf{k}')\right\rangle = \frac{(2\pi)^3}{2}\,\delta^{(3)}(\mathbf{k}-\mathbf{k}')\left(\delta_{ij}-\hat{k}_i\hat{k}_j\right)P_B(k)\ , \tag{6.1}$$

with $P_B(k) = A_B\, k^{n_B}$ and $\hat{k}_i$ being the cartesian component of the normalized wave vector. Hence, the two key quantities which specify the characteristics of the PMF are the amplitude of the power spectrum, A_B, and the spectral index, n_B. In particular, the latter is strictly related to the generation mechanism and hence provides a powerful tool to discriminate between different generation scenarios (for example we remind that post-inflationary mechanisms generate PMF with $n_B \geq 2$ [15, 20]).

It is customary to smooth the fields on a comoving scale λ, which is usually taken to be 1 Mpc (that is similar to the typical coherence lengths of large scale magnetic fields). Such smoothed amplitude is expressed as [62]

$$B_\lambda^2 = \int_0^\infty \frac{\mathrm{d}k\, k^2}{2\pi^2}\, \mathrm{e}^{-\lambda^2 k^2}\, P_B(k) = \frac{A_B}{4\pi^2\, \lambda^{n_B+3}}\, \Gamma\left(\frac{n_B+3}{2}\right) . \tag{6.2}$$

Note that the condition $n_B > -3$ must be satisfied in order to avoid infrared divergences.

Magnetic modes have the interesting property to not suffer from Silk damping, which instead causes the suppression of high multipoles in the CMB angular power spectrum. However, PMFs are still suppressed on small scales by radiation viscosity [39], although on scales much smaller than the Silk one. This damping is modelled by a sharp cut-off in the PMF power spectrum at the damping scale k_D, whose expression is [86]

$$k_D = (5.5\times 10^4)^{\frac{1}{n_B+5}} \left(\frac{B_\lambda}{\mathrm{nG}}\right)^{-\frac{2}{n_B+5}} \left(\frac{2\pi}{\lambda/\mathrm{Mpc}}\right)^{\frac{n_B+3}{n_B+5}} h^{\frac{1}{n_B+5}} \left(\frac{\Omega_\mathrm{b} h^2}{0.022}\right)^{\frac{1}{n_B+5}} \mathrm{Mpc}^{-1} . \tag{6.3}$$

The root mean square of the field is instead given by

$$\left\langle B^2 \right\rangle = \left\langle B_i(\mathbf{x})\, B_i^*(\mathbf{x}') \right\rangle|_{\mathbf{x}=\mathbf{x}'} = \frac{1}{2\pi^2} \int_0^{k_D} \mathrm{d}k\, k^2\, P_B(k) . \tag{6.4}$$

The relation between the root mean square of PMFs and the smoothed amplitude is

$$\left\langle B^2 \right\rangle = B_\lambda^2\, \frac{(k_D\,\lambda)^{n_B+3}}{(n_B+3)\,\Gamma\left(\frac{n_B+3}{2}\right)} . \tag{6.5}$$

6.1.2 PMF energy-momentum tensor

PMFs source scalar, vector and tensor perturbations. There are mainly three way in which PMFs influence the evolution of cosmological perturbations:

- PMFs carry energy and momentum which are treated at the same level of first-order perturbations, therefore gravitating and influencing the metric perturbations;
- PMFs carry anisotropic stress, which adds to the ones of neutrinos and photons[1];
- PMFs induce a Lorentz force on baryons, hence affecting their velocity and, due to the tight coupling, also having an indirect influence on photons.

[1] The photon anisotropic stress is however negligible before the decoupling.

Another important contribution which arises at next-to-leading order is the effect which magnetic fields have on the speed of sound due to the presence of MHD waves [2] in the magnetized plasma and becomes particularly important as approaching to recombination. Such effect, which is not included in the standard (ideal MHD) treatment, is particularly important for the purpose of this work and it will be discussed in the next chapter. The PMF energy-momentum tensor components are

$$\tau_0^0 = -\rho_B = -\frac{\mathbf{B}^2(\mathbf{x})}{8\pi\, a^4}\ , \tag{6.6}$$

$$\tau_i^0 = 0\ , \tag{6.7}$$

$$\tau_j^i = \frac{1}{4\pi\, a^4}\left(\frac{\mathbf{B}^2(\mathbf{x})}{2}\,\delta^i_j - \mathbf{B}_j(\mathbf{x})\,\mathbf{B}^i(\mathbf{x})\right)\ . \tag{6.8}$$

Note that the components are all quadratic in the magnetic field. Hence, since we are assuming the PMF EMT to contribute at first order in the cosmological perturbations, we can equivalently state that the magnetic field itself is a *half-order* perturbation, which in a perturbative expansion reads $B \sim \epsilon^{1/2}$. Another consequence of such quadratic dependence is that, even if the magnetic fields are Gaussian distributed, the EMT provides a non-Gaussian contribution to CMB anisotropies, since it approximately follows χ^2 statistics.

The Fourier transform of the PMF energy-momentum tensor, being quadratic in the magnetic fields, is a convolution. The two-point correlation function of the spatial part of EMT is

$$\begin{aligned}\left\langle \tau^*_{ab}(\mathbf{k})\,\tau_{cd}(\mathbf{k}')\right\rangle = &\int \frac{\mathrm{d}^3q\,\mathrm{d}^3p}{64\pi^5}\,\delta_{ab}\,\delta_{cd}\left\langle B_l(\mathbf{q})\,B_l(\mathbf{k}-\mathbf{q})\,B_m(\mathbf{p})\,B_m(\mathbf{k}'-\mathbf{p})\right\rangle \\ &- \int \frac{\mathrm{d}^3q\,\mathrm{d}^3p}{32\pi^5}\left\langle B_a(\mathbf{q})\,B_b(\mathbf{k}-\mathbf{q})\,B_c(\mathbf{p})\,B_d(\mathbf{k}'-\mathbf{p})\right\rangle\ .\end{aligned} \tag{6.9}$$

The scalar, vector and tensor correlation functions are then obtained as follows

$$\begin{aligned}\left\langle \Pi^{*(\mathrm{S})}(\mathbf{k})\,\Pi^{(\mathrm{S})}(\mathbf{k}')\right\rangle &= \delta_{ab}\,\delta_{cd}\left\langle \tau^*_{ab}(\mathbf{k})\,\tau_{cd}(\mathbf{k}')\right\rangle\ , \\ \left\langle \Pi^{*(\mathrm{V})}_i(\mathbf{k})\,\Pi^{(\mathrm{V})}_j(\mathbf{k}')\right\rangle &= k_a\,P_{ib}(\mathbf{k})\,k'_c\,P_{jd}(\mathbf{k}')\left\langle \tau^*_{ab}(\mathbf{k})\,\tau_{cd}(\mathbf{k}')\right\rangle\ , \\ \left\langle \Pi^{*(\mathrm{T})}_{ij}(\mathbf{k})\,\Pi^{(\mathrm{T})}_{tl}(\mathbf{k}')\right\rangle &= \left[P_{ia}(\mathbf{k})\,P_{jb}(\mathbf{k}) - \frac{1}{2}\,P_{ij}(\mathbf{k})\,P_{ab}(\mathbf{k})\right]\times \\ &\quad \left[P_{tc}(\mathbf{k}')\,P_{ld}(\mathbf{k}') - \frac{1}{2}\,P_{tl}(\mathbf{k}')\,P_{cd}(\mathbf{k}')\right]\left\langle \tau^*_{ab}(\mathbf{k})\,\tau_{cd}(\mathbf{k}')\right\rangle\ ,\end{aligned} \tag{6.10}$$

[2] In a magnetized plasma, three different kind of waves can be generated: the transversal *shear Alfvén* wave and the longitudinal *slow and fast magnetosonic* waves.

where $P_{ij} = \delta_{ij} - \hat{k}_i\,\hat{k}_j$ and a sum over repeated indices is implied. We can write such convolutions in terms of spectra, namely

$$\begin{aligned}
\left\langle \Pi^{*(\mathrm{S})}(\mathbf{k})\,\Pi^{(\mathrm{S})}(\mathbf{k}')\right\rangle &= |\Pi^{(\mathrm{S})}(k)|^2\,\delta(\mathbf{k}-\mathbf{k}')\ ,\\
\left\langle \Pi_i^{*(\mathrm{V})}(\mathbf{k})\,\Pi_j^{(\mathrm{V})}(\mathbf{k}')\right\rangle &= \frac{1}{2}|\Pi^{(\mathrm{V})}(k)|^2\,P_{ij}(\mathbf{k})\,\delta(\mathbf{k}-\mathbf{k}')\ ,\\
\left\langle \Pi_{ij}^{*(\mathrm{T})}(\mathbf{k})\,\Pi_{tl}^{(\mathrm{T})}(\mathbf{k}')\right\rangle &= \frac{1}{4}|\Pi^{(\mathrm{T})}(k)|^2\,\mathcal{M}_{ijtl}(\mathbf{k})\,\delta(\mathbf{k}-\mathbf{k}')\ ,
\end{aligned} \tag{6.11}$$

where $\mathcal{M}_{ijtl}(\mathbf{k}) = P_{it}\,P_{jl} + P_{il}\,P_{jt} - P_{ij}\,P_{tl}$. With this choice, the spectra take the form

$$\begin{aligned}
|\rho_B(k)|^2 &= \frac{1}{1024\,\pi^5}\int_\Omega \mathrm{d}^3p\,P_B(p)\,P_B(|\mathbf{k}-\mathbf{p}|)\,(1+\mu^2)\ ,\\
|\Pi^{(\mathrm{V})}(k)|^2 &= \frac{1}{512\,\pi^5}\int_\Omega \mathrm{d}^3p\,P_B(p)\,P_B(|\mathbf{k}-\mathbf{p}|)\left[(1+\beta^2)\,(1-\gamma^2)+\gamma\,\beta\,(\mu-\gamma\,\beta)\right]\ ,\\
|\Pi^{(\mathrm{T})}(k)|^2 &= \frac{1}{512\,\pi^5}\int_\Omega \mathrm{d}^3p\,P_B(p)\,P_B(|\mathbf{k}-\mathbf{p}|)\,(1+2\,\gamma^2+\gamma^2\,\beta^2)\ ,
\end{aligned} \tag{6.12}$$

where $\mu = \hat{\mathbf{p}}\cdot(\mathbf{k}-\mathbf{p})/|\mathbf{k}-\mathbf{p}|$, $\gamma = \hat{\mathbf{k}}\cdot\hat{\mathbf{p}}$, $\beta = \hat{\mathbf{k}}\cdot(\mathbf{k}-\mathbf{p})/|\mathbf{k}-\mathbf{p}|$ and Ω is the volume with $p < k_D$. The general expression for the Lorentz force is [41]

$$L_i(x,\tau_0) = \frac{1}{4\pi}\left[B_j(\mathbf{x})\,\nabla_j B_i(\mathbf{x}) - \frac{1}{2}\nabla_i B^2(\mathbf{x})\right] \tag{6.13}$$

and $\mathbf{L}(x,\tau) = \mathbf{L}(x,\tau_0)/a^4(\tau)$. Since we are interested in the scalar sector, its scalar part, which is defined as $\nabla^2 L^{(\mathrm{S})} \equiv \nabla_i L_i$, is

$$\nabla^2 L^{(\mathrm{S})} = \frac{1}{4\pi}\left[\nabla_i B_j(\mathbf{x})\,\nabla_j B_i(\mathbf{x}) - \frac{1}{2}\nabla^2 B^2(\mathbf{x})\right] \tag{6.14}$$

The Fourier power spectra of the Lorentz force reads

$$|L^{(\mathrm{S})}(k)|^2 = \frac{1}{128\,\pi^2\,a^8}\int_\Omega \mathrm{d}^3p\,P_B(p)\,P_B(|\mathbf{k}-\mathbf{p}|)\left[1+\mu^2+4\,\gamma\,\beta\,(\gamma\,\beta-\mu)\right]\ . \tag{6.15}$$

The conservation equations for the PMF energy-momentum tensor are given by

$$\nabla_\mu \tau^\mu_\nu = -F^\mu_\nu\,J_\nu\ . \tag{6.16}$$

which, for $\nu = 0$, give the energy conservation equation, $\rho_B \propto a^{-4}$, while from $\nu = i$ give a nice relation between the scalar anisotropic stress (σ_B) [3], the energy density and the Lorentz force, that is

$$\sigma_B = \frac{\rho_B}{3} + L\ , \tag{6.17}$$

[3]Here we are using the notation of Ma&Bertschinger [54] for the scalar anisotropic stress, see Appendix A for more details

This useful relation, which is also model-independent, allows us to compute only two of the three convolution integrals for ρ_B, L and σ_B.

CMB anisotropies are strongly affected by the infrared behavior of the spectra. In particular, for indices greater than $n_B = -3/2$, the spectra show white noise, while for smaller indices they are infrared-dominated as k^{2n_B+3}.

6.1.3 Compensated modes

In this work, we analyzed the effects of PMFs directly on the adiabatic modes, *i.e.* we properly modified the fluid and Einstein equations to account for the presence of PMFs, but keeping the adiabatic initial conditions. This is however an original approach with respect to what is usually done. In fact, magnetically induced perturbations are typically associated with different initial conditions, which are obtained by solving the Einstein and Boltzmann equations, with in addition the magnetic terms, on large scales deep in the radiation era. With this approach, the presence of PMF induces, in addition to the usual adiabatic ones, new independent fully magnetic modes in matter and metric perturbations, which are indeed the particular solutions of the (now) inhomogeneous[4] system of the Einstein-Boltzmann differential equations. At linear order, such modes decouple and evolve independently. The post inflationary evolution leads to two types of them, the *compensated* and the *passive* modes.

The compensated modes are magnetically induced modes which are sourced by the PMF energy-momentum tensor after neutrino decoupling. The term "compensated" comes from the fact that the magnetic contributions to the metric perturbations in the initial conditions are compensated by those of the fluids to leading order in $k\tau$. Thanks to this compensation, the curvature potential ζ remains constant outside the Hubble radius, since it is affected by PMF only at order $\sim (k\tau)^2$ [26, 65].

The passive modes are instead generated before neutrino decoupling. Hence, without the neutrino free-streaming, the anisotropic stress of PMF is not balanced and a logarithmic growing mode (in conformal time) is therefore generated. As neutrinos decouple, their anisotropic stress can compensate the PMF one, leading to the compensated mode previously described; however, such logarithmic growing mode leaves an imprint in form of a constant offset on the amplitude of the inflationary (non-magnetic) mode [80].

There is also another class of magnetic modes, the inflationary ones, which are directly related to the inflationary generation mechanism for PMFs [11].

We now focus only on the compensated modes and show what are their contributions to the angular power spectra. We will then present, in Sec. 6.2.2, the comparison of such effects with our results, which were instead obtained by looking at the effects of PMFs

[4]The SB of PMF, if treated as a stiff source, acts as a force term in the Einstein-Boltzmann system, making them inhomogeneous. Thus, the solution will be the sum of that of the homogeneous system (the primary adiabatic modes) and that of the inhomogeneous one (the fully magnetic modes).

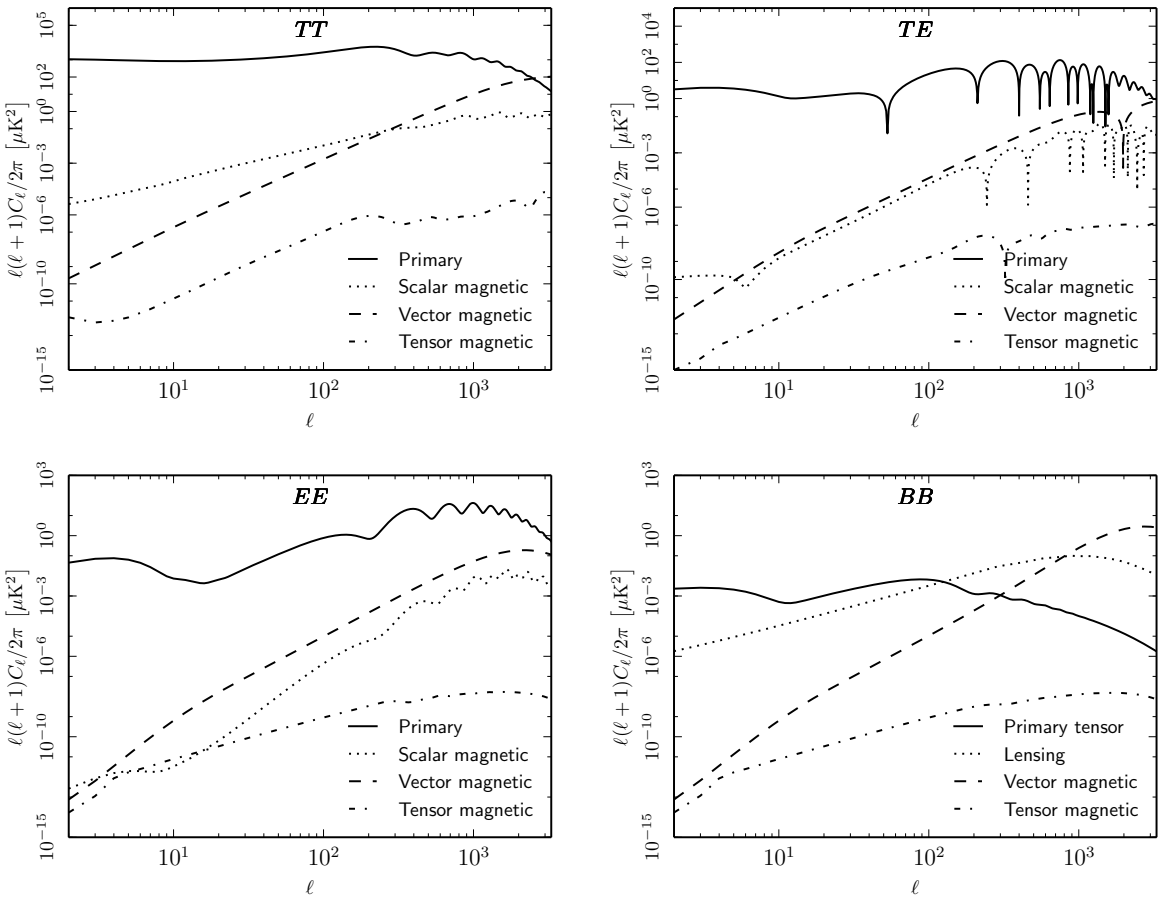

Figure 6.1: Magnetically-induced CMB TT (*top left*), TE (*top right*), EE (*bottom left*) and BB (*bottom right*) power spectra, for PMFs with $B_{1\,\mathrm{Mpc}} = 4.5$ nG and $n_B = -1$. The solid lines represent primary CMB anisotropies, while the dotted, dashed and dot-dashed lines represent magnetically-induced compensated scalar, vector and tensor modes, respectively (for the BB panel. the solid and dotted lines represent the primary tensor modes with a tensor-to-scalar ratio of $r = 0.1$ and the lensing contributions, respectively) [62].

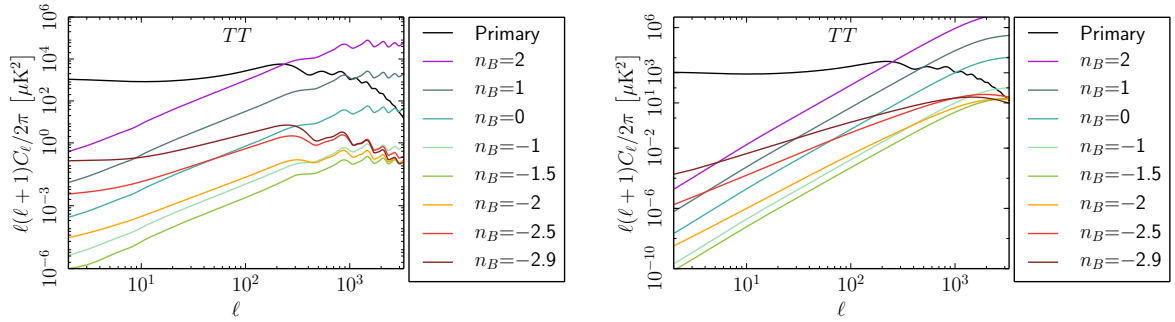

Figure 6.2: Dependence of the magnetically-induced CMB temperature power spectrum on the spectral index, for scalar (*left*) and vector (*right*) contributions. The amplitude of PMF is fixed at $B_{1\,\mathrm{Mpc}} = 4.5$ nG [62].

directly on the primary adiabatic modes. For the explicit expression of initial conditions for the compensated modes, see [26].

In Figure 6.1 the spectra for magnetically-induced compensated modes are shown. The dominant contributions to the angular power spectra for compensated initial conditions come from scalar and vector modes. Moreover, it can be noticed that the magnetic contributions become relevant at small scales, since magnetically-induced perturbations do not suffer from Silk damping, contrary to the primary ones [5]. Hence, a careful analysis of such scales is crucial for the constraining of PMFs. Another property of the magnetically-induced spectra is that their shape are strongly dependent on the PMF spectral index. This can be explicitly see in Figure 6.2, where such dependence for the temperature power spectrum, for scalar and vector perturbations, is displayed. In particular, one can see that, as n_B changes, for indices greater than $n_B = -3/2$ there is just a rescaling of the amplitude, while for smaller indices there is a change of the tilt, which reflects the infrared domination of the PMF EMT.

6.2 Effects for scalar adiabatic initial conditions

We show now our original results of the effects of PMFs for adiabatic initial conditions. Contrary to the usual approach of analyzing the PMF contribution for magnetized initial conditions and evolving magnetically induced independent modes, as shown in Sec. 6.1.3, we instead study the impact of PMFs directly on the primary adiabatic modes.

For this purpose, we select the usual adiabatic initial conditions, those presented in Sec. 2.5, and we developed a dedicated extension of the SONG code which includes the PMF contributions to the Einstein and Boltzmann equations. With this dedicated

[5] Alfvén waves behave as overdamping oscillators, hence being suppressed at scales smaller then the Silk one.

extension we see how the cosmological perturbations and the CMB power spectrum are affected. However, in the original version of SONG the PMF terms into the Einstein and Boltzmann equations were not implemented. Hence, we modified the code by introducing PMF contribution in the first order Einstein equations and in the first order evolution equation for baryons. The final goal would be to include all the next-to-leading effects which arise from the presence of PMFs in the primordial plasma. In fact, particularly at small scales non-linear effects induced by PMFs may be relevant and we would enter the realm of non-ideal MHD. So far, such effects are tested mainly with small-scale MHD simulations, but a complete and careful analysis of such physics with the use of the full Einstein and Boltzmann system is still lacking. In our work, we performed the first step towards this promising treatment by considering the coupling of the adiabatic modes with the magnetic field with the inclusion of the main PMF contributions: energy density, anisotropic stress, Lorentz force, Alfvén velocity; into the first-order Einstein and fluid equations, in such a way to capture the relevant next-to-leading order effects. We stress however that this is an approximate calculation, since we are for this first step neglecting the backreaction of the fluid into the PMF and hence the non-linear evolution of the magnetic field itself.

In this chapter we focus on the PMF effects for the first-order temperature power spectrum. In particular, we see the contributions of the Lorentz force and the PMF terms in the Einstein equations individually. In Chapter 7 instead we will focus on the next-to-leading effects of PMFs, showing in particular how baryon inhomogeneities are affected and their possible non-linear behaviour around recombination, especially for blue magnetic spectra; we will also introduce the effect of PMFs on the speed of sound, which is usually neglected in standard linear treatments, and show the correspondent impact on the baryon density perturbations and on the temperature power spectrum.

We finally stress that our treatment is limited to the scalar perturbations, but an extension to vector and tensor ones can be surely an interesting subject of future studies.

6.2.1 Lorentz force contribution

The presence of PMFs induces a Lorentz force on baryons and affects their velocity. In particular, being electrically charged, their conservation equations are modified by the introduction of an electromagnetic source term as

$$\nabla_\mu \delta T^{\mu\nu}_{\rm baryons} \propto F^{\mu\nu} J_\mu \ . \tag{6.18}$$

Since the primordial plasma can be considered globally neutral, $J_0 = 0$ and hence the energy conservation equation for baryons is not modified. The Euler equation, however, gets an additional term which is the Lorentz force contribution and becomes

$$\left({}_1b_0^1\right)' = -\mathcal{H}\,{}_1b_0^1 + 3\,k\,c_s^2\,{}_0b_0^0 + 3\,k\,\Psi - r\kappa'\left(4u_{[0]} - \mathcal{I}_0^1\right) - \frac{3\,k}{\rho_b}\,L \ , \tag{6.19}$$

The new term $-3\,k\,L/\rho_b$ encodes the Lorentz force contribution on baryon velocity and scales as $1/a(\tau)$.

Prior to recombination, photons and baryons are tightly coupled and therefore an indirect influence of the Lorentz force is present also for photons during this regime. The combination of the photon and baryon equations gives

$$\begin{aligned}(1+r)\left({}_1b_0^1\right)' = &-\mathcal{H}\,{}_1b_0^1 + 3\,k\,c_s^2\,{}_0b_0^0 + (1+r)\,3\,k\,\Psi \\ &+ 3\,k\,r\left(\frac{1}{4}\mathcal{I}_0^0 - \frac{1}{10}\mathcal{I}_0^2\right) + r\left[\frac{3}{4}\left(\mathcal{I}_0^1\right)' - \left({}_1b_0^1\right)'\right] - \frac{3\,k}{\rho_b}\,L\ , \end{aligned} \tag{6.20}$$

with $r = \bar{\rho}_\gamma/\bar{\rho}_b$ and

$$\begin{aligned}\left({}_1b_0^1\right)' - \frac{3}{4}\left(\mathcal{I}_0^1\right)' = &\frac{2\,r}{1+r}\,\mathcal{H}\left({}_1b_0^1 - \frac{3}{4}\mathcal{I}_0^1\right) + \frac{\tau}{1+r}\Bigg[-\frac{a''}{a}\,{}_1b_0^1 \\ &- 3\,k\,\mathcal{H}\left(\frac{1}{2}\mathcal{I}_0^0 + \Psi\right) + 3\,k\left(c_s^2\left({}_0b_0^0\right)' - \frac{1}{4}\left(\mathcal{I}_0^0\right)'\right) + \mathcal{H}\,\frac{3\,k}{\rho_b}\,L\Bigg]\ . \end{aligned} \tag{6.21}$$

The photon Euler equation in the tight-coupling regime becomes

$$\begin{aligned}\left(\mathcal{I}_0^1\right)' = &-\frac{1}{r}\left(\frac{4}{3}\left({}_1b_0^1\right)' + \frac{4}{3}\,\mathcal{H}\,{}_1b_0^1 - 4\,k\,c_s^2\,{}_0b_0^0 + \frac{4\,k}{\rho_b}\,L\right) \\ &+ 2\,k\left(\frac{1}{2}\mathcal{I}_0^0 - \frac{1}{5}\mathcal{I}_0^2\right) + \frac{1+r}{r}\,4\,k\,\Psi\ . \end{aligned} \tag{6.22}$$

Hence, we note the appearance of the Lorentz term which however disappears once the tight-coupling ends, as we would expect.

For the expression of the Lorentz force, we use the analytic solutions to the convolution integral 6.15 derived in [26] and [65] for fixed spectral indices. In particular, one finds that there is a non-vanishing contribution only for $0 < k < 2\,k_D$, as a consequence of the sharp cut-off of the power spectrum at the damping scale k_D. The explicit expressions of the Lorentz Fourier spectra are given in Appendix C.

In Figure 6.3 we show, in the top panel, how the CMB temperature power spectrum is affected by the presence of the Lorentz force, for different spectral indices and for $B_{1\mathrm{Mpc}} = 1$ nG, while in the lower panel percentage differences from the case without PMFs are shown (for a better visualization of the small percentage differences for negative indices, see Appendix D). It can be noticed that the effect progressively increases for larger values of n_B, but remains pretty subdominant up to $n_B = 1$ ($\lesssim 2\%$), with a quite appreciable contribution only for $n_B = 2$ (up to 10% of difference). However, for indices smaller than $n_B = -3/2$ we note an increasing effect at large angular scales: this may reflect the change in the infrared behaviour of the Lorentz spectra, which from white noise for indices greater than $-3/2$ become infrared dominated for smaller indices.

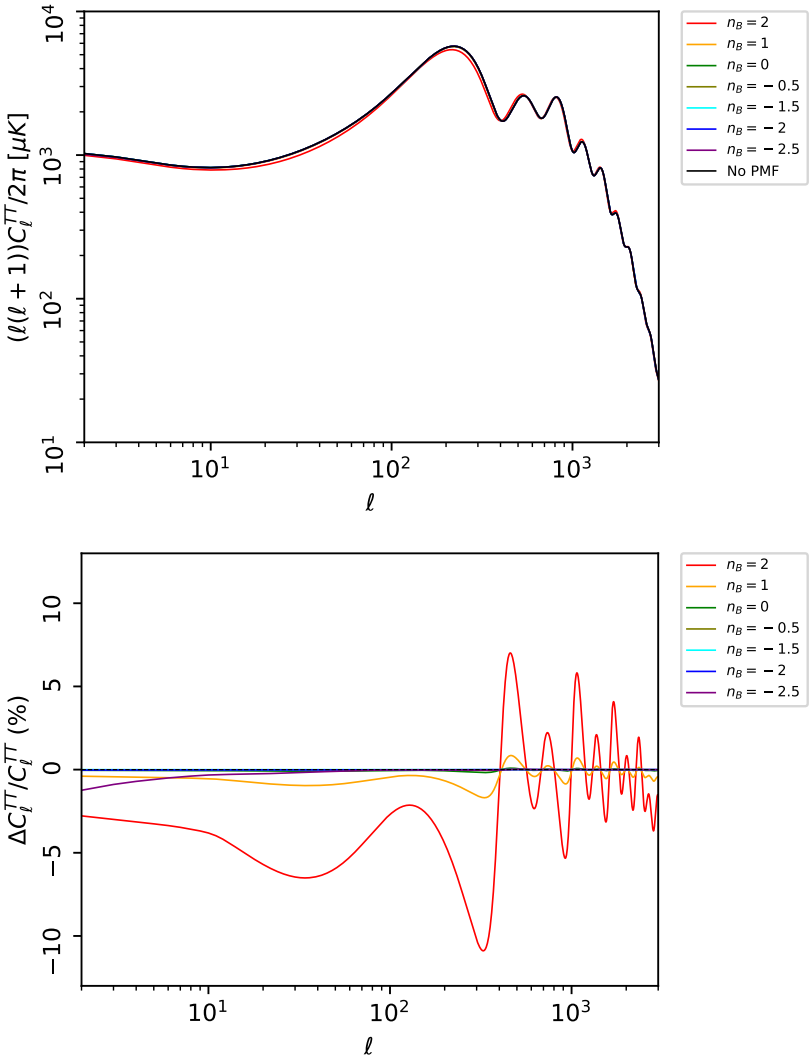

Figure 6.3: In the *top* panel, CMB temperature power spectrum without (black line) and with Lorentz force contribution for different spectral indices (coloured lines, see the legend); in the *lower* panel, the percentage differences with respect the case without PMFs for different indices (see the legend). In all cases with PMFs, $B_{1\mathrm{Mpc}} = 1$ nG.

6.2.2 PMF contribution in the Einstein equations

We associated to PMFs an energy-momentum tensor which is treated at the same level of first-order perturbations. Hence, at linear order PMFs gravitate and affect all the components of the cosmological fluid. The perturbed Einstein equations now read

$$\delta G_{\mu\nu} = 8\pi G \left(\delta T_{\mu\nu} + \tau_{\mu\nu}\right) . \tag{6.23}$$

where $\delta T_{\mu\nu}$ and $\tau_{\mu\nu}$ are the EMTs of the fluid and of PMF, respectively.

In Newtonian gauge, we then have

$$\begin{aligned}
6\mathcal{H}^2\Psi + 6\mathcal{H}\,\Phi' + 2k^2\Phi =& -8\pi G a^2 \left(\sum_n \bar{\rho}_{n\,0}\Delta_{00}^{(n)} + \rho_B\right) , \\
6\ddot{\Phi} + \Psi(6\mathcal{H}^2 + 12\dot{\mathcal{H}}) + 6\mathcal{H}(\dot{\Psi} + 2\dot{\Phi}) + 2k^2(\Phi - \Psi) =& 8\pi G a^2 \left(3\sum_n c_{sn}^2\,\bar{\rho}_{n\,0}\Delta_{00}^{(n)} + \rho_B\right) , \\
-2k(\dot{\Phi} + \mathcal{H}\Psi) =& 8\pi G a^2 \sum_n (\bar{\rho}_n + \bar{P}_n)\, V_{[0]n} , \\
-\frac{2k^2}{3}(\Phi - \Psi) =& 8\pi G a^2 \left(\sum_n \Sigma_{[0]n} + \sigma_B\right) ,
\end{aligned} \tag{6.24}$$

where $n = \gamma, \nu, b, c$ labels the different components. For the expression of ρ_B we again used the analytic solutions of the convolution integral (6.12) in [26] and [65] (see Appendix C), while σ_B is directly obtained through equation (6.17). We see then that additional terms due to the presence of the PMF EMT appear in the time-time, trace and space-space equation, while the space-time one is not affected. It is also evident, from the space-space equation, that PMFs provide anisotropic stress in addition to that of photons and neutrinos.

In Figure 6.4 we see the impact of such terms on the CMB temperature angular power spectrum for different spectral indices and the percentage differences. As in the Lorentz case, the effect becomes larger as the considered spectral increases (for $n_B = 2$ we observe a difference up to 15%), except for indices smaller than $-3/2$, where an increasing effect at larger angular scales as n_B becomes smaller is observed (but always below 2%). However, the impact on CMB power spectrum due to the modification of the Einstein equations seems to have an opposite behaviour with respect to that of the Lorentz force. Such feature is quite evident looking at the percentage differences in Figure 6.3 and Figure 6.4, where one can clearly see the opposite contributions due to the two effects (for example, the modification to the Einstein equations enhances the odd peaks and suppresses the even ones, at least till $\ell \sim 2000$ where an overall raising takes place, while the opposite happens for the Lorentz contribution).

In Figure 6.5 the same plots are shown for the combined effects of the PMF EMT in the Einstein equations and the Lorentz force. We see that there is an overall suppression

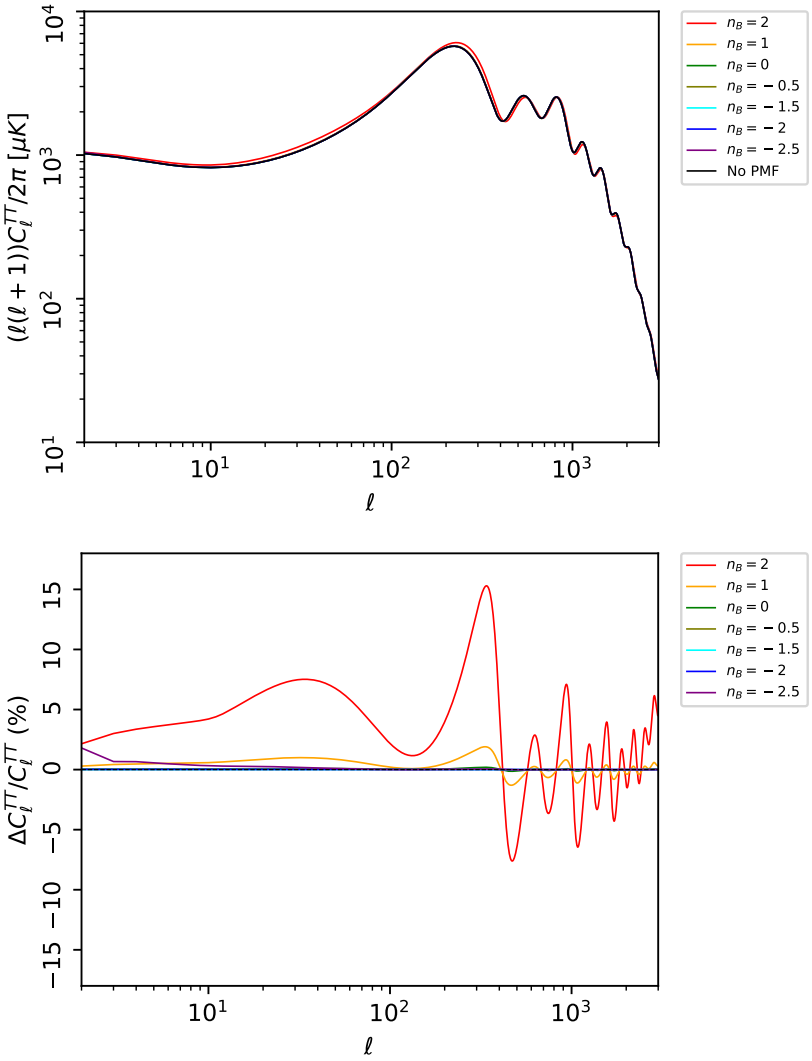

Figure 6.4: In the *top* panel, CMB temperature power spectrum without (black line) and with PMF EMT contribution in the Einstein equations for different spectral indices (coloured lines, see the legend); in the *lower* panel, the percentage differences with respect the case without PMFs for different indices (see the legend). In all cases with PMFs, $B_{1\mathrm{Mpc}} = 1$ nG.

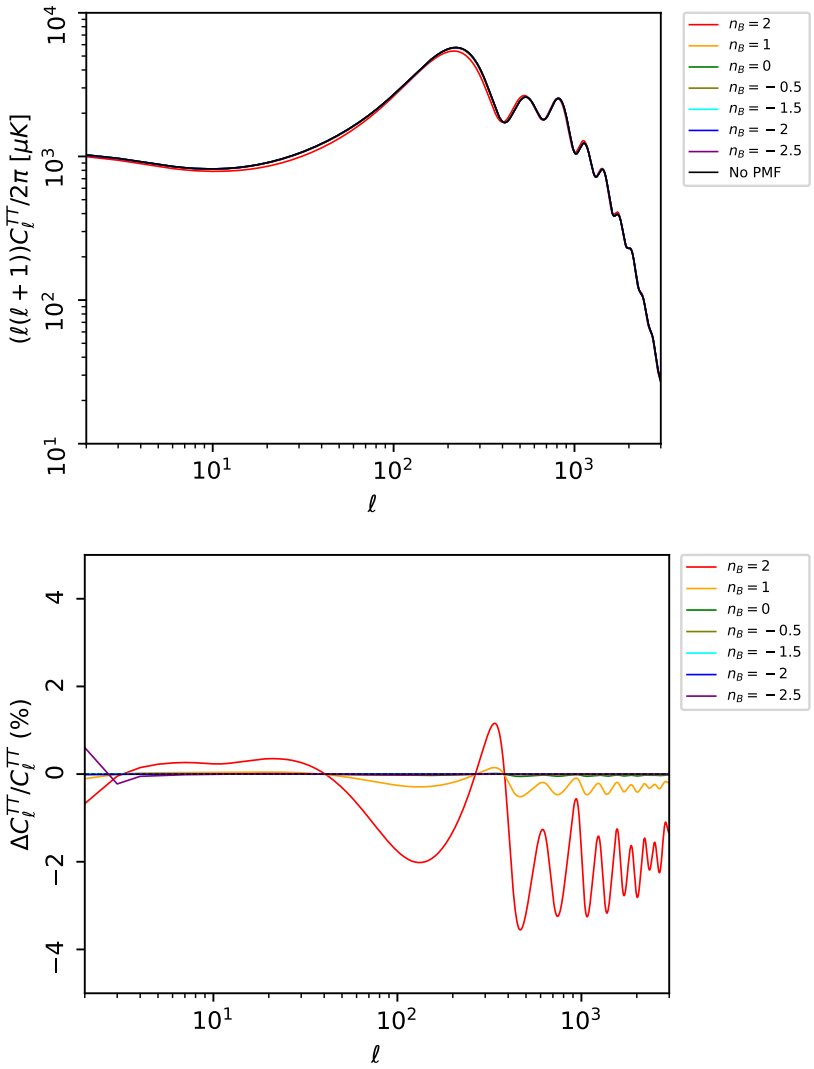

Figure 6.5: In the *top* panel, CMB temperature power spectrum without (black line) and with both the PMF EMT in the Einstein equations and Lorentz contributions for different spectral indices (coloured lines, see the legend); in the *lower* panel, the percentage differences with respect the case without PMFs for different indices (see the legend). In all cases with PMFs, $B_{1\mathrm{Mpc}} = 1$ nG.

of anisotropies for scales smaller than the horizon at recombination especially for the largest indices, while at larger scales the spectrum is only slightly increased for $n_B = 2$. The combination of the two effects provides a smaller contribution with respect to the individual cases, with differences below 4% at all scales. A comparison with the magnetically-induced compensated power spectra is shown in Figure 6.6.

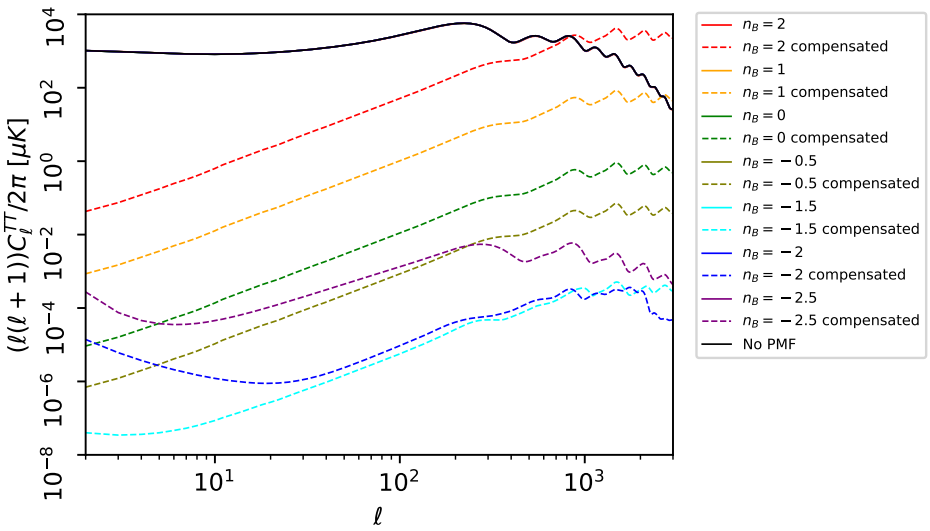

Figure 6.6: Comparison of adiabatic CMB angular power spectra (solid lines) with magnetically-induced compensated spectra (dashed lines), for different spectral indices (see the legend). In all cases with PMFs, $B_{1\mathrm{Mpc}} = 1$ nG and both the PMF EMT in the Einstein equations and the Lorentz force are included.

Chapter 7

Next-to-leading effects for PMF in CMB

The presence of PMFs in the cosmological plasma introduces several complex effects which are beyond the linear and ideal MHD regimes. Despite countless studies, a general and exhaustive treatment of PMFs within the general relativistic framework of the Einstein-Boltzmann equations is still lacking. So far, such non-linear effects, which are relevant mostly at small scales, are investigated through MHD simulations of small cells of plasma, which however completely miss the large-scale physics and the possible effects into the cosmological observables, like the CMB anisotropies.

A crucial effect which arises at small scales and which is particularly important for the purpose of this work is the generation, induced by PMFs, of baryon density inhomogeneites of considerable magnitude [38]. Shortly before recombination, photons and baryons are no longer tightly coupled and the photon mean free path (l_γ) progressively increases; hence, below this scale, photons do not co-move with the fluid anymore and they start to free stream. However, they still strongly affect the fluid by occasionally scattering with the moving electrons and therefore they introduce a drag force on the baryon fluid, leaving the plasma in a highly viscous state at small scales, before recombination. As the photons decouple from the fluid, there is a dramatic decrease in the speed of sound and the magnetic pressure becomes dominant with respect to the radiation one. It was shown [38] that such magnetic fields, with strengths of ~ 0.1 nG, can induce compressional flows at scales smaller than l_γ and hence density fluctuations as large as $\delta\rho/\rho \sim 1$ may be generated before recombination. The presence of such inhomogeneities on $\sim$ kpc scales may profoundly change the recombination history. In fact, the recombination rate is proportional to the electron density square n_e^2. As an inhomogeneous Universe has $\langle n_e^2\rangle > \langle n_e\rangle^2 = \langle n_e^2\rangle|_{\rm homo}$ (with $\langle n_e^2\rangle|_{\rm homo}$ being referred to an homogeneous Universe), the generation of baryon inhomogeneities would increase the average recombination rate and makes it happen at earlier times. An earlier recombination in turn would imply a smaller sound horizon (r_*) at recombination and hence a

shift of the Doppler peaks at smaller scales. According to a recent proposal by Jedamzik and Pogosian [40], since the positions of the peaks, $\ell \propto r_{\rm ls}/r_*$, are accurately measured by the Planck satellite, it becomes necessary to have a smaller conformal distance to last scattering ($r_{\rm ls}$) to compensate for the shift, hence requiring a larger value of the Hubble constant, H_0. The presence of PMFs could therefore provide a promising way to relieve the tension with the measurements of H_0 from the local Universe through type Ia supernovae, according to which H_0 is up to 5 standard deviations higher than the one determined from CMB [74, 73].

Another important effect which is usually neglected in the standard approach is the one that a magnetic fields induce on the baryon speed of sound, due to the possible excitation of magneto-hydrodynamics waves. It is in principle a second-order effect and further hidden by the large value of c_s, but its contribution may become relevant once approaching to recombination, when the baryon speed of sound experiences a large decrease due to the photon decoupling.

In this chapter we focus on these two effects. In particular, we show the influence of PMFs on the evolution of baryon density perturbations and investigate their impact around recombination; we then study the effect on CMB angular spectrum and baryon evolution with the modification of the speed of sound. We conclude by giving an outlook showing the second-order spectra within our approach. The results show how the base treatment we use may be insufficient for the full second order spectra, that might require the involvement of more terms; hence an expansion of our work in this direction can surely be an attractive goal for future studies.

As said before, an exhaustive treatment of all these effects within the use of Einstein-Boltzmann codes still misses. In the perspective of future cosmological data, with a precision which is progressively increasing, the modeling of this kind of physics may become crucial. In this context, our work represents a first step, that is to capture such effects by including the PMF energy-momentum tensor, together with the Lorentz force and the Alfvén velocity contributions, in the linear equations and using the second-order Einstein-Boltzmann code SONG to compute the evolution of cosmological perturbations and CMB anisotropies. It is already known that non-linear effects induced by PMFs are potentially relevant for structure formation, but their impact at earlier times on CMB anisotropies is still unclear.

In our work, we ignored the backreaction of the fluid into the magnetic field, *i.e.* we did not consider the non-linear evolution of the field due to the coupling with the plasma and therefore we simply evolved it as $1/a^2$. The idea could be to use the induction equation (5.18) and include the Harrison mechanism, already implemented in SONG, to evolve the field beyond linear order, but such treatment would surely require a deeper and longer study. This probably represents the major limitation of our work and the most natural extension for future, more complete, studies.

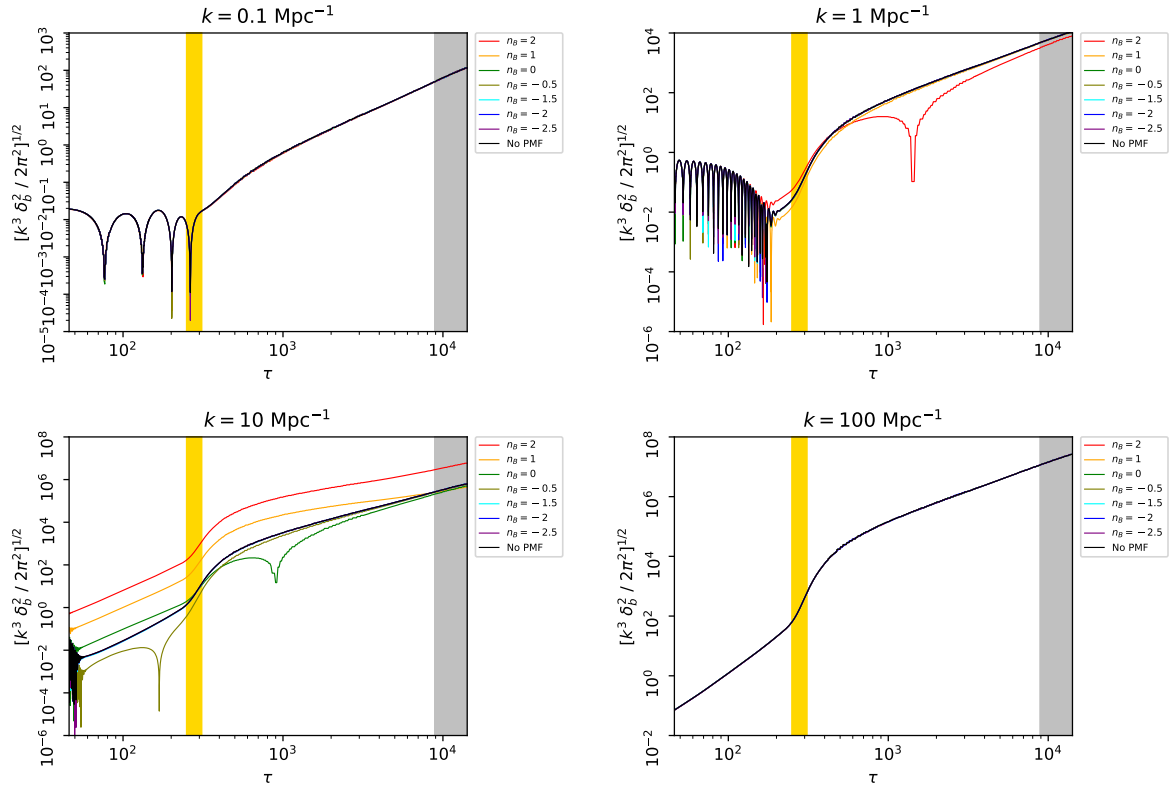

Figure 7.1: Time evolution of baryons for 4 different wavenumbers without (black line) and with PMFs for different spectral indices (coloured lines, see the legend). The golden and silver bands refer to the recombination epoch and $z < 2$, respectively. For all the cases with PMFs, $B_{1\mathrm{Mpc}} = 1$ nG and both the PMF EMT and Lorentz contributions are considered.

7.1 Effect on baryon inhomogeneities

We now focus on the influence that PMFs have on baryon inhomogeneities and test if, under our assumptions, such effects may be relevant during recombination and lead to possible non-linearities already during this epoch, in particular for blue magnetic spectra. In Figure 7.1 we show the time evolution of baryons [1] for 4 different wavenumbers (k=0.1 ,1, 10, 100 Mpc^{-1}) in presence of PMFs (with both the PMF EMT and Lorentz contributions) for different spectral indices, with in addition the case of no PMFs as reference. The golden and silver bands refer to the recombination epoch and $z < 2$, respectively. The first important thing to note is that the maximum contribution of PMFs is for $k = 10$ Mpc^{-1}, whereas for $k = 100$ Mpc^{-1} the effect almost disappears;

[1] In this chapter, all the baryon perturbations are represented in synchronous gauge, in order to be allowed to perform comparisons with results in the literature, that are available in synchronous gauge.

this behaviour is indeed expected, since at such small scales like $k = 100$ Mpc^{-1} we are well below the damping scale k_D for the chosen field configurations and furthermore for $k > 2k_D$ the EMT and Lorentz spectra have no support (see Appendix C). In accordance with what has been seen for the angular power spectra in Chapter 6, the case for $n_B = 2$ provides the maximum contribution also for the evolution of baryons. Particularly interesting is the case for $k = 10$ Mpc^{-1}, where unlike the other cases we observe an enhancement of the growth of baryon perturbations for blue spectral indices like $n_B = 2$ and $n_B = 1$, even at recombination. Although this may be a good argument in favour of the claim in [40] concerning the inhomogeneous recombination and the possible affection to the Hubble constant, a few considerations have to be made. First of all, the result we obtained are for $B_{1\mathrm{Mpc}} = 1$ nG, which however is larger than the current upper 95% C.L. bound of 3 pG [64], for $n_B = 2$ and for the same assumptions we have used. Moreover, we are so far neglecting the contribution of the magnetic pressure, which however at sufficiently small scales causes an opposite force against the growth of perturbations and may profoundly affect the results in Figure 7.1, as we will see in Sec. 7.2. A similar argument about the importance of the magnetic pressure for the perturbation growth is also made in [81]: below the magnetic Jeans scale, the restoring force due to the magnetic pressure gradient is significant and cannot be neglected anymore.

We also tested our result by comparing it with the approximated analytic solution found in [81] for the evolution of δ_b. This solution was found by considering a magnetized plasma in the limit of ideal MHD (so $\eta = 0$ and $B \propto a^{-2}$) and weak magnetic fields, hence obtaining the following evolution equation for δ_b (in real space) [81]:

$$\frac{\partial^2 \delta_b}{\partial t^2} + \left(2H + \frac{4\rho_\gamma}{3\bar{\rho}_b} n_e \sigma_T\right) \frac{\partial \delta_b}{\partial t} - c_s^2 \frac{1}{a^2} \nabla^2 \delta_b = 4\pi G\, \delta\rho_\mathrm{m} + \frac{1}{a^3} S_0(\mathbf{x}) \ , \tag{7.1}$$

where $\delta\rho_\mathrm{m} = \bar{\rho}_b\, \delta_b + \bar{\rho}_c\, \delta_c$ and $S_0 = \nabla \cdot [\mathbf{B} \times (\nabla \times \mathbf{B})]/[4\pi\bar{\rho}_b(t_0)]$ is the magnetic source of the density perturbations (here $\mathbf{B}$ is the physical field, *i.e.* non-comoving) which takes into account the induced Lorentz force on baryons. We see that whereas gravity enhances the growth of perturbations (the first term in the right hand side), the expansion of the Universe, the radiative viscosity and the baryonic pressure provide the opposite contribution (second, third and fourth terms in the left hand side, respectively). At sufficiently small scales, we are in the free-streaming regime where radiation viscosity dominates, hence the contributions of gravitational instability and the expansion of the Universe can be neglected. In this regime, the evolution of baryon inhomogeneities is therefore controlled by the balance of the viscous and Lorentz forces in equation 7.1. In this particular case, the equation can be integrated and yield [81]

$$\delta_b \simeq 3.5 \times 10^{-5}\, B_{-9}^2 \left(\frac{k}{\mathrm{Mpc}^{-1}}\right)^2 \left(\frac{\Omega_\mathrm{m} h^2}{0.15}\right)^{-1/2} \left(\frac{1+z}{10^3}\right)^{-5/2} \ , \tag{7.2}$$

which represents the baryon inhomogeneity induced by the magnetic field. B_{-9} is the smoothed field on the scale k in units of nG. This solution is however valid only around

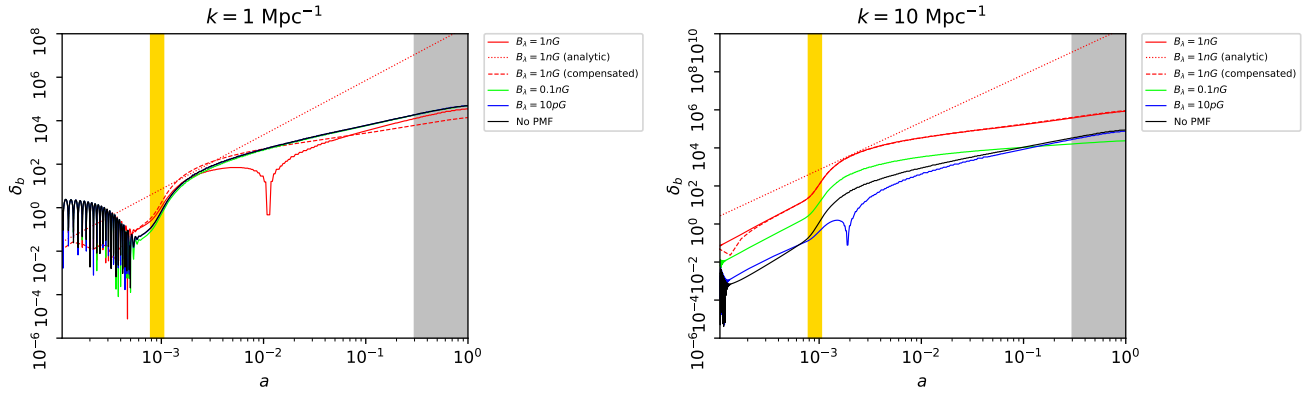

Figure 7.2: Baryon evolution for $k = 1$ Mpc$^{-}1$ (*left*) and for $k = 1$ Mpc$^{-}1$ (*right*). The dotted red line represents a rendering of the analytic solution (7.2) (equation (16.31) in [81]) for $B_\lambda = 1$ nG and $n_B = 2$, for all the other cases see the legend. For all the cases with PMFs, the spectral index is $n_B = 2$ and the contributions of both the Lorentz force and the EMT in the Einstein equations are considered.

recombination and for scales greater than the magnetic Jeans scale [81]

$$k_J \simeq 14.8\,\mathrm{Mpc}^{-1} \left(\frac{\Omega_\mathrm{m}}{0.3}\right)^{1/2} \left(\frac{h}{0.7}\right) \left(\frac{B_J}{\mathrm{nG}}\right)^{-1} f_b^{1/2}\,, \tag{7.3}$$

where $f_b = \Omega_b h^2/0.022$ and B_J is the smoothed field at the magnetic Jeans scale k_J.

In Figure 7.2 we show the comparison of our numerical result with the analytic approximation 7.2 for $B_{1\mathrm{Mpc}} = 1$ nG, $n_B = 2$ and for $k = 1$, 10 Mpc^{-1}. We observe a good agreement around recombination, which we remind is the period of validity of equation 7.2, although the analytic approximation seems to give a slightly larger values than our results, which however may be due to the different underlying assumptions with respect to ours. Moreover, in equation (7.2) we used as a first approximation the root mean square of the field (obtained from equation (6.5) and setting $B_{1\mathrm{Mpc}} = 1$ nG), but a more solid treatment, taking also into account the exact relations between the two notations, may be an interesting goal for future analyses to establish a more accurate comparison (which however is already at good level). An interesting feature that can be further noted is that for $k = 10$ Mpc^{-1} the slopes of our numerical result seems to roughly match the analytic estimates till recombination.

In Figure 7.2 it is also represented the baryon evolution for smaller values of B_λ (0.1 nG and 10 pG). We clearly see that the enhancement of baryon inhomogeneities progressively reduces as the smoothed amplitude decreases, and for $B_\lambda = 10$ pG (which is not far from the upper bound of 3 pG in [64]) the impact around recombination is particularly suppressed. All these arguments, together with the possible further suppression provided by the magnetic pressure (whose contribution will be investigated in Sec. 7.2), reinforces

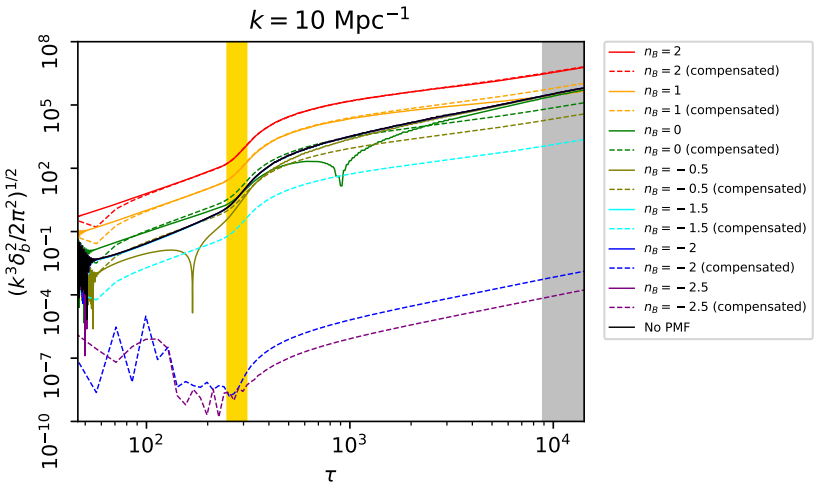

Figure 7.3: Comparison of baryon evolution for adiabatic perturbations (solid lines) with that for compensated modes (dashed lines), for different spectral indices (see the legend) and for $k = 10$ Mpc$^{-}1$. The golden and silver bands refer to the recombination epoch and $z < 2$, respectively. For all cases with PMFs, $B_{1\mathrm{Mpc}} = 1$ nG and both the PMF EMT in the Einstein equations and the Lorentz force are included.

the necessity to perform a more accurate and exhaustive treatment of all the non-trivial effects introduced by PMFs at such small scales before drawing firm conclusions about the impact on recombination and the cosmological implications that would follow, as also stressed in [81]. Moreover, we remark the fact that all the results we obtained are dependent on our underlying assumptions, like for example the use of equation (6.3) as sharp cut-off in the magnetic power spectrum, and hence slightly different conclusions might be made for other choices.

7.1.1 Comparison with compensated modes

In Figure 7.3 we show the baryon evolution for $k = 10$ Mpc$^{-}1$ for different spectral indices, with both the Lorentz and the PMF EMT contributions, in comparison with that for compensated modes, again for different spectral indices and for $B_{1\mathrm{Mpc}} = 1$ nG. An interesting fact which can be noted is that as the spectral index increases, the two cases become more and more overlapping, while such coincidence is gradually lost for smaller values of n_B. This can be due to the fact that at such scales and for high spectral indices the contribution of the PMF terms for the adiabatic mode starts becoming dominant and therefore a similar behavior of the pure magnetic case is achieved.

7.2 Effect on the speed of sound

A relevant, non-linear contribution we included in our work is the magnetic counterpart of the Jeans effect. When a perturbation grows due to gravitational collapse, the pressure of the gas increases and eventually stops the growth. A magnetic field, if present, gives a contribution to the pressure, hence providing additional support against the collapse. A magnetic Jeans scale can therefore been identified, given by the balance between the gravitational force and the magnetic pressure. We expect that the Jeans effect is primarily mediated by the fast magnetosonic mode, which is the fastest one that can arise in a magnetized plasma and reduces to the usual acoustic mode in the limit of small magnetic field. A way to model this effect and hence to include the contribution of the magnetic pressure is to take into account such modes and properly modify the speed of sound. A pioneering work in this direction was made by Adams et al. [1], who however considered the case of an homogeneous magnetic field. We followed instead the approach for a stochastic background presented in [79] and we modified the baryon speed of sound as

$$c_s^2 \to c_s^2 + \frac{2}{9}\, v_A^2 \ , \tag{7.4}$$

where v_A is the Alfvén velocity defined as

$$v_A^2 = \frac{1}{4\pi\rho_b\, a^4}\, \langle B^2 \rangle \ . \tag{7.5}$$

The factor 2/9 is an angular factor which depends on the exact velocity and field orientation (see [79] for the computation). We however remark that, while the authors in [79] in the definition of v_A^2 used $\langle B^2 \rangle_k$, that is the variance of the field from scales larger than k, we instead used the mean square of the field, $\langle B^2 \rangle$.

In Figure 7.4 the time evolution of baryon density perturbations are represented, for different values of n_B. As it can be clearly noted, the addition of the Alfvén velocity to the speed of sound has the effect of strongly suppressing the growth of the baryon overdensities and this effect becomes larger as the spectral index increases. This is in agreement with the fact that with this modification of the speed of sound we are encapsulating the effect of the magnetic pressure, which provides additional support against gravitational collapse and hence hinders the growth of baryon overdensities. Moreover, this suppression starts at earlier times and becomes stronger as the considered scale of perturbations decreases and the spectral index increases; in particular, for $k = 0.1$, 1 Mpc^{-1} we observe an appreciable deviation from the case without PMFs only from recombination, while for greater wavenumbers and for the largest indices such effect begins even earlier. This is again an expected result, since, as already said, either approaching to recombination or considering smaller scales, photons progressively decouple from baryon as their mean free path increases and hence the baryon speed of sound decreases, which in turn implies that the contribution of the Alfvén velocity starts becoming relevant.

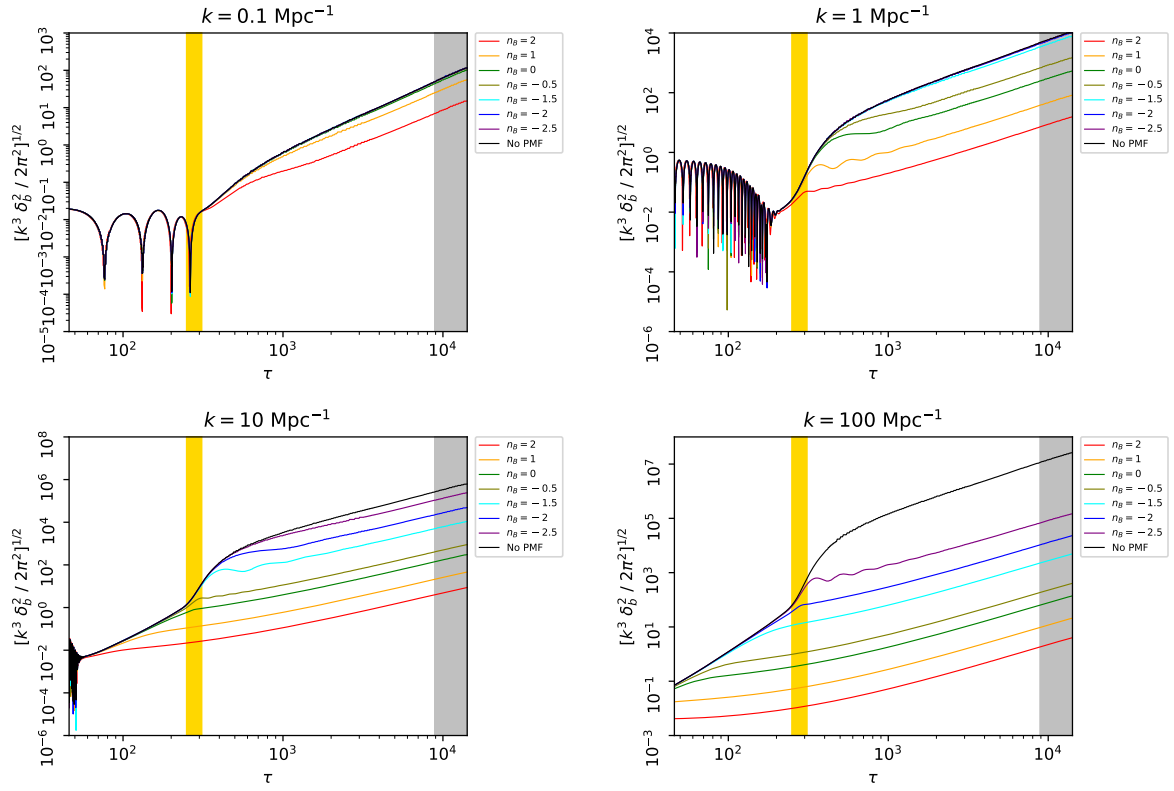

Figure 7.4: Time evolution of baryons for 4 different wavenumbers without (black line) and with the Alfvén velocity contribution for different spectral indices (coloured lines, see the legend). The golden and silver bands refer to the recombination epoch and $z < 2$, respectively. For all the cases with PMFs, $B_{1\mathrm{Mpc}} = 1$ nG.

In Figure 7.5 we show the impact on CMB power spectrum and the percentage differences due to the modification of the speed of sound. As in the previous cases, the effect becomes progressively more important as n_B increases; now, however, we do not observe a raising of the contribution at large scales for indices smaller than $-3/2$, since in equation (7.5) the Alfvén velocity just depends on the root mean square of the magnetic field and therefore no Fourier spectra is involved. It provides a stronger contribution with respect to the other effects seen so far, with differences up to 20% for $n_B = 2$. It should be remarked, though, that the used smoothed amplitude is $B_{1\mathrm{Mpc}} = 1$ nG, which is however larger than the upper bound of 3 pG at 95% C.L. [64] for $n_B = 2$. Another feature that can be noted is that the acoustic peaks are slightly shifted at larger scales, this effect being more evident for $n_B = 2$: this is exactly what we expect when increasing the speed of sound, since in this way also the sound horizon at recombination becomes correspondingly larger and hence the peaks get shifted at larger scales, *i.e.* at lower multipoles.

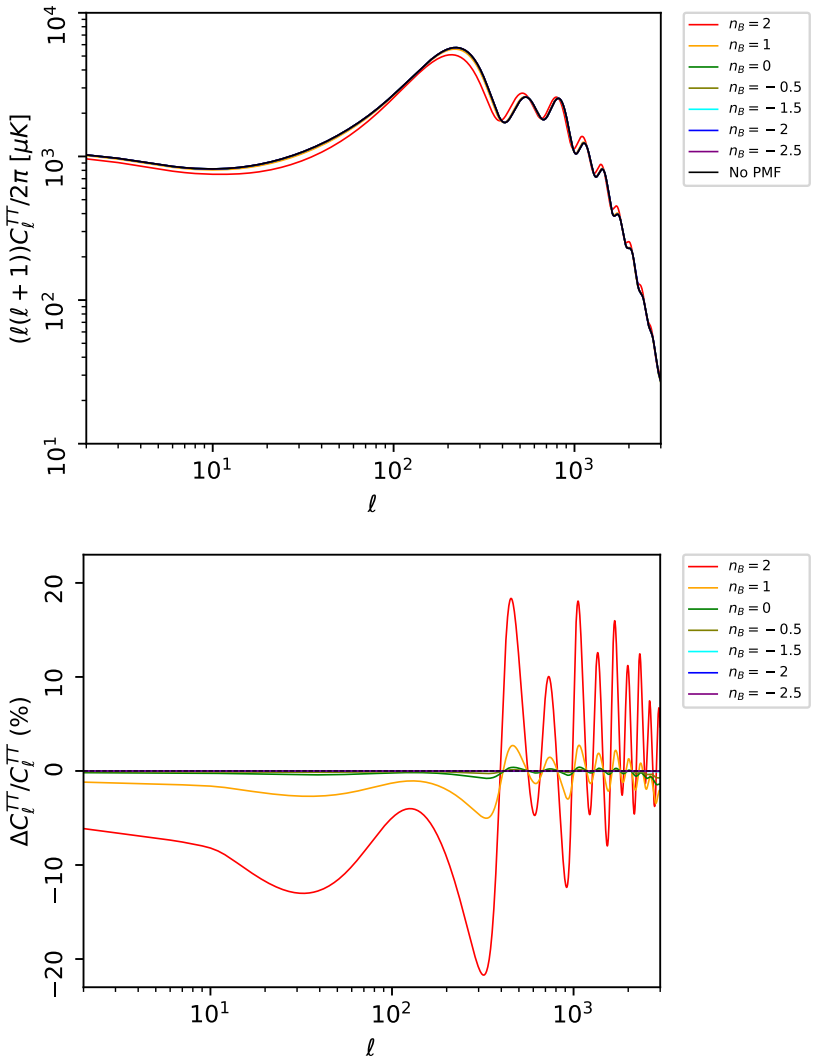

Figure 7.5: In the *top* panel, CMB temperature power spectrum without (black line) and with Alfvén velocity contribution for different spectral indices (coloured lines, see the legend); in the *lower* panel, the percentage differences with respect the case without PMFs for different indices (see the legend). In all cases with PMFs, $B_{1\mathrm{Mpc}} = 1$ nG.

7.3 Total PMF contribution and comparison with compensated modes

We now consider the combined effect of all the PMF contributions considered so far (Lorentz force, PMF EMT in the Einstein equations, the Alfvén velocity) and show their impact on baryon density perturbations and on CMB angular power spectrum. In

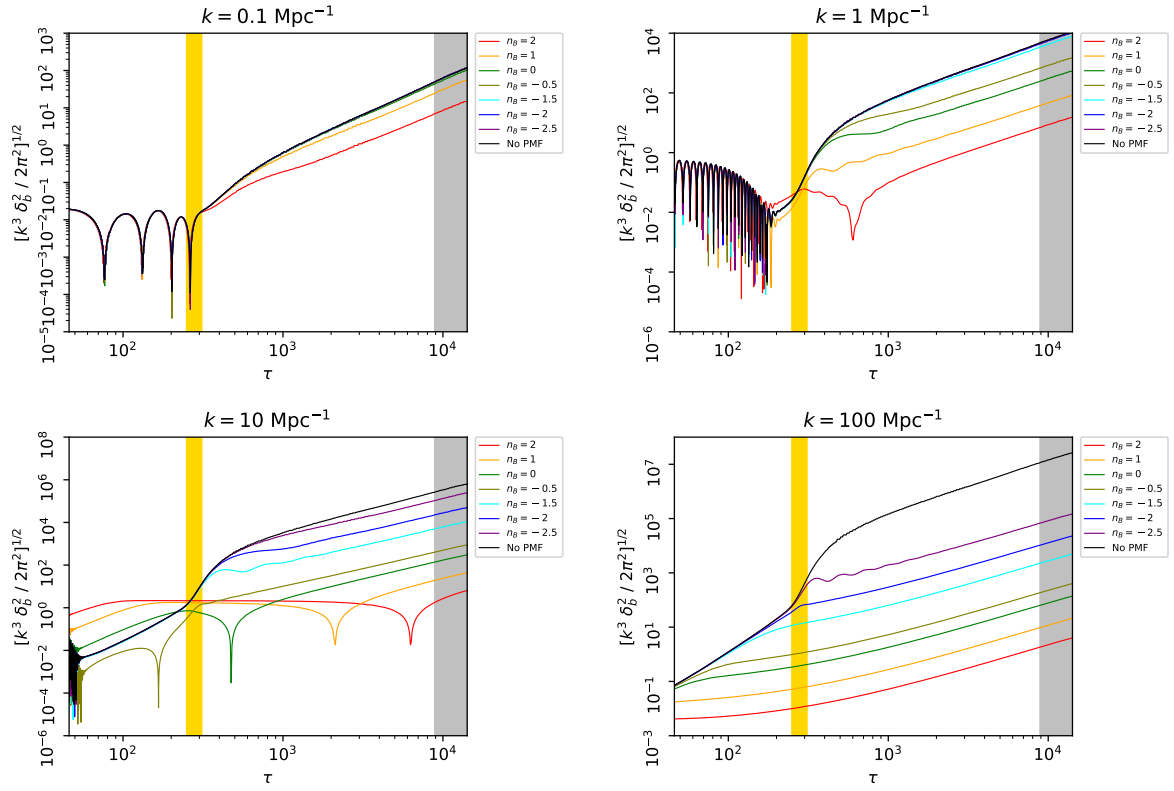

Figure 7.6: Time evolution of baryons for 4 different wavenumbers without (black line) and with the total PMF contribution for different spectral indices (coloured lines, see the legend). The golden and silver bands refer to the recombination epoch and $z < 2$, respectively. For all the cases with PMFs, $B_{1\mathrm{Mpc}} = 1$ nG.

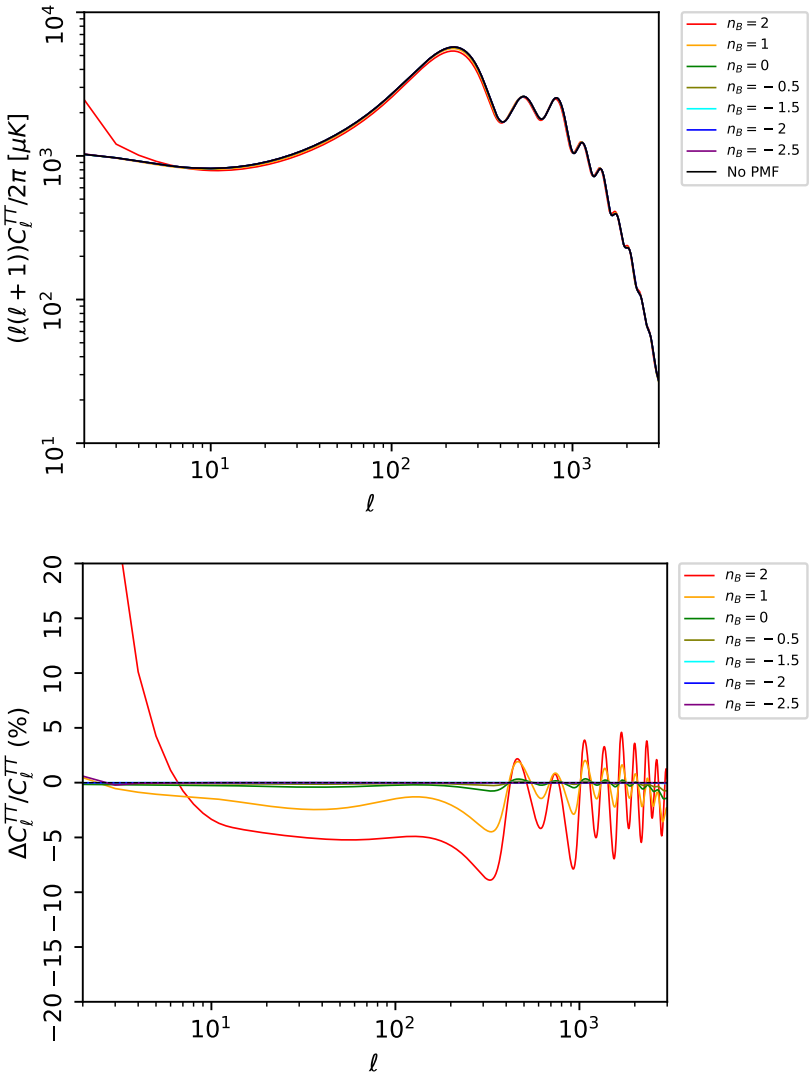

Figure 7.7: In the *top* panel, CMB temperature power spectrum without (black line) and with the total PMF contribution for different spectral indices (coloured lines, see the legend); in the *lower* panel, the percentage differences with respect the case without PMFs for different indices (see the legend). In all cases with PMFs, $B_{1\mathrm{Mpc}} = 1$ nG.

Figure 7.6 we see that the evolution of baryons is similar to the one for the only Alfvén contribution, suggesting that this one dominates over the other two effects. Particularly interesting is the case for $k = 10$ Mpc^{-1}, where we saw in Figure 7.1 that the introduction of the Lorentz contribution and the PMF terms in the Einstein equation produced the maximum effect at recombination and the growth of baryon overdensities were enhanced. We see however that the support against gravitational collapse provided by the magnetic pressure is dominant and even for $n_B = 2$ the perturbation growth is not enhanced anymore around recombination. At $k = 100$ Mpc^{-1} the contribution come almost exclusively from the introduction of the Alfvén velocity in the speed of sound, because we have already discussed the fact that at such scales the Lorentz and PMF EMT spectra were zero or very close to it.

In Figure 7.7 we show the total impact of PMFs into CMB angular power spectrum and the percentage differences. We note again an increasing effect for larger indices and a quite important raise of the very first multipoles for $n_B = 2$ (even beyond 20%), while for the lowest indices the overall contribution is particularly tiny for almost all the scales, with the exception of a small raise in the spectrum at the largest ones.

7.4 Second-order CMB angular power spectra

We conclude this chapter showing some examples of second-order CMB temperature spectra in presence of PMFs. We remark again that, since we are including PMF contributions only in the first-order equations, the second-order spectra are affected only through the quadratic terms in the first-order perturbations appearing in the second-order equations. This is not however a complete way to include all possible next-to-leading effects brought by the presence of PMFs; in fact, a full non-ideal MHD approach would require the presence of additional quadratic terms due to the coupling of the fluid with the magnetic field, which however are not considered in this work. The implementation of such terms would indeed require the solution of new (quite complicated) convolution integrals and their coding would not be immediate, hence their inclusion will surely be more suitable for future long-term projects in the direction we have taken. The backreaction of the fluid into PMFs should also be taken into account for a proper analysis of this kind of physics beyond linearity and ideal MHD. In Figure 7.8 we show the second-spectra for the individual contributions of the Lorentz force, the PMF EMT in the Einstein equations and the Alfvén velocity. As one can immediately see, the second-order spectra in the case of the PMF terms in the Einstein equations are very large and even larger than the first-order ones. As said before, this may be a direct consequence of our approximations and of the lack of coupling terms between the magnetic field and the fluid at second order, which might suppress such a large non-linear contribution. Moreover, we remind that beyond linear theory different scales couple with each other, hence small-scale effects (which is sensible to non-linear physics) propagate towards large

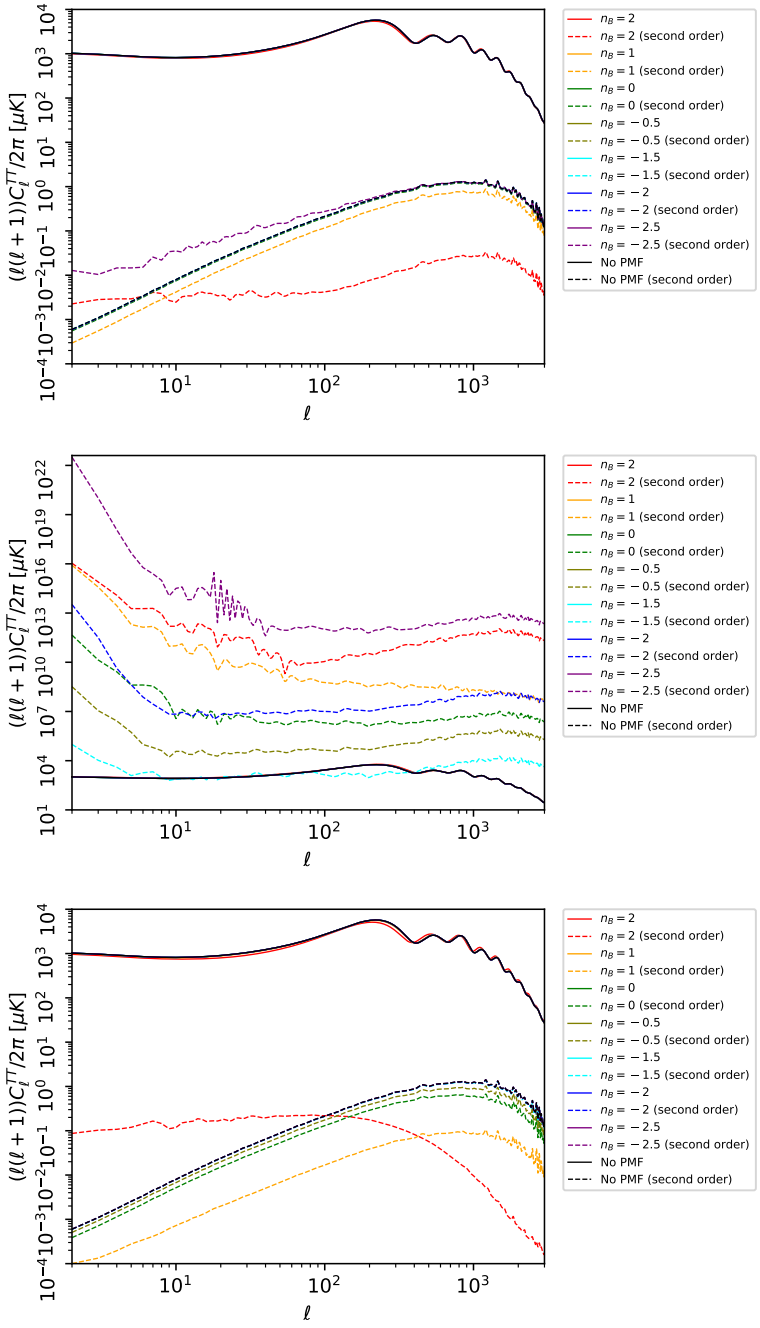

Figure 7.8: First-order (solid lines) and second-order (dashed lines) CMB temperature spectra without (black lines) and with PMFs for different spectral indices (coloured lines, see the legend). In particular, in the *top*, *middle* and *lower* panel the individual contributions of the Lorentz force, the PMF EMT in the Einstein equations and the Alfvén velocity are considered, respectively. In all cases with PMFs, $B_{1\mathrm{Mpc}} = 1$ nG.

scales and therefore have a strong impact on the CMB spectrum. Hence, a careful and more exhaustive treatment of the physics in presence of PMFs at such small scales, which would be an interesting subject of future studies, should be considered before drawing conclusions from these second-order spectra.

Conclusions

The study of PMFs and their impact on CMB anisotropies and other key cosmological observables represents a crucial tool for the investigation of fundamental physics in the early Universe and at the same time their existence provides the ideal theoretical setting for explaining the observed large scale magnetic fields in galaxies, galaxy clusters and voids. Accounting for the ever increasing precision of CMB anisotropies measurements, together with the perspective of future cosmological data, a solid analysis of PMF effects beyond the standard assumptions of linearity and ideal MHD represents nowadays one of the most compelling challenges of modern cosmology. Furthermore, these non-linearities may have a considerable impact on the recombination history, leading to the possibility of changing the value of the Hubble constant from CMB data and alleviating the tension with the measurements from supernovae, not to mention smaller scales relevant for matter tracers at low redshift.

For all these reasons, this thesis has the objective to perform a step towards a fully non-linear treatment of the impact of PMFs on the evolution of cosmological perturbations and CMB anisotropies. We selected adiabatic initial conditions, instead of the compensated ones which are widely used in literature, and treated the contribution of PMFs (quadratic in the magnetic field) at the same footing of first order perturbations. We studied the impact of the Lorentz force on baryon velocity, the gravitational contribution of PMFs through the introduction of their energy-momentum tensor in the Einstein equations and the effect of increasing the baryon speed of sound with the Alfvén velocity, which has the meaning of including the contribution of the magnetic pressure in the fluid; the last-mentioned one, in particular, represents an effect which is usually neglected in the standard literature, since it would provide a next-to-leading order contribution in perturbation theory that, however, is of much interest for us. Apart from the impact on CMB angular power spectrum, it was particularly interesting to investigate how PMFs affect baryon inhomogeneities, and see if relevant non-linearities can arise around recombination. For these purposes, we improved and extended the publicly available Einstein-Boltzmann code SONG [70, 69], which is able to compute cosmological observables taking into account all second-order contributions in cosmological perturbation theory. We chose to use this code because it had already implemented the study of the Harrison mechanism within second-order cosmological perturbation theory [25]:

although this mechanism was not explicitly studied in this thesis SONG might be particularly interesting for future studies including non-linear/beyond ideal MHD effects.

Concerning the CMB temperature angular power spectrum, for $B_{1\mathrm{Mpc}} = 1$ nG we observed for all the cases the maximum impact for blue spectral indices and in particular for $n_B = 2$. The most important contribution is provided by the introduction of the Alfvén velocity in the speed of sound, with deviations up to 20% from the ΛCDM spectrum. In this last case, we observed a shift towards larger scales of the acoustic peaks as expected, while the Lorentz force and the PMF EMT have the characteristic to provide individually similar contributions but with opposite sign. The contribution of all the combined PMF effects gives deviations in the spectrum up to 10% without any overall suppression or enhancement, except for the very first multiples that are instead increased up to a deviation of $\sim 20\%$.

Particular attention was then devoted on the analysis of baryon inhomogeneities, especially on the impact that PMFs have on them around the recombination epoch. If baryon inhomegeinities were anomalously large with respect to ΛCDM at such epoch, inhomogeneous recombination would indeed need further investigation. We first investigated the combined effect of the Lorentz force and the presence of the PMF EMT in the Einstein equations for the wavenumbers $k = 0.1$, 1, 10, 100 Mpc^{-1} and $B_{1\mathrm{Mpc}} = 1$. We noted that the contribution, that increases for higher indices as already experienced for the C_ℓ's, is maximum for $k = 10$ Mpc^{-1}, showing for both $n_B = 1$ and $n_B = 2$ an important enhancement of baryon inhomogeneities at all times and, in particular, around recombination. We also performed a comparison with the analytic estimate given in [81] for $n_B = 2$ and $k = 1$, 10 Mpc; we observed a good agreement around recombination (which is indeed the epoch of validity of the analytic estimate) for both the cases, with a small deviation that may be due to different underlying assumptions. Although baryon inhomogeneities of appreciable amplitude seem to form around recombination with the presence of PMFs, more careful considerations should be made before drawing firm conclusions. First of all, for $n_B = 2$ the current upper bound for $B_{1\mathrm{Mpc}}$ is 3 pG at 95% C.L. [64], and we saw that even for a slightly larger value ($B_{1\mathrm{Mpc}} = 10$ pG) the enhancement of the baryon inhomogeneities around recombination is absent. Moreover, we are so far neglecting the contribution of the magnetic pressure, which together with the one of the baryon-photon fluid provides, at sufficiently small scale, additional support against gravitational collapse and hence hinders the growth of perturbations. We indeed encapsulated the effect of the magnetic pressure by increasing the baryon speed of sound with the Alfvén velocity. We observed, as expected, that with this further modification baryon inhomogeneities are strongly suppressed and, even for $n_B = 2$ and $k = 10$ Mpc^{-1}, they do not experience any enhancement around recombination. This reinforces the idea that a careful analysis of the small-scale physics in presence of PMFs is necessary to perform more reliable statement about the impact of possible non-linearities around recombination, with the consequent effect on the Hubble constant as claimed in [40]. Moreover, it should be stressed that the results we obtained are based on our assumptions, like for

example the introduction of a sharp cut-off k_D in the magnetic power spectrum to take into account the radiative viscosity; slightly different results might be obtained with different choices, therefore a more in-depth analysis of the conventions and the underlying assumptions assumed in [40] may be an interesting topic for future discussions.

We finally gave a preliminary look at the second-order CMB power spectrum in presence of PMFs. We saw immediately that they are more strongly affected by PMFs with respect to the first-order spectra; however, the fact that in the case of the sole presence of the PMF EMT in the Einstein equations the second-order contribution becomes particularly large may suggest that to obtain the full second-order spectra our treatment requires a more complete involvement of all terms which may arise at second order, due to the coupling between the magnetic field and the fluid.

This issue, together with all the considerations made so far, opens the way to a lot of attractive challenges for future studies, making this thesis an important first step towards a more robust and exhaustive treatment of the full non-linear contribution of PMFs in the primordial plasma. We summarize the most relevant future perspectives in the following:

- To perform a treatment which goes fully beyond linearity and ideal-MHD, the involvement of additional coupling terms between the magnetic field and the fluid may be crucial, especially to avoid that unaccounted small-scale non-linear effects causes unexpected results like some of the second-order spectra we obtained (beyond linearity different scales are coupled, so a non-complete treatment of small-scales physics might propagate towards large scales and strongly affect the angular power spectrum). These quadratic terms require the resolution of new (not immediate) convolution integrals and their implementation in the code, being therefore more suitable for a future long-term project.

- In this thesis, we treated as a first approximation the magnetic field as a stiff source, but for a more accurate analysis, the back-reaction of the fluid into the PMF which drives its second-order evolution should be included. This would require the resolution of the induction equation, together with the implementation of the Harrison mechanism with a non-vanishing initial condition.

- We focused on the impact of PMFs on scalar cosmological perturbations, but an extension to vector modes which is the dominant contribution for PMFs into CMB anisotropies is important. Since the evolution equation for the vorticity part of baryon velocity perturbations is similar to the scalar part, it may be interesting to evaluate the possible non-linearity also in this sector and its possible impact on cosmological observables.

Appendix A

Connection to the Ma&Bertschinger notation

We briefly give here a connection of our beta-moment notation to the one of the most common ones used in the literature for scalar linear cosmological perturbation theory, that is the one introduced in 1995 by Ma and Bertschinger [54]. In fact, although the beta-moment notation provides a unified framework for describing both relativistic and non-relativistic species, it has the disadvantage of not being so intuitive at first sight and therefore an explanation of how it is related to a more common notation like the one in [54], at least at first order in perturbations, may be useful. From now on we always refer to first-order variables.

The scalar energy density, velocity and anisotropic stress are expressed in [54] through the following variables:

$$\delta = \frac{\rho - \bar{\rho}}{\bar{\rho}} \qquad \text{energy density contrast ,}$$

$$\theta = \frac{ik^j\, \delta T^0{}_j}{\bar{\rho} + \bar{P}} \qquad \text{velocity gradient ,}$$

$$\sigma = -\frac{(\hat{\mathbf{k}}_i \cdot \hat{\mathbf{k}}_j - \frac{1}{3}\delta_{ij})\Sigma^i{}_j}{\bar{\rho} + \bar{P}} \qquad \text{anisotropic stress ,}$$

with $\Sigma^i{}_j = T^i{}_j - \delta^i{}_j T^k{}_k/3$ being the traceless component of $T^i{}_j$.

Whereas at linear order the density contrast δ corresponds to the first beta-moment for $\ell = m = 0$ for both relativistic and non-relativistic cases, the other two variables connect with our scalar dipoles and quadrupoles as follows:

$$\theta = \frac{k}{3}\frac{{}_1\Delta_{10}}{\omega + 1} , \qquad \sigma = \frac{2}{15}\frac{{}_2\Delta_{20}}{\omega + 1} . \tag{A.1}$$

Concerning the adiabatic initial conditions, comparing equation (2.59) with equation

(98) of [54], we find that

$$\zeta = -2\,C\ , \tag{A.2}$$

where C denotes in that reference the amplitude of the fastest growing mode.

Appendix B

Spherical projection

During all the discussion of this thesis we often encountered the necessity to split a tensor into its scalar, vector and tensor components. It was possible to do that by employing the projection vectors ξ and matrices χ, whose explicit expressions are now given. We do not give here a exhaustive discussion of all the geometrical properties of such objects, but a more extensive and detailed treatment about this topic can be found in [70].

B.1 The projection vectors ξ and matrices χ

The $\xi^i_{[m]}$ vectors are an orthogonal [1] set of spherical basis, whose cartesian components are

$$\xi_{[0]} = \begin{pmatrix} 0 \\ 0 \\ 1 \end{pmatrix} \quad , \quad \xi_{[+1]} = \sqrt{\frac{1}{2}} \begin{pmatrix} -1 \\ i \\ 0 \end{pmatrix} \quad , \quad \xi_{[-1]} = \sqrt{\frac{1}{2}} \begin{pmatrix} +1 \\ i \\ 1 \end{pmatrix} \tag{B.1}$$

and through which a generic direction $\hat{\mathbf{n}}$ can be expressed as

$$n^i = \sqrt{\frac{4\pi}{3}} \sum_{m=-1}^{1} \xi^i_{[m]} Y_{1m} \ . \tag{B.2}$$

Their indices are lowered and raised with the Euclidean metric δ_{ij} and its inverse δ^{ij} respectively and under complex conjugation they transform as

$$\xi^i_{[-m]} = (-1)^m \xi^{*i}_m \ . \tag{B.3}$$

[1] Their orthogonality holds for both their indices, i and m.

The $\chi^{ij}_{2,[m]}$ matrices are symmetric and traceless matrices defined as

$$\chi_{2,0} = \frac{1}{3}\begin{pmatrix} -1 & 0 & 0 \\ 0 & -1 & 0 \\ 0 & 0 & 2 \end{pmatrix} \quad , \quad \chi_{2,\pm1} = \sqrt{\frac{1}{6}}\begin{pmatrix} 0 & 0 & \mp 1 \\ 0 & 0 & i \\ \mp 1 & i & 0 \end{pmatrix} \quad , \quad \chi_{2,\pm2} = \sqrt{\frac{1}{6}}\begin{pmatrix} 1 & \mp i & \mp 0 \\ \mp i & -1 & 0 \\ \mp 0 & 0 & 0 \end{pmatrix} \ . \tag{B.4}$$

The rank-2 tensor $n^i n^j$ can be expressed as

$$n^i n^j = \frac{\delta^{ij}}{3} + \sqrt{\frac{4\pi}{5}} \sum_{m=-2}^{2} \chi^{ij}_{2,[m]} Y_{2m} \ . \tag{B.5}$$

Under complex conjugation they transform as

$$\chi^{ij*}_{2,[m]} = (-1)^m \chi^{ij}_{2,[-m]} \ . \tag{B.6}$$

B.2 The coupling coefficients

We saw in Sec. 4.3.1 the appearance in the quadratic parts of the Liouville and collision terms of coupling coefficients C, which arise from the application of the operator $L_{\ell m}$ on the wavevector $\mathbf{k}$ (for the Liouville term) and on the electron velocity (for the collision term), and D, which instead comes from the action of $L_{\ell m}$ on $\partial f/\partial n^i$ in the lensing term. Their expressions are

$$C^{\pm,\ell}_{m_1 m} = (-1)^m (2\ell+1) \begin{pmatrix} 1 & \ell \pm 1 & \ell \\ 0 & 0 & 0 \end{pmatrix} \begin{pmatrix} 1 & \ell \pm 1 & \ell \\ m - m_1 & m_1 & -m \end{pmatrix} \ , \tag{B.7}$$

$$R^{\pm,\ell}_{m_1 m} = (-1)^m (2\ell+1) \sqrt{2(\ell \pm 1)(\ell \pm 1 + 1)} \begin{pmatrix} 1 & \ell \pm 1 & \ell \\ 1 & -2 & 0 \end{pmatrix} \begin{pmatrix} 1 & \ell \pm 1 & \ell \\ m - m_1 & m_1 & -m \end{pmatrix} \ . \tag{B.8}$$

Here we have made use of the Wigner $3j$ symbols,

$$\begin{pmatrix} \ell_1 & \ell_2 & \ell_3 \\ m_1 & m_2 & m_3 \end{pmatrix} \ , \tag{B.9}$$

which encode the geometrical properties of a system of three vectors that form a triangle, that is $\boldsymbol{\ell_1} + \boldsymbol{\ell_2} + \boldsymbol{\ell_3} = 0$; ℓ_1, ℓ_2 and ℓ_3 represent the magnitudes of the three vectors and must be positive, while m_1, m_2 and m_3 are the projections of the three vectors on the zenith and must satisfy $-\ell_i \leq m_i \leq \ell_i$. These symbols are non-vanishing only if the triangular inequality is satisfied, *i.e.* $|\ell_i - \ell_j| \leq \ell_k \leq \ell_i + \ell_j$, and if $m_1 + m_2 + m_3 = 0$.

Appendix C

Convolution integrals

The convolution integrals for the Fourier spectra $|\rho_B(k)|^2$ and $|L(k)|^2$ have to be computed, assuming that the magnetic power spectrum is parametrized as $P_B(k) = A_B k^{n_B}$ and $P_B(k) = 0$ for $k > k_D$. Hence, two conditions must be taken into account, that is $p < k_D$ and $|\mathbf{k} - \mathbf{p}| < k_D$, which in turn allow the spectra to be non-zero only for $0 < k < 2k_D$ (or equivalently, for $0 < \tilde{k} < 2$, with $\tilde{k} = k/k_D$). We give now the results, derived in [26] and [65], for particular values of n_B; σ_B can be directly obtained from equation (6.17). Details on the integration technique can be found in [65].

$\mathbf{n_B = 2}$

$$|\rho_B(k)|^2_{n_B=2} = \frac{A_B^2\, k_D^7}{512\,\pi^4}\left[\frac{4}{7} - \tilde{k} + \frac{8\tilde{k}^2}{15} - \frac{\tilde{k}^5}{24} + \frac{11\tilde{k}^7}{2240}\right] ,$$

$$|L(k)|^2_{n_B=2} = \frac{A_B^2\, k_D^7}{512\,\pi^4}\left[\frac{44}{105} - \frac{2\tilde{k}}{3} + \frac{8\tilde{k}^2}{15} - \frac{\tilde{k}^3}{6} - \frac{\tilde{k}^5}{240} + \frac{13\tilde{k}^7}{6720}\right] .$$

$\mathbf{n_B = 1}$

$$|\rho_B(k)|^2_{n_B=1} = \frac{A_B^2\, k_D^5}{512\,\pi^4}\begin{cases} \frac{44}{575} - \frac{2\tilde{k}}{3} + \frac{32\tilde{k}^2}{105} + \frac{4\tilde{k}^4}{315} - \frac{\tilde{k}^5}{25} & \text{for } 0 \le \tilde{k} \le 1 \\ -\frac{44}{75} + \frac{64}{1575\tilde{k}^4} - \frac{16}{105\tilde{k}^3} + \frac{8}{15\tilde{k}} + \frac{2\tilde{k}}{3} - \frac{32\tilde{k}^2}{105} - \frac{4\tilde{k}^4}{315} + \frac{\tilde{k}^5}{75} & \text{for } 1 \le \tilde{k} \le 2 \end{cases} ,$$

$$|L(k)|^2_{n_B=1} = \frac{A_B^2\, k_D^5}{512\,\pi^4}\begin{cases} \frac{4}{5} - \tilde{k} + \frac{\tilde{k}^3}{4} - \frac{4\tilde{k}^4}{15} - \frac{\tilde{k}^5}{5} & \text{for } 0 \le \tilde{k} \le 1 \\ \frac{8}{15\tilde{k}} - \frac{4}{5} + \frac{\tilde{k}}{3} + \frac{\tilde{k}^3}{4} - \frac{4\tilde{k}^4}{15} + \frac{\tilde{k}^5}{15} & \text{for } 1 \le \tilde{k} \le 2 \end{cases} .$$

$\mathbf{n_B = 0}$

$$|\rho_B(k)|^2_{n_B=0} = \frac{A_B^2\, k_D^3}{512\,\pi^4}\left[\frac{29}{24} - \frac{17\tilde{k}}{16} + \frac{7\tilde{k}^2}{8} + \frac{53\tilde{k}^3}{96} + \frac{\pi^2\tilde{k}^3}{24} - \frac{\log|1-\tilde{k}|}{8\tilde{k}} + \frac{\tilde{k}\log|1-\tilde{k}|}{2} - \frac{3\tilde{k}^3\log|1-\tilde{k}|}{8} + \frac{\tilde{k}^3\log|1-\tilde{k}|\log\tilde{k}}{2} - \frac{\tilde{k}^3\log^2\tilde{k}}{4} - \frac{\tilde{k}^3\mathrm{PolyLog}[2,\frac{-1+\tilde{k}}{\tilde{k}}]}{2}\right],$$

$$|L(k)|^2_{n_B=0} = \frac{A_B^2\, k_D^3}{512\,\pi^4}\left[\frac{43}{48} - \frac{1}{16\tilde{k}^4} - \frac{1}{32\tilde{k}^3} + \frac{7}{48\tilde{k}^2} + \frac{13}{192\tilde{k}} - \frac{67\tilde{k}}{96} + \frac{\tilde{k}^2}{48} + \frac{17\tilde{k}^3}{384} - \frac{\log|1-\tilde{k}|}{16\tilde{k}^5} + \frac{\log|1-\tilde{k}|}{6\tilde{k}^3} - \frac{\log|1-\tilde{k}|}{8\tilde{k}} + \frac{\tilde{k}^3\log|1-\tilde{k}|}{48}\right].$$

$\mathbf{n_B = -3/2}$

$$|\rho_B(k)|^2_{n_B=-3/2} = \frac{A_B^2}{512\,\pi^4}\begin{cases} \frac{232}{45\sqrt{1-\tilde{k}}} + \frac{88}{15\tilde{k}} - \frac{88}{15\sqrt{1-\tilde{k}}\tilde{k}} - 2\pi + \frac{4\tilde{k}}{3} - \frac{32\tilde{k}}{45\sqrt{1-\tilde{k}}} \\ + \frac{64\tilde{k}^2}{45\sqrt{1-\tilde{k}}} + \frac{\tilde{k}^3}{9} + 8\log[1+\sqrt{1-\tilde{k}}] - 4\log\tilde{k} & \text{for } 0 \le \tilde{k} \le 1 \\ - \frac{232}{45\sqrt{-1+\tilde{k}}} + \frac{88}{15\tilde{k}} - \frac{88}{15\sqrt{-1+\tilde{k}}\tilde{k}} & \\ + \frac{4\tilde{k}}{3} + \frac{32\tilde{k}}{45\sqrt{-1+\tilde{k}}} - \frac{64\tilde{k}^2}{45\sqrt{-1+\tilde{k}}} & \\ + \frac{\tilde{k}^3}{9} - 4\arctan\left[\frac{1}{\sqrt{-1+\tilde{k}}}\right] + 4\arctan\left[\sqrt{-1+\tilde{k}}\right] & \text{for } 1 \le \tilde{k} \le 2 \end{cases},$$

$$|L(k)|^2_{n_B=-3/2} = \frac{A_B^2}{512\,\pi^4}\begin{cases} \frac{10616}{1755\sqrt{1-\tilde{k}}} - \frac{2048}{2925\tilde{k}^5} + \frac{2048}{2925\sqrt{1-\tilde{k}}\tilde{k}^5} - \frac{22\pi}{15} \\ + \frac{128}{135\tilde{k}^3} - \frac{9088}{8775\sqrt{1-\tilde{k}}\tilde{k}^3} + \frac{88}{15\tilde{k}} - \frac{10136}{1775\sqrt{1-\tilde{k}}\tilde{k}} \\ + \frac{32\tilde{k}}{1755\sqrt{1-\tilde{k}}} - \frac{64\tilde{k}^2}{1775\sqrt{1-\tilde{k}}} + \frac{88\log\left[1+\sqrt{1-\tilde{k}}\right]}{15} - \frac{44\log\tilde{k}}{15} & \text{for } 0 \le \tilde{k} \le 1 \\ - \frac{10616}{1755\sqrt{-1+\tilde{k}}} - \frac{2048}{2925\tilde{k}^5} - \frac{2048}{2925\sqrt{-1+\tilde{k}}\tilde{k}^5} + \frac{1024}{2925\sqrt{-1+\tilde{k}}\tilde{k}^4} & \\ + \frac{128}{135\tilde{k}^3} + \frac{9088}{8775\sqrt{-1+\tilde{k}}\tilde{k}^3} - \frac{3776}{8775\sqrt{-1+\tilde{k}}\tilde{k}^2} + \frac{88}{15\tilde{k}} + & \\ \frac{10136}{1755\sqrt{-1+\tilde{k}}} - \frac{32\tilde{k}}{1775\sqrt{-1+\tilde{k}}} + \frac{64\tilde{k}^2}{1775\sqrt{-1+\tilde{k}}\tilde{k}^4} - & \\ \frac{44\arctan\left[\frac{1}{\sqrt{-1+\tilde{k}}}\right]}{15} + \frac{44\arctan\left[\sqrt{-1+\tilde{k}}\right]}{15} & \text{for } 1 \le \tilde{k} \le 2 \end{cases}.$$

$\mathbf{n_B = -2}$

$$|\rho_B(k)|^2_{n_B=-2} = \frac{A_B^2}{512\,\pi^4}\begin{cases} -\frac{1}{2}+\frac{\tilde{k}^3}{16}+\frac{\pi^2}{4\tilde{k}}-\frac{\log[1-\tilde{k}]}{2\tilde{k}}(-1+\tilde{k}^2-6\log[1-\tilde{k}]) & \\ -\frac{3\log^2\tilde{k}}{2\tilde{k}}-\frac{3\mathrm{PolyLog}[2,\frac{-1+\tilde{k}}{\tilde{k}}]}{\tilde{k}} & \text{for } 0\le\tilde{k}\le 1 \\ -\frac{1}{2}+\frac{\tilde{k}^3}{16}+\frac{\log[-1+\tilde{k}]}{2\tilde{k}}-\frac{\tilde{k}\log[-1+\tilde{k}]}{2}+\frac{3\log[-1+\tilde{k}]\log\tilde{k}}{2\tilde{k}} & \\ +\frac{3\mathrm{PolyLog}[2,\frac{1}{\tilde{k}}]}{2\tilde{k}}-\frac{3\mathrm{PolyLog}[2,\frac{-1+\tilde{k}}{\tilde{k}}]}{2\tilde{k}} & \text{for } 1\le\tilde{k}\le 2 \end{cases},$$

$$|L(k)|^2_{n_B=-2} = \frac{A_B^2}{512\,\pi^4}\begin{cases} \frac{\log[1-\tilde{k}]}{2\tilde{k}^5}(1-\tilde{k}^2+6\tilde{k}^4\log\tilde{k})+\frac{1}{2\tilde{k}^4}+\frac{1}{4\tilde{k}^3}-\frac{1}{3\tilde{k}^2}+\frac{1}{24} & \\ +\frac{-3+6\pi^2}{24\tilde{k}}-\frac{3\log^2\tilde{k}}{2\tilde{k}}-\frac{3\mathrm{PolyLog}[2,\frac{-1+\tilde{k}}{\tilde{k}}]}{\tilde{k}} & \text{for } 0\le\tilde{k}\le 1 \\ \frac{(-2+k)k(1+\tilde{k})(-6+\tilde{k}^2+\tilde{k}^3)}{24\tilde{k}^5}+\frac{\log[-1+\tilde{k}](1-\tilde{k}^2+3\tilde{k}^4\log\tilde{k}}{2\tilde{k}^5} & \\ +\frac{3}{2\tilde{k}}\left(\mathrm{PolyLog}\left[2,\frac{1}{\tilde{k}}\right]-\mathrm{PolyLog}\left[2,\frac{-1+\tilde{k}}{\tilde{k}}\right]\right) & \text{for } 1\le\tilde{k}\le 2 \end{cases}.$$

$\mathbf{n_B = -5/2}$

$$|\rho_B(k)|^2_{n_B=-5/2} = \frac{A_B^2}{512\,\pi^4\,k_D^2}\left[-\frac{32}{75\sqrt{|1-\tilde{k}|}}+\frac{272}{25\sqrt{|1-\tilde{k}|}\tilde{k}^2}+\frac{88}{15\tilde{k}}-\frac{848}{75\sqrt{|1-\tilde{k}|}\tilde{k}}\right.$$
$$\left.-\frac{4\tilde{k}}{5}+\frac{64}{75\sqrt{|1-\tilde{k}|}}+\frac{\tilde{k}^3}{25}\right],$$

$$|L(k)|^2_{n_B=-5/2} = \frac{A_B^2}{512\,\pi^4\,k_D^2}\left[-\frac{32}{1155\sqrt{|1-\tilde{k}|}}+\frac{2048}{1155\tilde{k}^5}-\frac{2048}{1155\sqrt{|1-\tilde{k}|}\tilde{k}^5}\right.$$
$$+\frac{1024}{1155\sqrt{|1-\tilde{k}|}\tilde{k}^4}-\frac{128}{105\tilde{k}^3}+\frac{1664}{1155\sqrt{|1-\tilde{k}|}\tilde{k}^3}+\frac{12976}{1155\sqrt{|1-\tilde{k}|}\tilde{k}^2}$$
$$\left.+\frac{88}{15\tilde{k}}-\frac{13648}{1155\sqrt{|1-\tilde{k}|}\tilde{k}}+\frac{64\tilde{k}}{1155\sqrt{|1-\tilde{k}|}}\right].$$

Appendix D

CMB temperature power spectra percentage differences for negative spectral indices

We show in this appendix the CMB temperature power spectra percentage differences for negative indices (including the $n_B = 0$ case) for the various contributions with respect to the case without PMFs, since for these values of n_B the differences are all below the 1% and are not well visible in the plots showed so far.

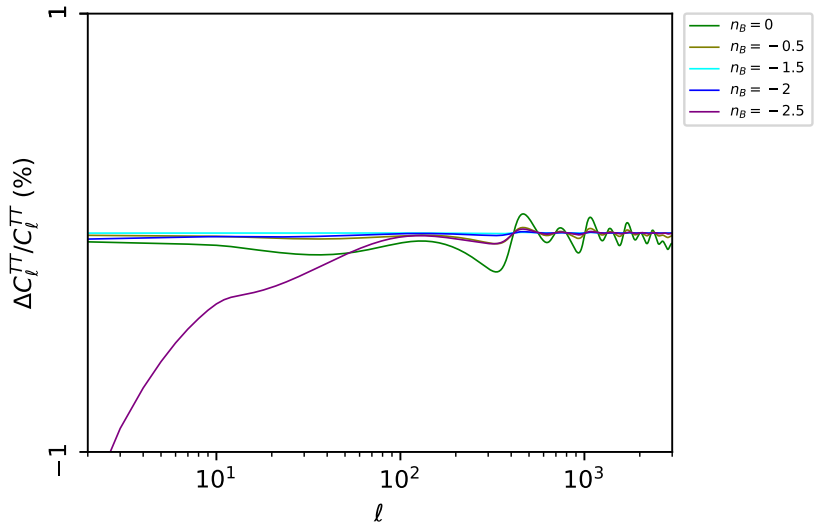

Figure D.1: CMB temperature power spectra percentage differences for the case of the sole Lorentz force contribution.

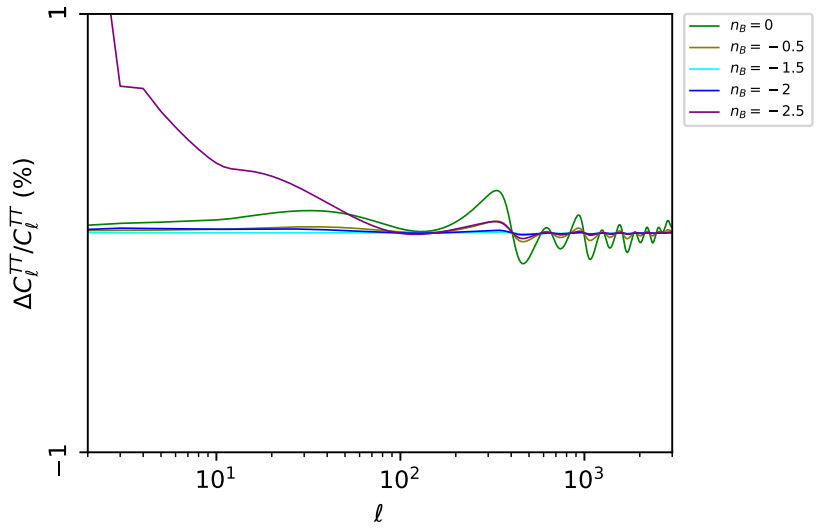

Figure D.2: CMB temperature power spectra percentage differences for the case of the sole PMF EMT contribution in the Einstein equations.

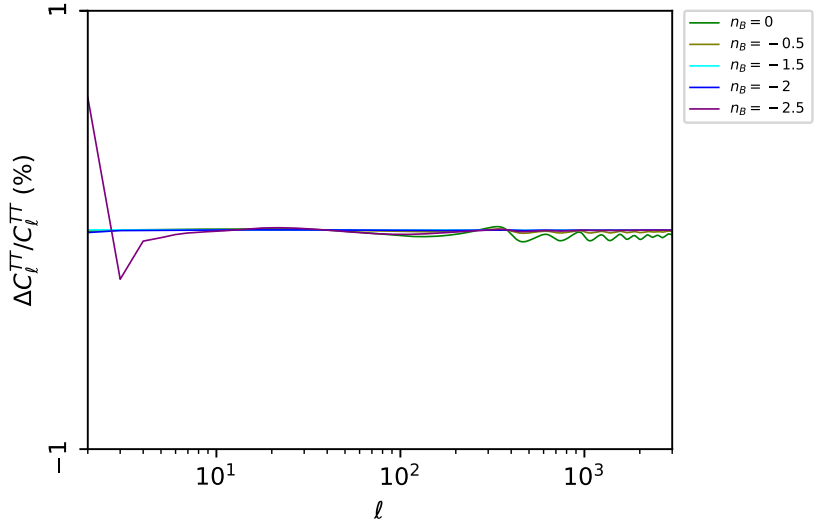

Figure D.3: CMB temperature power spectra percentage differences for the case of both the Lorentz force and PMF EMT contributions.

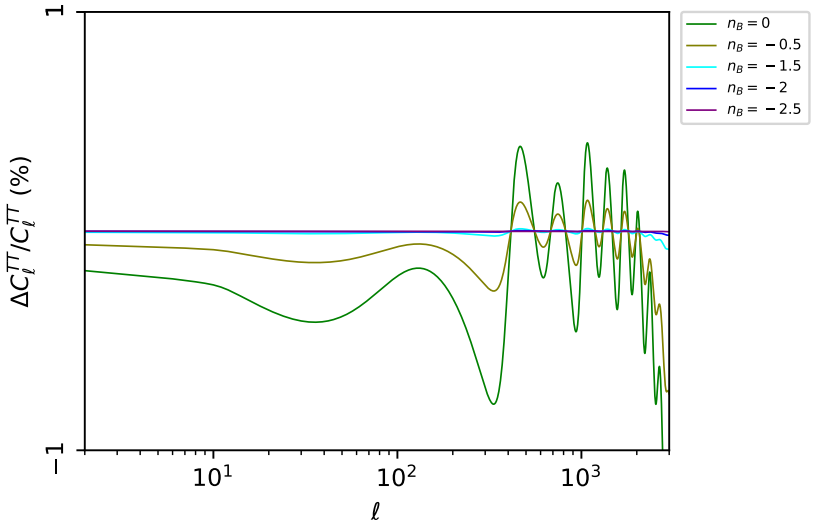

Figure D.4: CMB temperature power spectra percentage differences for the case of the sole Alfvén velocity contribution to the speed of sound.

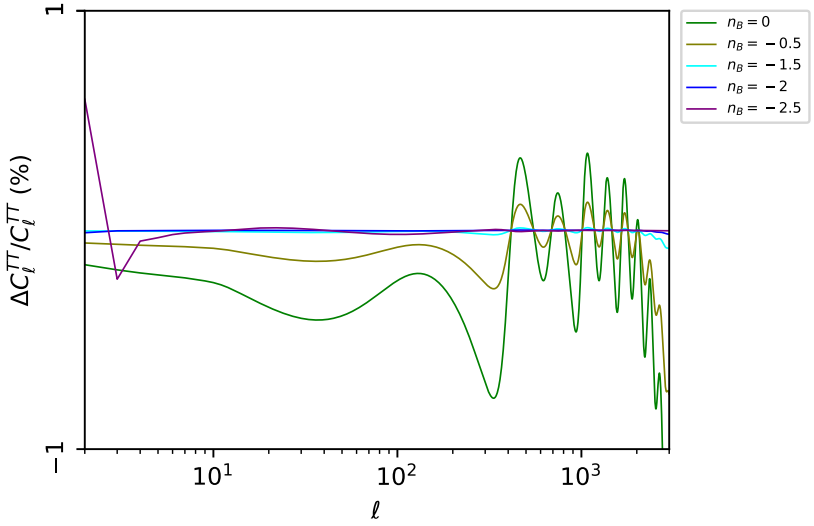

Figure D.5: CMB temperature power spectra percentage differences for the case of the total PMF contribution.

Bibliography

[1] Jennifer A. Adams et al. "Distortion of the acoustic peaks in the CMBR due to a primordial magnetic field". In: *Phys. Lett. B* 388 (1996), pp. 253–258. DOI: 10.1016/S0370-2693(96)01171-9. arXiv: astro-ph/9607043.

[2] Nabila Aghanim, Subhabrata Majumdar, and Joseph Silk. "Secondary anisotropies of the CMB". In: *Rept. Prog. Phys.* 71 (2008), p. 066902. DOI: 10.1088/0034-4885/71/6/066902. arXiv: 0711.0518 [astro-ph].

[3] James M. Bardeen. "Gauge-invariant cosmological perturbations". In: *Phys. Rev. D* 22 (8 Oct. 1980), pp. 1882–1905. DOI: 10.1103/PhysRevD.22.1882. URL: https://link.aps.org/doi/10.1103/PhysRevD.22.1882.

[4] N Bartolo, S Matarrese, and A Riotto. "Evolution of second-order cosmological perturbations and non-Gaussianity". In: *Journal of Cosmology and Astroparticle Physics* 2004.01 (Jan. 2004), pp. 003–003. DOI: 10.1088/1475-7516/2004/01/003. URL: https://doi.org/10.1088/1475-7516/2004/01/003.

[5] E. Battaner, E. Florido, and Jorge Jiménez-Vicente. "Magnetic Fields and Large Scale Structure in a hot Universe. I. General Equations". In: 326 (Mar. 1996).

[6] Daniel Baumann. *Cosmology*. 2013.

[7] M. Beneke and C. Fidler. "Boltzmann hierarchy for the cosmic microwave background at second order including photon polarization". In: *Phys. Rev. D* 82 (6 Sept. 2010), p. 063509. DOI: 10.1103/PhysRevD.82.063509. URL: https://link.aps.org/doi/10.1103/PhysRevD.82.063509.

[8] Martin L. Bernet et al. "Strong magnetic fields in normal galaxies at high redshifts". In: *Nature* 454 (2008), pp. 302–304. DOI: 10.1038/nature07105. arXiv: 0807.3347 [astro-ph].

[9] Diego Blas, Julien Lesgourgues, and Thomas Tram. "The Cosmic Linear Anisotropy Solving System (CLASS) II: Approximation schemes". In: *Journal of Cosmology and Astroparticle Physics - JCAP* 7 (Apr. 2011). DOI: 10.1088/1475-7516/2011/07/034.

[10] A. Bonafede et al. "Galaxy cluster magnetic fields from radio polarized emission". In: *PoS* ISKAF2010 (2010), p. 006. DOI: 10.22323/1.112.0006. arXiv: 1009.1233 [astro-ph.CO].

[11] Camille Bonvin, Chiara Caprini, and Ruth Durrer. "Magnetic fields from inflation: the transition to the radiation era". In: *Phys. Rev. D* 86 (2012), p. 023519. DOI: 10.1103/PhysRevD.86.023519. arXiv: 1112.3901 [astro-ph.CO].

[12] A Botteon et al. "A giant radio bridge connecting two galaxy clusters in Abell 1758". In: *Monthly Notices of the Royal Astronomical Society: Letters* 499.1 (Aug. 2020), pp. L11–L15. DOI: 10.1093/mnrasl/slaa142. eprint: https://academic.oup.com/mnrasl/article-pdf/499/1/L11/33779940/slaa142.pdf. URL: https://doi.org/10.1093/mnrasl/slaa142.

[13] Marco Bruni et al. "Perturbations of spacetime: Gauge transformations and gauge invariance at second order and beyond". In: *Classical and Quantum Gravity* 14 (Sept. 1996). DOI: 10.1088/0264-9381/14/9/014.

[14] Stefano Camera, Cosimo Fedeli, and Lauro Moscardini. "Magnification bias as a novel probe for primordial magnetic fields". In: *JCAP* 03 (2014), p. 027. DOI: 10.1088/1475-7516/2014/03/027. arXiv: 1311.6383 [astro-ph.CO].

[15] Chiara Caprini and Ruth Durrer. "Gravitational wave production: A Strong constraint on primordial magnetic fields". In: *Phys. Rev. D* 65 (2001), p. 023517. DOI: 10.1103/PhysRevD.65.023517. arXiv: astro-ph/0106244.

[16] C. L. Carilli and G. B. Taylor. "Cluster magnetic fields". In: *Ann. Rev. Astron. Astrophys.* 40 (2002), pp. 319–348. DOI: 10.1146/annurev.astro.40.060401.093852. arXiv: astro-ph/0110655.

[17] Subrahmanyan Chandrasekhar. *Radiative transfer*. 1960.

[18] Bao-lian Cheng et al. "Constraints on the strength of primordial magnetic fields from big bang nucleosynthesis revisited". In: *Phys. Rev. D* 54 (1996), pp. 4714–4718. DOI: 10.1103/PhysRevD.54.4714. arXiv: astro-ph/9606163.

[19] P.P. Coles and P.F. Lucchin. *Cosmology: The Origin and Evolution of Cosmic Structure*. Wiley, 2003. ISBN: 9780470852996. URL: https://books.google.it/books?id=BGYcivB1EtMC.

[20] Ruth Durrer and Chiara Caprini. "Primordial magnetic fields and causality". In: *JCAP* 11 (2003), p. 010. DOI: 10.1088/1475-7516/2003/11/010. arXiv: astro-ph/0305059.

[21] Ruth Durrer and Andrii Neronov. "Cosmological Magnetic Fields: Their Generation, Evolution and Observation". In: *Astron. Astrophys. Rev.* 21 (2013), p. 62. DOI: 10.1007/s00159-013-0062-7. arXiv: 1303.7121 [astro-ph.CO].

[22] Arthur Eddington. "The cosmological controversy". In: *Science Progress (1933-)* 34.134 (1939), pp. 225–236. ISSN: 00368504, 20477163. URL: http://www.jstor.org/stable/43412676 (visited on 06/13/2022).

[23] C. Fedeli and L. Moscardini. "Constraining Primordial Magnetic Fields with Future Cosmic Shear Surveys". In: *JCAP* 11 (2012), p. 055. DOI: 10.1088/1475-7516/2012/11/055. arXiv: 1209.6332 [astro-ph.CO].

[24] Elisa Fenu, Cyril Pitrou, and Roy Maartens. "The seed magnetic field generated during recombination". In: *Monthly Notices of The Royal Astronomical Society - MON NOTIC ROY ASTRON SOC* 414 (Dec. 2010). DOI: 10.1111/j.1365-2966.2011.18554.x.

[25] Christian Fidler, Guido Pettinari, and Cyril Pitrou. "Precise numerical estimation of the magnetic field generated around recombination". In: *Physical Review D* 93 (Nov. 2015). DOI: 10.1103/PhysRevD.93.103536.

[26] Fabio Finelli, Francesco Paci, and Daniela Paoletti. "Impact of stochastic primordial magnetic fields on the scalar contribution to cosmic microwave background anisotropies". In: *Physical Review D* 78.2 (July 2008). DOI: 10.1103/physrevd.78.023510. URL: https://doi.org/10.1103%2Fphysrevd.78.023510.

[27] D. J. Fixsen. "The Temperature of the Cosmic Microwave Background". In: *Astrophys. J.* 707 (2009), pp. 916–920. DOI: 10.1088/0004-637X/707/2/916. arXiv: 0911.1955 [astro-ph.CO].

[28] A. Friedman. "On the Curvature of space". In: *Z. Phys.* 10 (1922), pp. 377–386. DOI: 10.1007/BF01332580.

[29] Massimo Giovannini and M. E. Shaposhnikov. "Primordial magnetic fields, anomalous isocurvature fluctuations and big bang nucleosynthesis". In: *Phys. Rev. Lett.* 80 (1998), pp. 22–25. DOI: 10.1103/PhysRevLett.80.22. arXiv: hep-ph/9708303.

[30] F. Govoni et al. "A radio ridge connecting two galaxy clusters in a filament of the cosmic web". In: *Science* 364.6444 (2019), pp. 981–984. DOI: 10.1126/science.aat7500.

[31] Federica Govoni and Luigina Feretti. "Magnetic field in clusters of galaxies". In: *Int. J. Mod. Phys. D* 13 (2004), pp. 1549–1594. DOI: 10.1142/S0218271804005080. arXiv: astro-ph/0410182.

[32] Dario Grasso and H.R. Rubinstein. "Limits on possible magnetic fields at nucleosynthesis time". In: *Astroparticle Physics* 3.1 (1995), pp. 95–102. ISSN: 0927-6505. DOI: https://doi.org/10.1016/0927-6505(94)00030-7. URL: https://www.sciencedirect.com/science/article/pii/0927650594000307.

[33] Christophe Grojean, Géraldine Servant, and James D. Wells. "First-order electroweak phase transition in the standard model with a low cutoff". In: *Phys. Rev. D* 71 (3 Feb. 2005), p. 036001. DOI: 10.1103/PhysRevD.71.036001. URL: https://link.aps.org/doi/10.1103/PhysRevD.71.036001.

[34] E. R. Harrison. "Generation of magnetic fields in the radiation ERA". In: 147 (Jan. 1970), p. 279. DOI: 10.1093/mnras/147.3.279.

[35] Wayne Hu and Martin J. White. "A CMB polarization primer". In: *New Astron.* 2 (1997), p. 323. DOI: 10.1016/S1384-1076(97)00022-5. arXiv: astro-ph/9706147.

[36] Edwin Hubble. "A relation between distance and radial velocity among extragalactic nebulae". In: *Proc. Nat. Acad. Sci.* 15 (1929), pp. 168–173. DOI: 10.1073/pnas.15.3.168.

[37] Stephan J. Huber et al. "Electroweak Phase Transition and Baryogenesis in the nMSSM". In: *Nucl. Phys. B* 757 (2006), pp. 172–196. DOI: 10.1016/j.nuclphysb.2006.09.003. arXiv: hep-ph/0606298.

[38] Karsten Jedamzik and Tom Abel. "Small-scale primordial magnetic fields and anisotropies in the cosmic microwave background radiation". In: *Journal of Cosmology and Astroparticle Physics* 2013.10 (Oct. 2013), pp. 050–050. DOI: 10.1088/1475-7516/2013/10/050. URL: https://doi.org/10.1088/1475-7516/2013/10/050.

[39] Karsten Jedamzik, Vi šnja Katalini ć, and Angela V. Olinto. "Damping of cosmic magnetic fields". In: *Phys. Rev. D* 57 (6 Mar. 1998), pp. 3264–3284. DOI: 10.1103/PhysRevD.57.3264. URL: https://link.aps.org/doi/10.1103/PhysRevD.57.3264.

[40] Karsten Jedamzik and Levon Pogosian. "Relieving the Hubble Tension with Primordial Magnetic Fields". In: *Physical Review Letters* 125.18 (Oct. 2020). DOI: 10.1103/physrevlett.125.181302. URL: https://doi.org/10.1103%2Fphysrevlett.125.181302.

[41] Tina Kahniashvili and Bharat Ratra. "CMB anisotropies due to cosmological magnetosonic waves". In: *Phys. Rev. D* 75 (2 Jan. 2007), p. 023002. DOI: 10.1103/PhysRevD.75.023002. URL: https://link.aps.org/doi/10.1103/PhysRevD.75.023002.

[42] Tina Kahniashvili et al. "Constraining primordial magnetic fields through large scale structure". In: *Astrophys. J.* 770 (2013), p. 47. DOI: 10.1088/0004-637X/770/1/47. arXiv: 1211.2769 [astro-ph.CO].

[43] Tina Kahniashvili et al. "Primordial magnetic field limits from cosmological data". In: *Phys. Rev. D* 82 (2010), p. 083005. DOI: 10.1103/PhysRevD.82.083005. arXiv: 1009.2094 [astro-ph.CO].

[44] Peter J. Kernan, Glenn D. Starkman, and Tanmay Vachaspati. "Big bang nucleosynthesis constraints on primordial magnetic fields". In: *Phys. Rev. D* 54 (1996), pp. 7207–7214. DOI: 10.1103/PhysRevD.54.7207. arXiv: astro-ph/9509126.

[45] Hideo Kodama and Misao Sasaki. "Cosmological Perturbation Theory". In: *Prog. Theor. Phys. Suppl.* 78 (1984), pp. 1–166. DOI: 10.1143/PTPS.78.1.

[46] Edward W. Kolb and Michael S. Turner. *The Early Universe*. Vol. 69. 1990. ISBN: 978-0-201-62674-2. DOI: 10.1201/9780429492860.

[47] Philipp P. Kronberg. "Extragalactic magnetic fields". In: *Rept. Prog. Phys.* 57 (1994), pp. 325–382. DOI: 10.1088/0034-4885/57/4/001.

[48] Kerstin E. Kunze. "CMB and matter power spectra from cross correlations of primordial curvature and magnetic fields". In: *Phys. Rev. D* 87.10 (2013), p. 103005. DOI: 10.1103/PhysRevD.87.103005. arXiv: 1301.6105 [astro-ph.CO].

[49] Kerstin E. Kunze and Eiichiro Komatsu. "Constraining primordial magnetic fields with distortions of the black-body spectrum of the cosmic microwave background: pre- and post-decoupling contributions". In: *JCAP* 01 (2014), p. 009. DOI: 10.1088/1475-7516/2014/01/009. arXiv: 1309.7994 [astro-ph.CO].

[50] G. Lemaitre. "Evolution of the Expanding Universe". In: *Proceedings of the National Academy of Sciences* 20.1 (1934), pp. 12–17. DOI: 10.1073/pnas.20.1.12. eprint: https://www.pnas.org/doi/pdf/10.1073/pnas.20.1.12. URL: https://www.pnas.org/doi/abs/10.1073/pnas.20.1.12.

[51] G. Lemaıtre. "Un Univers homogène de masse constante et de rayon croissant rendant compte de la vitesse radiale des nébuleuses extra-galactiques". In: *Annales de la Société Scientifique de Bruxelles* 47 (Jan. 1927), pp. 49–59.

[52] Julien Lesgourgues. "The Cosmic Linear Anisotropy Solving System (CLASS) I: Overview". In: (Apr. 2011).

[53] Yudong Luo et al. "Big Bang Nucleosynthesis with an Inhomogeneous Primordial Magnetic Field Strength". In: *Astrophys. J.* 872.2 (2019), p. 172. DOI: 10.3847/1538-4357/ab0088. arXiv: 1810.08803 [astro-ph.CO].

[54] Chung-Pei Ma and Edmund Bertschinger. "Cosmological Perturbation Theory in the Synchronous and Conformal Newtonian Gauges". In: 455 (Dec. 1995), p. 7. DOI: 10.1086/176550. arXiv: astro-ph/9506072 [astro-ph].

[55] S. Matarrese et al. "Large-scale magnetic fields from density perturbations". In: *Phys. Rev. D* 71 (4 Feb. 2005), p. 043502. DOI: 10.1103/PhysRevD.71.043502. URL: https://link.aps.org/doi/10.1103/PhysRevD.71.043502.

[56] Sabino Matarrese, Silvia Mollerach, and Marco Bruni. "Relativistic second-order perturbations of the Einstein-de Sitter universe". English. In: *Physical Review D* 58.4 (Aug. 1998). ISSN: 1550-7998. DOI: 10.1103/PhysRevD.58.043504.

[57] Teppei Minoda et al. "Thermal Sunyaev–Zel'dovich Effect in the IGM due to Primordial Magnetic Fields". In: *Galaxies* 6.4 (2018), p. 143. DOI: 10.3390/galaxies6040143. arXiv: 1812.09813 [astro-ph.CO].

[58] V.F. Mukhanov, H.A. Feldman, and R.H. Brandenberger. "Theory of cosmological perturbations". In: *Physics Reports* 215.5 (1992), pp. 203–333. ISSN: 0370-1573. DOI: https://doi.org/10.1016/0370-1573(92)90044-Z. URL: https://www.sciencedirect.com/science/article/pii/037015739290044Z.

[59] Kouji Nakamura. "General formulation of general-relativistic higher-order gauge-invariant perturbation theory". In: *Classical and Quantum Gravity - CLASS QUANTUM GRAVITY* 28 (Nov. 2010). DOI: 10.1088/0264-9381/28/12/122001.

[60] Atsushi Naruko et al. "Second-order Boltzmann equation: Gauge dependence and gauge invariance". In: *Classical and Quantum Gravity* 30 (Aug. 2013). DOI: 10.1088/0264-9381/30/16/165008.

[61] A. Neronov and I. Vovk. "Evidence for strong extragalactic magnetic fields from Fermi observations of TeV blazars". In: *Science* 328 (2010), pp. 73–75. DOI: 10.1126/science.1184192. arXiv: 1006.3504 [astro-ph.HE].

[62] and P. A. R. Ade et al. "iPlanck/i2015 results". In: *Astronomy &amp Astrophysics* 594 (Sept. 2016), A19. DOI: 10.1051/0004-6361/201525821. URL: https://doi.org/10.1051%2F0004-6361%2F201525821.

[63] Kanhaiya L. Pandey and Shiv K. Sethi. "Probing Primordial Magnetic Fields Using Ly-alpha Clouds". In: *Astrophys. J.* 762 (2013), p. 15. DOI: 10.1088/0004-637X/762/1/15. arXiv: 1210.3298 [astro-ph.CO].

[64] D. Paoletti and F. Finelli. "Constraints on primordial magnetic fields from magnetically-induced perturbations: current status and future perspectives with LiteBIRD and future ground based experiments". In: *Journal of Cosmology and Astroparticle Physics* 2019.11 (Nov. 2019), pp. 028–028. DOI: 10.1088/1475-7516/2019/11/028. URL: https://doi.org/10.1088/1475-7516/2019/11/028.

[65] D. Paoletti, F. Finelli, and F. Paci. "The scalar, vector and tensor contributions of a stochastic background of magnetic fields to cosmic microwave background anisotropies". In: *Monthly Notices of the Royal Astronomical Society* 396.1 (June 2009), pp. 523–534. ISSN: 0035-8711. DOI: 10.1111/j.1365-2966.2009.14727.x. eprint: https://academic.oup.com/mnras/article-pdf/396/1/523/4078988/mnras0396-0523.pdf. URL: https://doi.org/10.1111/j.1365-2966.2009.14727.x.

[66] Daniela Paoletti and Fabio Finelli. "Constraints on primordial magnetic fields from magnetically-induced perturbations: current status and future perspectives with LiteBIRD and future ground based experiments". In: *JCAP* 11 (2019), p. 028. DOI: 10.1088/1475-7516/2019/11/028. arXiv: 1910.07456 [astro-ph.CO].

[67] P. J. E. Peebles. *The large-scale structure of the universe*. 1980.

[68] A. A. Penzias and R. W. Wilson. "A Measurement of Excess Antenna Temperature at 4080 Mc/s." In: 142 (July 1965), pp. 419–421. DOI: 10.1086/148307.

[69] Guido Pettinari et al. "The intrinsic bispectrum of the Cosmic Microwave Background". In: *Journal of Cosmology and Astroparticle Physics* 2013 (Feb. 2013). DOI: 10.1088/1475-7516/2013/04/003.

[70] Guido Walter Pettinari. *The Intrinsic Bispectrum of the Cosmic Microwave Background*. Springer International Publishing, 2016. DOI: 10.1007/978-3-319-21882-3. URL: https://doi.org/10.1007%2F978-3-319-21882-3.

[71] Cyril Pitrou. "The radiative transfer at second order: A full treatment of the Boltzmann equation with polarization". In: *Classical Quantum Gravity* 26 (Sept. 2008). DOI: 10.1088/0264-9381/26/6/065006.

[72] Planck Collaboration et al. "Planck 2018 results - VI. Cosmological parameters". In: *A&A* 641 (2020), A6. DOI: 10.1051/0004-6361/201833910. URL: https://doi.org/10.1051/0004-6361/201833910.

[73] Adam G. Riess et al. "A Comprehensive Measurement of the Local Value of the Hubble Constant with 1 km/s/Mpc Uncertainty from the Hubble Space Telescope and the SH0ES Team". In: (Dec. 2021). arXiv: 2112.04510 [astro-ph.CO].

[74] Adam G. Riess et al. "Cosmic Distances Calibrated to 1% Precision with Gaia EDR3 Parallaxes and Hubble Space Telescope Photometry of 75 Milky Way Cepheids Confirm Tension with ΛCDM". In: *Astrophys. J. Lett.* 908.1 (2021), p. L6. DOI: 10.3847/2041-8213/abdbaf. arXiv: 2012.08534 [astro-ph.CO].

[75] Adam G. Riess et al. "Observational Evidence from Supernovae for an Accelerating Universe and a Cosmological Constant". In: 116.3 (Sept. 1998), pp. 1009–1038. DOI: 10.1086/300499. arXiv: astro-ph/9805201 [astro-ph].

[76] R. K. Sachs and A. M. Wolfe. "Perturbations of a Cosmological Model and Angular Variations of the Microwave Background". In: 147 (Jan. 1967), p. 73. DOI: 10.1086/148982.

[77] Mohammadtaher Safarzadeh and Abraham Loeb. "An upper limit on primordial magnetic fields from ultra-faint dwarf galaxies". In: *Astrophys. J. Lett.* 877.2 (2019), p. L27. DOI: 10.3847/2041-8213/ab2335. arXiv: 1901.03341 [astro-ph.CO].

[78] Dominik J. Schwarz and Maik Stuke. "Lepton asymmetry and the cosmic QCD transition". In: 2009.11, 025 (Nov. 2009), p. 025. DOI: 10.1088/1475-7516/2009/11/025. arXiv: 0906.3434 [hep-ph].

[79] J. Richard Shaw and Antony Lewis. "Constraining primordial magnetism". In: *Phys. Rev. D* 86 (4 Aug. 2012), p. 043510. DOI: 10.1103/PhysRevD.86.043510. URL: https://link.aps.org/doi/10.1103/PhysRevD.86.043510.

[80] J. Richard Shaw and Antony Lewis. "Massive Neutrinos and Magnetic Fields in the Early Universe". In: *Phys. Rev. D* 81 (2010), p. 043517. DOI: 10.1103/PhysRevD.81.043517. arXiv: 0911.2714 [astro-ph.CO].

[81] A. Shukurov and K. Subramanian. *Astrophysical Magnetic Fields: From Galaxies to the Early Universe*. Cambridge Astrophysics. Cambridge University Press, 2021. ISBN: 9780521861052. URL: https://books.google.it/books?id=dK2BzgEACAAJ.

[82] George F. Smoot. "COBE observations and results". In: *Conference on 3K cosmology* (1999). DOI: 10.1063/1.59326. URL: http://dx.doi.org/10.1063/1.59326.

[83] Sebastiano Sonego and Marco Bruni. "Gauge dependence in the theory of nonlinear space-time perturbations". In: *Commun. Math. Phys.* 193 (1998), pp. 209–218. DOI: 10.1007/s002200050325. arXiv: gr-qc/9708068.

[84] Kandaswamy Subramanian. "Magnetic Fields in the Universe". In: (Sept. 2018). arXiv: 1809.03543 [astro-ph.CO].

[85] Kandaswamy Subramanian. "The origin, evolution and signatures of primordial magnetic fields". In: *Reports on Progress in Physics* 79 (Apr. 2015). DOI: 10.1088/0034-4885/79/7/076901.

[86] Kandaswamy Subramanian and John D. Barrow. "Magnetohydrodynamics in the early universe and the damping of nonlinear Alfvé n waves". In: *Physical Review D* 58.8 (Aug. 1998). DOI: 10.1103/physrevd.58.083502. URL: https://doi.org/10.1103%2Fphysrevd.58.083502.

[87] Hiroyuki Tashiro and Naoshi Sugiyama. "S-Z power spectrum produced by primordial magnetic fields". In: *Mon. Not. Roy. Astron. Soc.* 411 (2011), p. 1284. DOI: 10.1111/j.1365-2966.2010.17767.x. arXiv: 0908.0113 [astro-ph.CO].

[88] A. M. Taylor, I. Vovk, and A. Neronov. "Extragalactic magnetic fields constraints from simultaneous GeV-TeV observations of blazars". In: *Astron. Astrophys.* 529 (2011), A144. DOI: 10.1051/0004-6361/201116441. arXiv: 1101.0932 [astro-ph.HE].

[89] Kenji Tomita. "Non-Linear Theory of Gravitational Instability in the Expanding Universe". In: *Progress of Theoretical Physics* 37.5 (May 1967), pp. 831–846. ISSN: 0033-068X. DOI: 10.1143/PTP.37.831. eprint: https://academic.oup.com/ptp/article-pdf/37/5/831/5234391/37-5-831.pdf. URL: https://doi.org/10.1143/PTP.37.831.

[90] Tessa Vernstrom et al. "Discovery of Magnetic Fields Along Stacked Cosmic Filaments as Revealed by Radio and X-Ray Emission". In: (Jan. 2021). DOI: 10.1093/mnras/stab1301. arXiv: 2101.09331 [astro-ph.CO].

[91] Ievgen Vovk et al. "Fermi/LAT observations of 1ES 0229+200: implications for extragalactic magnetic fields and background light". In: *Astrophys. J. Lett.* 747 (2012), p. L14. DOI: 10.1088/2041-8205/747/1/L14. arXiv: 1112.2534 [astro-ph.CO].

[92] Steven Weinberg. *Gravitation and Cosmology: Principles and Applications of the General Theory of Relativity*. New York: John Wiley and Sons, 1972. ISBN: 978-0-471-92567-5, 978-0-471-92567-5.

[93] Lawrence M. Widrow. "Origin of galactic and extragalactic magnetic fields". In: *Rev. Mod. Phys.* 74 (2002), pp. 775–823. DOI: 10.1103/RevModPhys.74.775. arXiv: astro-ph/0207240.

[94] Lawrence M. Widrow et al. "The First Magnetic Fields". In: *Space Sci. Rev.* 166 (2012), pp. 37–70. DOI: 10.1007/s11214-011-9833-5. arXiv: 1109.4052 [astro-ph.CO].

[95] Matias Zaldarriaga and Uros Seljak. "An all sky analysis of polarization in the microwave background". In: *Physical Review D* 55 (1997), pp. 1830–1840.

Acknowledgements

At the end of this work and of my master degree course, some thanks are due.

First of all, I would like to thank my supervisor Prof. Roberto Casadio for his kind availability and for having increasing my interest in cosmology during these years of study.

Special thanks go to my two co-supervisors. I thank Dr. Fabio Finelli for always showing me passion and enthusiasm for this thesis and inspiring me to always give my best, I am really grateful to have worked with him. I thank Dr. Daniela Paoletti for her immense patience and for all the time she spent helping me and solving all my doubts, she has been always available and kind to me.

I would like to thank Dr. Christian Fidler for having kindly provided useful information about the SONG code and Prof. Kandaswamy Subramanian for having shared his precious opinions and considerations throughout the course of this thesis.

I want to express all my gratitude to my family. Thank you for the unconditional support you gave me for all these years. Even if I do not often show it explicitly, I want you to know that I always feel lucky to have a supportive and lovely family like yours.

Finally, I am really happy to express my gratitude to Camilla for being always there for me and for supporting me even in my most difficult periods. I am really glad to have had the opportunity to share with you all my thoughts, worries and dreams during these years. Thank you.